

Diamond-based Fabry-Perot microcavities for quantum networks

Bogdanovic, Stefan

DOI

[10.4233/uuid:29c23e60-9f4c-4d5e-9ab9-9bf6c520df01](https://doi.org/10.4233/uuid:29c23e60-9f4c-4d5e-9ab9-9bf6c520df01)

Publication date

2017

Document Version

Final published version

Citation (APA)

Bogdanovic, S. (2017). *Diamond-based Fabry-Perot microcavities for quantum networks*. [Dissertation (TU Delft), Delft University of Technology]. <https://doi.org/10.4233/uuid:29c23e60-9f4c-4d5e-9ab9-9bf6c520df01>

Important note

To cite this publication, please use the final published version (if applicable).
Please check the document version above.

Copyright

Other than for strictly personal use, it is not permitted to download, forward or distribute the text or part of it, without the consent of the author(s) and/or copyright holder(s), unless the work is under an open content license such as Creative Commons.

Takedown policy

Please contact us and provide details if you believe this document breaches copyrights.
We will remove access to the work immediately and investigate your claim.

DIAMOND-BASED FABRY-PEROT MICROCAVITIES FOR QUANTUM NETWORKS



DIAMOND-BASED FABRY-PEROT MICROCAVITIES FOR QUANTUM NETWORKS

Proefschrift

ter verkrijging van de graad van doctor
aan de Technische Universiteit Delft,
op gezag van de Rector Magnificus prof. ir. K.C.A.M. Luyben,
voorzitter van het College voor Promoties,
in het openbaar te verdedigen op vrijdag 3 november 2017 om 10:00 uur

door

Stefan BOGDANOVIĆ

Master of Science in Physics,
University of Belgrade, Belgrado, Servië
geboren te Čačak, Servië.

Dit proefschrift is goedgekeurd door de promotor:

Prof. dr. ir. R. Hanson

Samenstelling promotiecommissie:

Rector Magnificus,
Prof. dr. ir. R. Hanson

Voorzitter
Technische Universiteit Delft, promotor

Onafhankelijke leden:

Prof. dr. ir. L. M. K. Vandersypen	Technische Universiteit Delft
Prof. dr. L. Kuipers	Technische Universiteit Delft
Prof. dr. C. Degen	Eidgenössische Technische Hochschule, Zürich
Dr. S. Groeblacher	Technische Universiteit Delft
Prof. dr. ir. L. P. Kouwenhoven,	Technische Universiteit Delft, reservelid



Printed by: Gildeprint

Front & Back: Designed by Tanja Vuksanović, Önder Gül and Stefan Bogdanović

Copyright © 2017 by S. Bogdanović

Casimir PhD series, Delft-Leiden 2017-37

ISBN 978-90-8593-321-2

An electronic version of this dissertation is available at
<http://repository.tudelft.nl/>.

To everyone I love



CONTENTS

1	Introduction	1
1.1	The Implementation of Quantum Networks	2
1.2	Quantum networks using NV centers in diamond.	3
1.3	Thesis overview	4
	References	6
2	The nitrogen-vacancy center in diamond	9
2.1	Energy level structure of the NV center	10
2.2	Properties of the optically excited state	12
2.3	NV center as a qubit.	14
	References	16
3	Fabry-Perot resonators and emitter-cavity coupling	19
3.1	One-dimensional Fabry-Perot Cavity	20
3.2	Gaussian beams in spherical-mirror resonators.	23
3.3	Emitters in cavities	24
3.4	An overview of Nitrogen-vacancy centers in cavities so far	28
	References	30
4	Experimental methods	33
4.1	Fiber interface	34
4.2	Mirror properties	34
4.3	Diamond membrane	36
4.4	Piezo positioner.	38
4.5	Cryostation	38
	References	41
5	Robust nano-fabrication of an integrated platform for spin control in a tunable micro-cavity	43
5.1	Introduction	44
5.2	Fiber dimple	44
5.3	Mirror coatings	46
5.4	Striplines and marker field	46
5.5	Cavity finesse	47
5.6	Diamond membrane preparation and bonding.	47
5.7	Conclusion	50
5.8	Methods	51
	References	52

6 Design and low-temperature characterization of a tunable microcavity for diamond-based quantum networks	57
6.1 Introduction	58
6.2 Cavity design	58
6.3 Cavity mode study	58
6.4 Finesse measurement	60
6.5 Cavity stability measurement	62
6.6 Conclusion	64
6.7 Supplementary Material	64
References	65
7 Outlook	69
7.1 Summary	70
7.2 Towards Purcell enhancement of the NV center emission	70
7.3 Possible experimental advancement	71
7.4 Future experiments	73
7.5 Conclusion	74
References	75
Summary	77
Samenvatting	79
Acknowledgements	81
List of Publications	87
Curriculum Vitæ	89

1

INTRODUCTION

S. Bogdanović

The realization of quantum networks would represent a remarkable implementation of quantum technologies in a real-world setting. Here, we present the basic principles of these networks (Section 1.1) and discuss their implementation in different experimental systems. Section 1.2 will describe the first building blocks of these quantum networks based on the NV centers in diamond and outline the current bottlenecks for their full realization. Finally, Section 1.3 will propose an approach to overcome these drawbacks and give the overview of this thesis.

1.1. THE IMPLEMENTATION OF QUANTUM NETWORKS

Ever since the proposal of a universal quantum simulator[1], the possibility of the application of quantum mechanics in a real-world setting has opened up many exciting research avenues. From a fundamental point of view, this new perspective has contributed to a deeper understanding of the principles of quantum mechanics and enabled testing of some of its fundamental predictions. From an applied perspective, meeting the requirements for these new applications necessitated a dramatic improvement of our ability to isolate and control quantum systems. This stimulated the emergence of a range of accompanying quantum technologies in step with the development of this fundamental research. A prime example of these emerging technologies is the symbiosis of quantum mechanics and classical information theory which gave rise to the concepts of quantum computing and quantum networks.

Quantum networks allow for the creation of quantum many-body systems distributed across many spatially separated nodes[2]. Reflecting the architecture of classical networks, in leading proposals for the design of quantum networks the quantum information is generated, processed, and stored locally in quantum nodes[3]. By entangling these nodes through quantum communication channels, quantum information can be transmitted between the nodes using teleportation protocols[4, 5] over arbitrarily long distances[6].

Long range quantum communication protocols running on a quantum network would enable secret key distribution with guaranteed secure communication. In addition, such a network would allow distributed quantum computing[7] through the connection of smaller quantum processors into larger units. The benefits of this design would be that it would overcome the spatial scaling and error correlations which limit the size and the processing power of a single quantum node, instead allowing for an alternative multi-node processing paradigm that may lead to more effective scaling[3]. Furthermore, increasing the separation between two quantum nodes has already enabled fundamental tests of quantum mechanics to be performed, including a loophole-free Bell test[8–11].

Finally, it is likely that, aside from the proposed examples of the utility of these networks, their full potential will be realized through not yet foreseen applications, as was the case with their classical communication counterpart.

Having broadly described the design of a quantum network, in the remainder of this section we shall discuss their practical implementation. A natural pick for long distance quantum information carriers in quantum networks are optical photons, ideally at a telecom wavelength, which enables high-speed propagation with low loss in optical fibers. In contrast, in order to implement quantum protocols, local nodes will require the ability to initialize, manipulate and measure quantum states, making material qubits an ideal choice.

These considerations narrow the selection of the candidates for a quantum network platform to a hybrid system of isolated matter qubits which can store and preserve the quantum information for long times, interfaced with photons which carry the informa-

tion to large distances, connecting several nodes.

A significant appeal of this experimental field lies in the range of potential physical platforms for the implementation of such a quantum network. These platforms range from laser-cooled atomic gasses[12] and rare-earth ion doped crystals[13, 14] where information can be stored in a collective excitation of the atomic ensembles, to systems where the quantum information is localized in individual particles which possess the capability to manipulate and process stored quantum information.

The latter approach relies on isolating an individual particle and decoupling it from its environment either by advanced optical or electromagnetic trapping in trapped ion[15] and atom[16] experiments or by utilizing solid state systems reinforced by the plethora of available fabrication techniques. The application of these techniques has already facilitated tremendous progress in the field of quantum information with quantum dots[17], superconducting qubits[18] and diamond color centers.

1.2. QUANTUM NETWORKS USING NV CENTERS IN DIAMOND

Since the first observation of the single nitrogen-vacancy (NV) color center in diamond[19], this defect attracted considerable interest in experimental physics. It displays many desirable quantum properties of a trapped single ion while being embedded in the robust diamond matrix which largely shields it from environmental disturbances. Some of these properties, like its stable single photon emission, initialization, manipulation and optical readout of its electron spin, which remarkably persist even at room temperatures, can adapt well to the requirements of a quantum network node with the photonic interface, introduced in the previous section. Furthermore, its natural incorporation into the diamond lattice during diamond growth greatly reduces the experimental overhead of trapping the single quantum object, highlighting its promise of easier scalability compared to other systems.

Expanding on the adaptation to the quantum networks framework, the NV center electron spin along with the neighboring nuclear spins form a multi-qubit quantum node that can be addressed and manipulated using the microwave and optical pulses[20]. The ability to create entanglement between the state of the NV center spin and a photon introduces a way of transferring quantum information from the stationary NV node to a flying photonic qubit[21], enabling long distance transmission of quantum information using this optical channel. This trait will be essential in establishing entanglement between two macroscopically separated NV center spins in a Barrett-Kok protocol[22].

In the heart of this protocol lies the quantum interference of the two photons emitted by two macroscopically separated NV centers on a 50:50 beamsplitter. The beamsplitter acts as an eraser of a "which-path" information enabling heralded NV spin-spin entanglement after successful photon detection events. However, for this scheme to work the impinging photons need to be indistinguishable. This requirement renders only photons emitted from the NV center resonant line useful in establishing entanglement between two quantum nodes and it is clear that the ability to collect and detect these resonant

photons will be crucial for the success probability of this protocol.

To achieve this goal, a hemispherical solid immersion lens was fabricated around the NV center position using a focused beam of gallium ions. The purpose of this design is to establish a normal angle of incidence of the emitted photons from the center of the fabricated hemisphere to the diamond surface, reducing the probability of total internal reflection. These fabricated structures increased the collection efficiency by an order of magnitude which enabled experiments establishing long distance entanglement of the NV center spins over distances of 3 meters[23] and 1.3 kilometers[24], demonstrating essential components of the NV center based quantum network.

However pushing the existing experiments beyond a proof-of-principle demonstration will require addressing the central issue of low success rates of the described entanglement protocol which lies in the NV center resonant emission probability. Only $\approx 3\%$ of the NV center emission is resonant and thus useful in the long distance entanglement schemes. In addition, the solid immersion lens can collect only a fraction of a total solid angle of the NV center emission meaning that a majority of the emitted photons are inaccessible for detection.

Addressing these issues would clearly represent a crucial step towards the realization of the quantum networks based on NV centers. This solution will, however, require a significant overhaul of our current experimental design which we introduce in the following section.

1.3. THESIS OVERVIEW

The goal of this thesis is to provide a solution to the key outstanding problem of the low success probability of photonic links for NV-based diamond quantum networks. This will be achieved by coupling NV centers to open, tunable, Fabry-Perot microcavities.

The thesis overview is:

In Chapter 2 we will introduce the main properties of the NV centers starting with an analysis of its electron structure, and the features of its optical transitions.

Chapter 3 will introduce the theoretical background governing properties of optical resonators and their coupling to emitters. We present an overview of experiments aimed at demonstrating NV-cavity coupling and highlight their strengths and weaknesses.

In Chapter 4 we describe the procedures for fabricating cavity components and diamond samples and present and discuss several design choices of our experimental setup.

We continue the description of the fabrication procedure in Chapter 5 providing additional details of the process. We modify the cavity components to enable NV center searching and demonstrate NV center spin addressing in our current experimental de-

sign.

Chapter 6 focuses on the design and characterization of the open tunable Fabry-Perot cavity. It contains details of the cavity finesse measurement and investigates the finesse dependency on various experimental regimes. Special attention is given to the effects of the system vibrations and the cavity performance is estimated versus the expected speedup of the long distance entanglement protocol.

Finally, Chapter 7 summarizes the work presented in this thesis, outlines possible improvements to the current experiment and discusses several future experimental directions.

REFERENCES

- [1] R. P. Feynman, “Simulating physics with computers,” *International Journal of Theoretical Physics*, vol. 21, pp. 467–488, Jun 1982.
- [2] S. Ritter, C. Nolleke, C. Hahn, A. Reiserer, A. Neuzner, M. Uphoff, M. Mücke, E. Figueroa, J. Bochmann, and G. Rempe, “An elementary quantum network of single atoms in optical cavities,” *Nature*, vol. 484, pp. 195–200, Apr 2012.
- [3] H. J. Kimble, “The quantum internet,” *Nature*, vol. 453, pp. 1023–1030, Jun 2008.
- [4] C. H. Bennett, G. Brassard, C. Crépeau, R. Jozsa, A. Peres, and W. K. Wootters, “Teleporting an unknown quantum state via dual classical and einstein-podolsky-rosen channels,” *Phys. Rev. Lett.*, vol. 70, pp. 1895–1899, Mar 1993.
- [5] W. Pfaff, B. J. Hensen, H. Bernien, S. B. van Dam, M. S. Blok, T. H. Taminiâu, M. J. Tiggelman, R. N. Schouten, M. Markham, D. J. Twitchen, and R. Hanson, “Unconditional quantum teleportation between distant solid-state quantum bits,” *Science*, vol. 345, no. 6196, pp. 532–535, 2014.
- [6] L. Childress, J. M. Taylor, A. S. Sørensen, and M. D. Lukin, “Fault-tolerant quantum repeaters with minimal physical resources and implementations based on single-photon emitters,” *Phys. Rev. A*, vol. 72, p. 052330, Nov 2005.
- [7] L. Jiang, J. M. Taylor, and M. D. Lukin, “Fast and robust approach to long-distance quantum communication with atomic ensembles,” *Phys. Rev. A*, vol. 76, p. 012301, Jul 2007.
- [8] B. Hensen, H. Bernien, A. E. Dreau, A. Reiserer, N. Kalb, M. S. Blok, J. Ruitenberg, R. F. L. Vermeulen, R. N. Schouten, C. Abellan, W. Amaya, V. Pruneri, M. W. Mitchell, M. Markham, D. J. Twitchen, D. Elkouss, S. Wehner, T. H. Taminiâu, and R. Hanson, “Loophole-free bell inequality violation using electron spins separated by 1.3 kilometres,” *Nature*, vol. 526, pp. 682–686, Oct 2015. Letter.
- [9] L. K. Shalm, E. Meyer-Scott, B. G. Christensen, P. Bierhorst, M. A. Wayne, M. J. Stevens, T. Gerrits, S. Glancy, D. R. Hamel, M. S. Allman, K. J. Coakley, S. D. Dyer, C. Hodge, A. E. Lita, V. B. Verma, C. Lambrocco, E. Tortorici, A. L. Migdall, Y. Zhang, D. R. Kumor, W. H. Farr, F. Marsili, M. D. Shaw, J. A. Stern, C. Abellán, W. Amaya, V. Pruneri, T. Jennewein, M. W. Mitchell, P. G. Kwiat, J. C. Bienfang, R. P. Mirin, E. Knill, and S. W. Nam, “Strong loophole-free test of local realism,” *Phys. Rev. Lett.*, vol. 115, p. 250402, Dec 2015.
- [10] M. Giustina, M. A. M. Versteegh, S. Wengerowsky, J. Handsteiner, A. Hochrainer, K. Phelan, F. Steinlechner, J. Kofler, J.-A. Larsson, C. Abellán, W. Amaya, V. Pruneri, M. W. Mitchell, J. Beyer, T. Gerrits, A. E. Lita, L. K. Shalm, S. W. Nam, T. Scheidl, R. Ursin, B. Wittmann, and A. Zeilinger, “Significant-loophole-free test of bell’s theorem with entangled photons,” *Phys. Rev. Lett.*, vol. 115, p. 250401, Dec 2015.

- [11] W. Rosenfeld, D. Burchardt, R. Garthoff, K. Redeker, N. Ortegel, M. Rau, and H. Weinfurter, “Event-ready bell test using entangled atoms simultaneously closing detection and locality loopholes,” *Phys. Rev. Lett.*, vol. 119, p. 010402, Jul 2017.
- [12] X.-H. Bao, A. Reingruber, P. Dietrich, J. Rui, A. Duck, T. Strassel, L. Li, N.-L. Liu, B. Zhao, and J.-W. Pan, “Efficient and long-lived quantum memory with cold atoms inside a ring cavity,” *Nat Phys*, vol. 8, pp. 517–521, Jul 2012.
- [13] C. Clausen, I. Usmani, F. Bussieres, N. Sangouard, M. Afzelius, H. de Riedmatten, and N. Gisin, “Quantum storage of photonic entanglement in a crystal,” *Nature*, vol. 469, pp. 508–511, Jan 2011.
- [14] M. Gundogan, P. M. Ledingham, K. Kutluer, M. Mazzera, and H. de Riedmatten, “Solid state spin-wave quantum memory for time-bin qubits,” *Phys. Rev. Lett.*, vol. 114, p. 230501, Jun 2015.
- [15] R. Blatt and D. Wineland, “Entangled states of trapped atomic ions,” *Nature*, vol. 453, pp. 1008–1015, Jun 2008.
- [16] A. Reiserer and G. Rempe, “Cavity-based quantum networks with single atoms and optical photons,” *Rev. Mod. Phys.*, vol. 87, pp. 1379–1418, Dec 2015.
- [17] A. Delteil, Z. Sun, W.-b. Gao, E. Togan, S. Faelt, and A. Imamoglu, “Generation of heralded entanglement between distant hole spins,” *Nat Phys*, vol. 12, pp. 218–223, Mar 2016. Letter.
- [18] D. Riste, M. Dukalski, C. A. Watson, G. de Lange, M. J. Tiggelman, Y. M. Blanter, K. W. Lehnert, R. N. Schouten, and L. DiCarlo, “Deterministic entanglement of superconducting qubits by parity measurement and feedback,” *Nature*, vol. 502, pp. 350–354, Oct 2013. Letter.
- [19] A. Gruber, A. Dräbenstedt, C. Tietz, L. Fleury, J. Wrachtrup, and C. v. Borczyskowski, “Scanning confocal optical microscopy and magnetic resonance on single defect centers,” *Science*, vol. 276, no. 5321, pp. 2012–2014, 1997.
- [20] M. V. G. Dutt, L. Childress, L. Jiang, E. Togan, J. Maze, F. Jelezko, A. S. Zibrov, P. R. Hemmer, and M. D. Lukin, “Quantum register based on individual electronic and nuclear spin qubits in diamond,” *Science*, vol. 316, no. 5829, pp. 1312–1316, 2007.
- [21] E. Togan, Y. Chu, A. S. Trifonov, L. Jiang, J. Maze, L. Childress, M. V. G. Dutt, A. S. Sørensen, P. R. Hemmer, A. S. Zibrov, and M. D. Lukin, “Quantum entanglement between an optical photon and a solid-state spin qubit,” *Nature*, vol. 466, no. 7307, pp. 730–734, 2010.
- [22] S. D. Barrett and P. Kok, “Efficient high-fidelity quantum computation using matter qubits and linear optics,” *Phys. Rev. A*, vol. 71, p. 060310, Jun 2005.
- [23] H. Bernien, B. Hensen, W. Pfaff, G. Koolstra, M. S. Blok, L. Robledo, T. H. Taminiau, M. Markham, D. J. Twitchen, L. Childress, and R. Hanson, “Heralded entanglement between solid-state qubits separated by three metres,” *Nature*, vol. 497, pp. 86–90, Apr. 2013.

- [24] B. Hensen, H. Bernien, A. E. Dreau, A. Reiserer, N. Kalb, M. S. Blok, J. Ruitenberg, R. F. L. Vermeulen, R. N. Schouten, C. Abellan, W. Amaya, V. Pruneri, M. W. Mitchell, M. Markham, D. J. Twitchen, D. Elkouss, S. Wehner, T. H. Taminiau, and R. Hanson, “Loophole-free bell inequality violation using electron spins separated by 1.3 kilometres,” *Nature*, vol. 526, p. 682, Oct 2015.

2

THE NITROGEN-VACANCY CENTER IN DIAMOND

S. Bogdanović

This chapter will introduce the NV center properties relevant for the scope of this thesis. We start with the analysis of the NV center ground and the excited state electronic structure (Section 2.1), discuss the properties of its optical transitions (Section 2.2) and define its spin states in the qubit framework (Section 2.3). For a more complete description of the NV center fundamental properties, the reader is pointed to the several comprehensive review papers[1–3].

2.1. ENERGY LEVEL STRUCTURE OF THE NV CENTER

The nitrogen-vacancy (NV) center is an optically active defect in diamond created by the substitution of two adjacent carbon atoms in the diamond crystal matrix by a nitrogen atom and a neighboring vacancy (Figure 2.1(a)). The presence of a vacancy breaks the covalent bonds in the diamond crystal creating four dangling bonds in their place. Three of them are centered on each of the carbon atoms adjacent to the vacancy while the fourth one is associated with the nitrogen atom and they transform under the symmetry operations of the C_{3v} group[2]. The NV center electron orbitals, displayed in Figure 2.1(b,c), are formed by the linear combination of these bonds.

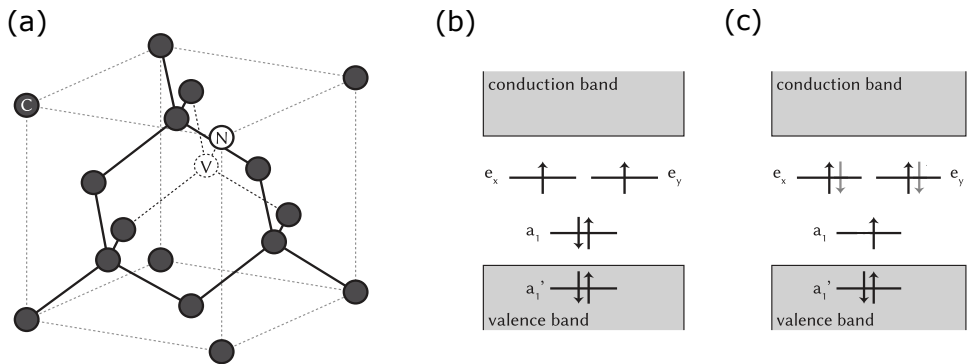


Figure 2.1: Nitrogen-vacancy center in diamond. a) Schematics of a diamond lattice containing a nitrogen atom (N) and an adjacent vacancy (V) substituting carbon atoms (C). b) The NV center ground state electron orbitals. c) Excited state NV center orbital structure. Optical excitation promotes one electron from the a_1 orbital to the first excited state. The figure is adapted from Bernien[4].

The electronic structure of the NV center is determined by the filling of these orbitals. An NV^0 charge state is formed by three neighboring carbons contributing with a single electron and two electrons originating from the nitrogen as a donor in diamond. An NV^- defect, the one relevant for this work (called just the NV center in the remainder of the thesis), is formed by capturing an additional electron from the environment. The ground state electron configuration of the NV^- $a_1^2e^2$ has four electrons in symmetric states a_1 and a_1' and an unpaired electron in each of the e_x and e_y energy orbitals forming a spin triplet $S = 1$ (Figure 2.1(b)). Optical excitation promotes one of the a_1' orbital electrons to one of the higher energy orbitals e_{xy} forming an $a_1'e^3$ configuration (Figure 2.1(c)). The ground and the excited state energy levels of the NV center are located within the 5.5 eV wide diamond bandgap, insulating it from the bulk electrons which is beneficial for the long coherence times of the NV center spin.

To fully describe the electron states, we consider several effects governing their configuration at low temperature (≈ 4 K) (Figure 2.2). The ground state spin triplet 3A_2 is separated by 1.945 eV from the excited state triplet 3E and can be reached via resonant (zero-phonon line) or off-resonant (phonon side band) optical excitation followed by

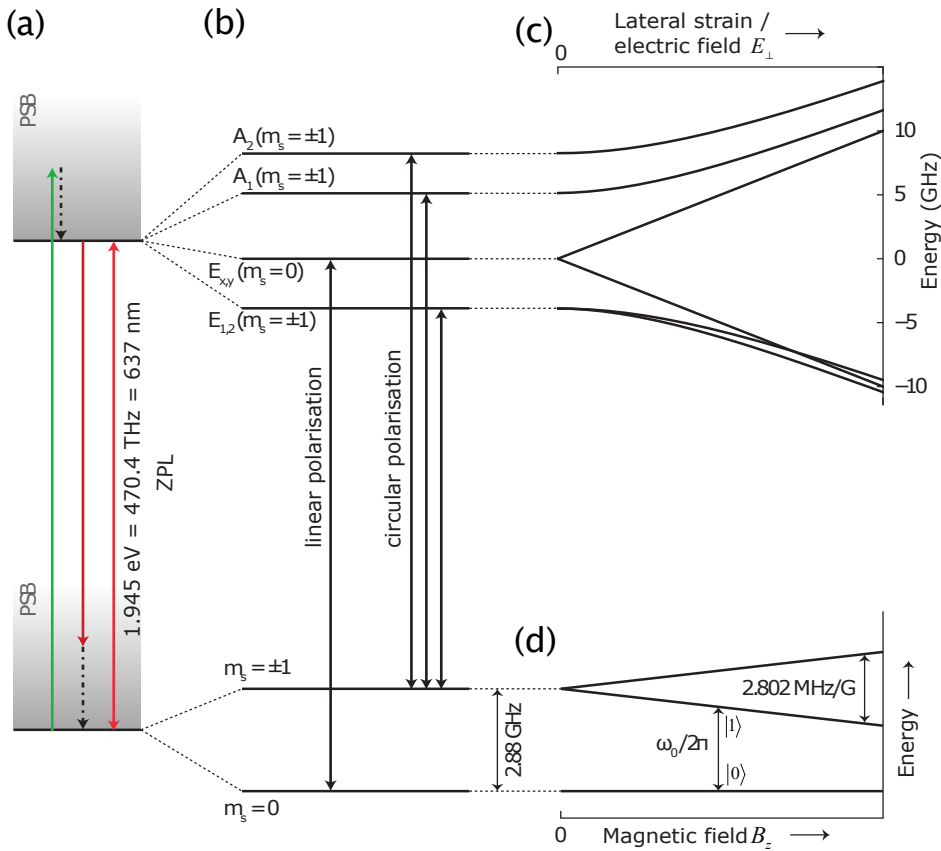


Figure 2.2: NV center electron level structure. a) Ground state triplet 3A_2 is coupled to the excited state triplet 3E through resonant (ZPL) or off-resonant (PSB) excitation and emission. b) The zero field splitting (2.88 GHz), separates $m_s = 0$ and the degenerate $m_s = \pm 1$ ground states. Spin-orbit and spin-spin interactions split the excited state into four levels. c) Lateral strain or applied electric fields can shift the energy levels of the NV excited state. d) Applying an external magnetic field along the NV axis lifts the degeneracy of the $m_s = \pm 1$ ground states, enabling microwave addressing of the individual transitions. The figure is adapted from Bernien[4].

subsequent emission as shown in Figure 2.2(a). The zero field splitting, separates the $m_s = 0$ and the degenerate $m_s = \pm 1$ ground states, while spin-orbit and spin-spin interactions split the excited state into four levels out of which two consist of two degenerate levels ($E_{1,2}$ and $E_{x,y}$) (Figure 2.2(b)). The optical transitions between the ground and the excited states are spin-selective and obey selection rules.

The excited state levels can be further split as a consequence of the electric fields or the lateral strain (Figure 2.2(c)). An externally applied magnetic field along the NV crystal axis lifts the degeneracy of the $m_s = \pm 1$ ground state levels by the Zeeman splitting (Figure 2.2(d)).

2.2. PROPERTIES OF THE OPTICALLY EXCITED STATE

Properties of the resonant zero-phonon line (ZPL) of the NV center will be of great importance in the consideration of the NV-cavity coupling mechanism and will be discussed here in more detail. In Figure 2.3(a) we present the NV center spectrum at $T = 7$ K and highlight a narrow ZPL at 637 nm containing only $\approx 3\%$ of the total NV center emission and a broad phonon side band (PSB). Scanning a tunable laser across the ZPL reveals its individual resonances displayed in Figure 2.3(b). Labels correspond to the spin selective transitions in Figure 2.2(b). Narrow linewidths of ZPL transitions are necessary for establishing the photon indistinguishability in long distance entanglement protocols as well as improving the NV-cavity coupling which will be further elaborated in Chapter 3. Lifetime limited linewidths set the lower boundary of the spectral width of the individual ZPL transitions to ≈ 13 MHz corresponding to the lifetime of ≈ 12 ns.

However, optical linewidths of these transitions are subject to broadening due to several effects. For temperatures higher than 10 K the linewidth increases following a T^5 dependence likely as a consequence of a two-phonon Raman process due to the dynamic Jahn-Teller effect[6, 7], illustrating the necessity of performing experiments at low temperatures.

Another mechanism of linewidth broadening is connected to the sensitivity of the NV center to local electric fields through Stark effect. This process is used to controllably tune the frequency of the NV center resonant transitions[8, 9]. However, shallow NV centers can suffer from the spectral diffusion induced by charge fluctuations on the diamond surface which inhomogeneously broadens their spectral line. This will be further discussed in the following chapter.

It is worth mentioning other color centers in diamond, such as silicon-vacancies[10] and germanium-vacancies[11], whose spectral lines are not susceptible at first order to the electric field changes. This makes them robust to the mentioned spectral diffusion effects, although at the expense of the necessity for more elaborate spectral tuning mechanisms[12].

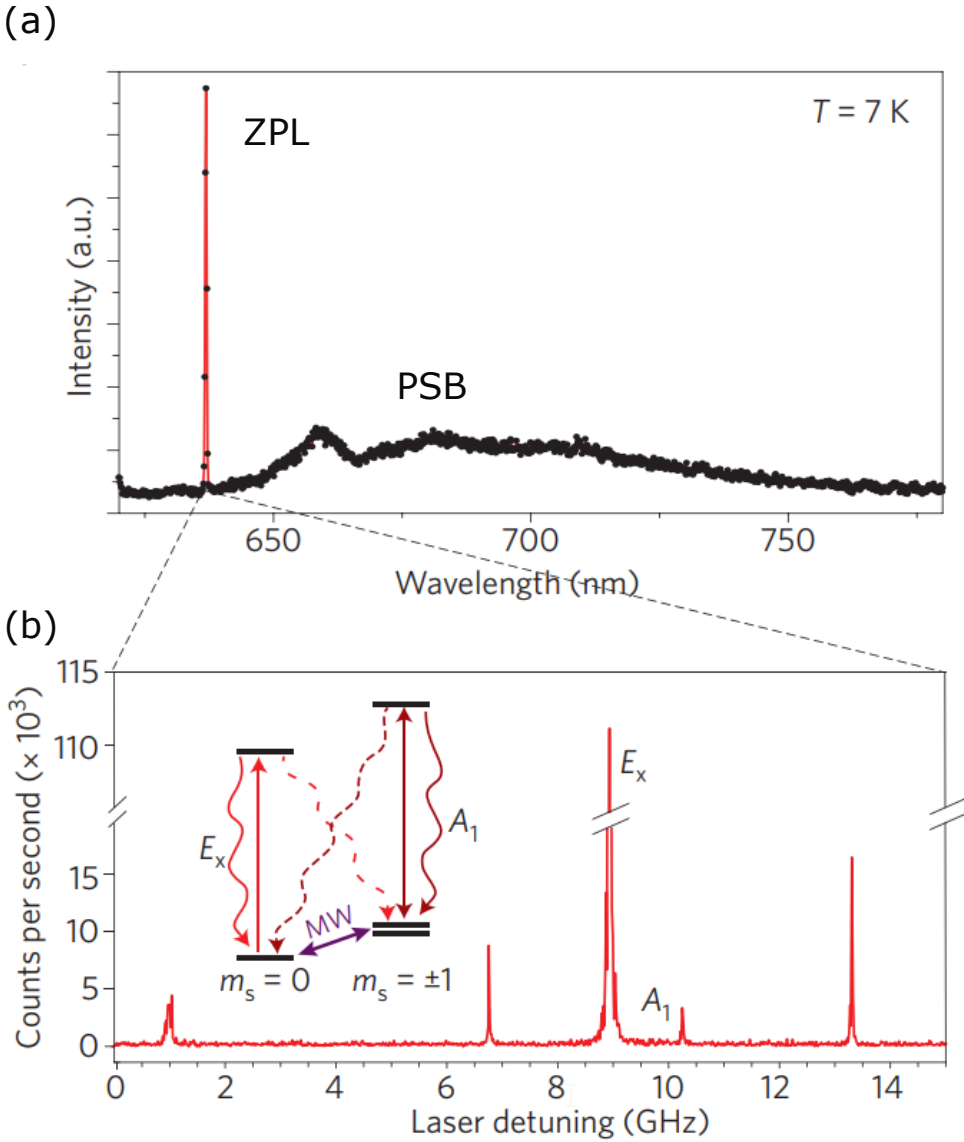


Figure 2.3: NV center spectrum. (a) Low temperature photoluminescence spectrum of the NV center obtained using off-resonant excitation at 532 nm. Narrow ZPL and a broad PSB are visible. (b) Scanning a tunable laser frequency over the ZPL reveals individual resonances of the electron transitions. The inset shows NV center energy level transitions labeled according to Figure 2.2(b). Dashed lines represent non-spin-conserving decay. The figure is adapted from Gao et al[5].

2.3. NV CENTER AS A QUBIT

2

The ability to separate and individually address two spin states in the NV center's ground state, allows describing this defect in the quantum information processing framework. We label the NV center's ground states $m_s = 0 \rightarrow |0\rangle$ and $m_s = -1$ (or $m_s = +1$) $\rightarrow |1\rangle$ and designate this two-level system as a qubit.

The NV center spin can be initialized into state $|0\rangle$ using individual spin-selective optical transitions within the NV center's ZPL that can be resolved at temperatures below 10 K (Figure 2.3). Relying on the technique of optical pumping, this qubit can be initialized with $> 99.7\%$ fidelity and read out in a single shot with high fidelity using spin dependent fluorescence detection[13]. In the microwave domain, application of the microwave pulses coherently drives the NV center electron spin between the states $|0\rangle$ and $|1\rangle$. Coherence times exceeding 10 ms have been observed for a single NV[14] in samples with a natural abundance of ^{13}C nuclear spins and up to 0.5 s for ensembles[15].

One of the limitations to the NV center spin coherence times is the presence of the residual ^{13}C spins within the diamond matrix which create fluctuating magnetic field and contribute to the NV center spin dephasing[16]. This issue can be addressed by using isotopically purified samples (concentration of $^{12}\text{C} \approx 99.99\%$)[17]. Another established method for the spin coherence time extension is applying a sequence of microwave pulses to the NV center spin, isolating it from the environmental noise using the principles of dynamical decoupling[18].

However, the coupling of the NV center spin to the spins in the environment can also be used as a resource. The hyperfine interaction that couples NV spin to nitrogen or ^{13}C nuclear spins allows spin selective control conditional on the state of nuclear spins enabling two-qubit quantum gates between them[19] transforming the NV center into a multi-qubit quantum node[20–23]. In addition, the nuclear spin coherence times are significantly larger compared to the NV center's due to their three orders of magnitude smaller gyromagnetic ratio, enabling storing of quantum information for much longer periods of time[24].

Utilizing NV centers for long distance quantum communication schemes relies on their spin dependent optical excitation and emission which enables spin-photon entanglement[25]. Photons as flying qubits, allow the transmission of quantum information over long distances, establishing remote entanglement protocols between two NV center nodes with meter[14, 25] and even kilometer[26] separation.

The demonstration of NV center high fidelity initialization, readout and qubit manipulation with long coherence times, as well as connecting the stationary and flying qubit through NV center spin-photon entanglement fulfills some of the key points of the DiVincenzo criteria for quantum computation and quantum communication[27]. However, the criterion of scalability remains the key challenge for any practical implementation of this system in the quantum communication protocols. The efficiency of quantum

networks greatly decreases with increasing node separation due to the large absorption of the 637 nm photon in optical fiber and low probability of the NV center resonant emission. An appealing approach for overcoming this problem and boosting the success rate of long distance entanglement protocols is coupling NV centers to optical cavities which will be introduced in the following chapter.

REFERENCES

- [1] F. Jelezko and J. Wrachtrup, "Single defect centres in diamond: A review," *phys. stat. sol. (a)*, vol. 203, pp. 3207–3225, Oct. 2006.
- [2] J. R. Maze, A. Gali, E. Togan, Y. Chu, A. Trifonov, E. Kaxiras, and M. D. Lukin, "Properties of nitrogen-vacancy centers in diamond: the group theoretic approach," *New J. Phys.*, vol. 13, p. 5025, Feb. 2011.
- [3] M. W. Doherty, N. B. Manson, P. Delaney, F. Jelezko, J. Wrachtrup, and L. C. L. Hollenberg, "The nitrogen-vacancy colour centre in diamond," *Physics Reports*, vol. 528, pp. 1–45, July 2013.
- [4] H. Bernien, *Control, measurement and entanglement of remote quantum spin registers in diamond*. Delft, University of Technology: PhD Thesis, 2014.
- [5] W. B. Gao, A. Imamoglu, H. Bernien, and R. Hanson, "Coherent manipulation, measurement and entanglement of individual solid-state spins using optical fields," *Nat. Photon.*, vol. 9, p. 363, Jun 2015.
- [6] K.-M. C. Fu, C. Santori, P. E. Barclay, L. J. Rogers, N. B. Manson, and R. G. Beausoleil, "Observation of the dynamic jahn-teller effect in the excited states of nitrogen-vacancy centers in diamond," *Phys. Rev. Lett.*, vol. 103, p. 256404, Dec 2009.
- [7] T. A. Abtew, Y. Y. Sun, B.-C. Shih, P. Dev, S. B. Zhang, and P. Zhang, "Dynamic jahn-teller effect in the nv^- center in diamond," *Phys. Rev. Lett.*, vol. 107, p. 146403, Sep 2011.
- [8] P. Tamarat, T. Gaebel, J. Rabeau, M. Khan, A. Greentree, H. Wilson, L. Hollenberg, S. Prawer, P. Hemmer, F. Jelezko, and J. Wrachtrup, "Stark Shift Control of Single Optical Centers in Diamond," *Phys. Rev. Lett.*, vol. 97, no. 8, p. 83002, 2006.
- [9] L. C. Bassett, F. J. Heremans, C. G. Yale, B. B. Buckley, and D. D. Awschalom, "Electrical Tuning of Single Nitrogen-Vacancy Center Optical Transitions Enhanced by Photoinduced Fields," *Phys. Rev. Lett.*, vol. 107, p. 266403, Dec. 2011.
- [10] A. Sipahigil, R. E. Evans, D. D. Sukachev, M. J. Burek, J. Borregaard, M. K. Bhaskar, C. T. Nguyen, J. L. Pacheco, H. A. Atikian, C. Meuwly, R. M. Camacho, F. Jelezko, E. Bielejec, H. Park, M. Lončar, and M. D. Lukin, "An integrated diamond nanophotonics platform for quantum-optical networks," *Science*, vol. 354, no. 6314, pp. 847–850, 2016.
- [11] T. Iwasaki, F. Ishibashi, Y. Miyamoto, Y. Doi, S. Kobayashi, T. Miyazaki, K. Tahara, K. D. Jahnke, L. J. Rogers, B. Naydenov, F. Jelezko, S. Yamasaki, S. Nagamachi, T. Inubushi, N. Mizuochi, and M. Hatano, "Germanium-vacancy single color centers in diamond," vol. 5, pp. 12882 EP –, Aug 2015. Article.
- [12] Y.-I. Sohn, S. Meesala, B. Pingault, H. A. Atikian, J. Holzgrafe, M. Gundogan, C. Stavrakas, M. J. Stanley, A. Sipahigil, J. Choi, M. Zhang, J. L. Pacheco, J. Abraham, E. Bielejec, M. D. Lukin, M. Atature, and M. Loncar, "Engineering a diamond spin-qubit with a nano-electro-mechanical system," 2017.

- [13] L. Robledo, L. Childress, H. Bernien, B. Hensen, P. F. A. Alkemade, and R. Hanson, “High-fidelity projective read-out of a solid-state spin quantum register,” *Nature*, vol. 477, pp. 574–578, Sep 2011.
- [14] H. Bernien, B. Hensen, W. Pfaff, G. Koolstra, M. S. Blok, L. Robledo, T. H. Taminiau, M. Markham, D. J. Twitchen, L. Childress, and R. Hanson, “Heralded entanglement between solid-state qubits separated by three metres,” *Nature*, vol. 497, pp. 86–90, Apr. 2013.
- [15] N. Bar-Gill, L. M. Pham, A. Jarmola, D. Budker, and R. L. Walsworth, “Solid-state electronic spin coherence time approaching one second.,” *Nature Commun.*, vol. 4, p. 1743, 2013.
- [16] V. V. Dobrovitski, A. E. Feiguin, R. Hanson, and D. D. Awschalom, “Decay of Rabi oscillations by dipolar-coupled dynamical spin environments.,” *Phys. Rev. Lett.*, vol. 102, p. 237601, June 2009.
- [17] G. Balasubramanian, P. Neumann, D. Twitchen, M. Markham, R. Kolesov, N. Mizuochi, J. Isoya, J. Achard, J. Beck, J. Tissler, V. Jacques, P. R. Hemmer, F. Jelezko, and J. Wrachtrup, “Ultralong spin coherence time in isotopically engineered diamond,” *Nat Mater*, vol. 8, pp. 383–387, May 2009.
- [18] G. de Lange, Z. H. Wang, D. Ristè, V. V. Dobrovitski, and R. Hanson, “Universal dynamical decoupling of a single solid-state spin from a spin bath,” *Science*, vol. 330, no. 6000, pp. 60–63, 2010.
- [19] F. Jelezko, T. Gaebel, I. Popa, A. Gruber, and J. Wrachtrup, “Observation of coherent oscillations in a single electron spin.,” *Phys. Rev. Lett.*, vol. 92, p. 076401, Feb. 2004.
- [20] M. V. G. Dutt, L. Childress, L. Jiang, E. Togan, J. Maze, F. Jelezko, A. S. Zibrov, P. R. Hemmer, and M. D. Lukin, “Quantum register based on individual electronic and nuclear spin qubits in diamond,” *Science*, vol. 316, no. 5829, pp. 1312–1316, 2007.
- [21] P. Neumann, J. Beck, M. Steiner, F. Rempp, H. Fedder, P. R. Hemmer, J. Wrachtrup, and F. Jelezko, “Single-shot readout of a single nuclear spin,” *Science*, vol. 329, no. 5991, pp. 542–544, 2010.
- [22] T. H. Taminiau, J. J. T. Wagenaar, T. van der Sar, F. Jelezko, V. V. Dobrovitski, and R. Hanson, “Detection and control of individual nuclear spins using a weakly coupled electron spin,” *Phys. Rev. Lett.*, vol. 109, p. 137602, Sep 2012.
- [23] A. Reiserer, N. Kalb, M. S. Blok, K. J. M. van Bemmelen, T. H. Taminiau, R. Hanson, D. J. Twitchen, and M. Markham, “Robust quantum-network memory using decoherence-protected subspaces of nuclear spins,” *Phys. Rev. X*, vol. 6, p. 021040, Jun 2016.
- [24] P. C. Maurer, G. Kucsko, C. Latta, L. Jiang, N. Y. Yao, S. D. Bennett, F. Pastawski, D. Hunger, N. Chisholm, M. Markham, D. J. Twitchen, J. I. Cirac, and M. D. Lukin, “Room-Temperature Quantum Bit Memory Exceeding One Second,” *Science*, vol. 336, pp. 1283–1286, June 2012.

- [25] E. Togan, Y. Chu, A. S. Trifonov, L. Jiang, J. Maze, L. Childress, M. V. G. Dutt, A. S. Sørensen, P. R. Hemmer, A. S. Zibrov, and M. D. Lukin, “Quantum entanglement between an optical photon and a solid-state spin qubit,” *Nature*, vol. 466, no. 7307, pp. 730–734, 2010.
- [26] B. Hensen, H. Bernien, A. E. Dreau, A. Reiserer, N. Kalb, M. S. Blok, J. Ruitenberg, R. F. L. Vermeulen, R. N. Schouten, C. Abellan, W. Amaya, V. Pruneri, M. W. Mitchell, M. Markham, D. J. Twitchen, D. Elkouss, S. Wehner, T. H. Taminiau, and R. Hanson, “Loophole-free bell inequality violation using electron spins separated by 1.3 kilometres,” *Nature*, vol. 526, p. 682, Oct 2015.
- [27] D. P. DiVincenzo, “The physical implementation of quantum computation,” 2000.

3

FABRY-PEROT RESONATORS AND EMITTER-CAVITY COUPLING

S. Bogdanović

Coupling emitters to optical cavities is a promising approach for boosting their emission properties. In this chapter, we will provide the theoretical background necessary to describe the mechanism of an emitter-cavity coupling. We begin by introducing the basic properties of a planar Fabry-Perot resonator (Section 3.1) and discuss a more general case of Gaussian beams in spherical-mirror cavities (Section 3.2) following the approach from Saleh[1]. Section 3.3 describes the interaction between the light and an atom inside a cavity with the emphasis on the weak coupling regime and the case of an NV center in a cavity. We finish the chapter by providing an overview of different experimental designs aimed at demonstrating NV center-cavity coupling (Section 3.4).

3.1. ONE-DIMENSIONAL FABRY-PEROT CAVITY

A one-dimensional Fabry-Perot cavity is a linear optical resonator consisting of two parallel mirrors M_1 and M_2 with transmissions T_1 and T_2 and losses L_1 and L_2 , suitable for spatial and temporal confinement of light at frequencies ν determined by the mirror separation (Figure 3.1). The amplitude of a monochromatic wave $U(\mathbf{r})$ inside the lossless cavity with mirror separation L , satisfies the Helmholtz equation:

3

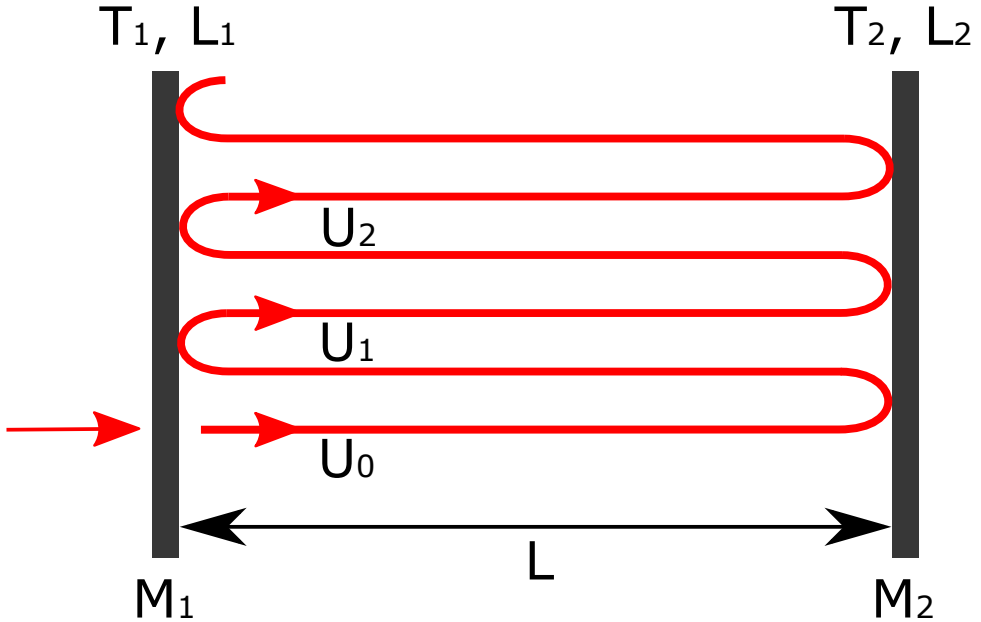


Figure 3.1: Schematics of a wave roundtrip inside a planar cavity consisting of two mirrors with transmissions T_1 and T_2 and losses L_1 and L_2 separated by distance L . The wave amplitude after N roundtrips around the cavity is U_N .

$$\nabla^2 U(\mathbf{r}) + k^2 U(\mathbf{r}) = 0, \quad (3.1)$$

where $k = \frac{2\pi\nu}{c}$ is the wavenumber and c is the speed of light. This cavity geometry imposes boundary conditions requiring that upon reflection the field components parallel to the mirror surface must be zero while the perpendicular component of the incident wave must have equal magnitude and a phase shift of π . This translates to: $U(\mathbf{r}) = 0$ at the planes $z = 0$ and $z = L$ with standing waves as cavity modes satisfying the solution to Equation (3.1):

$$U(\mathbf{r}) = A_q \sin k_q z, \quad k_q = q \frac{\pi}{L}, \quad q = 1, 2, \dots \quad (3.2)$$

Therefore the resonant frequencies take discrete values $\nu_q = q \frac{c}{2L}$ and the separation between two resonant frequencies is called the Free Spectral Range (FSR):

$$\nu_{FSR} = \nu_{q+1} - \nu_q = \frac{c}{2L}. \quad (3.3)$$

This result can also be derived from the condition that resonant modes reproduce themselves after a round-trip. The accumulated phase during propagation has to be an integer of 2π :

$$\phi = k \cdot 2L = q \cdot 2\pi, \quad q = 1, 2, \dots \quad (3.4)$$

obtaining the same expression for resonant frequencies.

To model cavity losses in the resonant mode analysis, we multiply the complex wave amplitude after each cavity round-trip (Figure 3.1.) with the attenuation factor $h = |r|e^{-i\phi}$ where $|r| = \sqrt{(1 - T_1 - L_1)(1 - T_2 - L_2)}$ represents cavity mirrors of finite transmittance and loss. The total wave amplitude is therefore:

$$U = U_0 + U_1 + U_2 + \dots = U_0 + hU_0 + h^2U_0 + \dots = \frac{U_0}{1-h}, \quad (3.5)$$

with the field intensity inside the cavity described as the Lorentzian function (Figure 3.2):

$$I = |U|^2 = \frac{|U_0|^2}{|1 - |r|e^{-i\phi}|^2} = \frac{I_0}{1 + |r|^2 - 2|r|\cos\phi}. \quad (3.6)$$

Defining $I_{max} = \frac{I_0}{(1-|r|)^2}$ for $\phi = 2\pi q$ allows us to express the field intensity as:

$$I = \frac{I_{max}}{1 + (2F/\pi)^2 \sin^2(\phi/2)}, \quad (3.7)$$

where we introduce the parameter F as the Finesse of the cavity:

$$F = \frac{\pi\sqrt{|r|}}{1-|r|} \approx \frac{2\pi}{T_1 + T_2 + L_1 + L_2}; \quad 1 - |r| \ll 1. \quad (3.8)$$

For resonant condition near $\phi \approx 0$ we can rewrite (3.7) as:

$$I = \frac{I_{max}}{1 + (F\phi/\pi)^2}. \quad (3.9)$$

The intensity of field is at the half of its maximum value for $\phi = \frac{\pi}{F}$ so the Full Width at Half Maximum (FWHM) of the intensity peak becomes:

$$\Delta\phi \approx \frac{2\pi}{F}. \quad (3.10)$$

Defined like this, the cavity finesse represents the sensitivity of the field intensity inside the cavity to deviations from the resonant frequency. It is a measure of spectral resolving capability of the Fabry-Perot cavity. Expressing this value in frequency, using (3.4) gives us:

$$\Delta\nu = \frac{c}{2LF} = \frac{\nu_{FSR}}{F}. \quad (3.11)$$

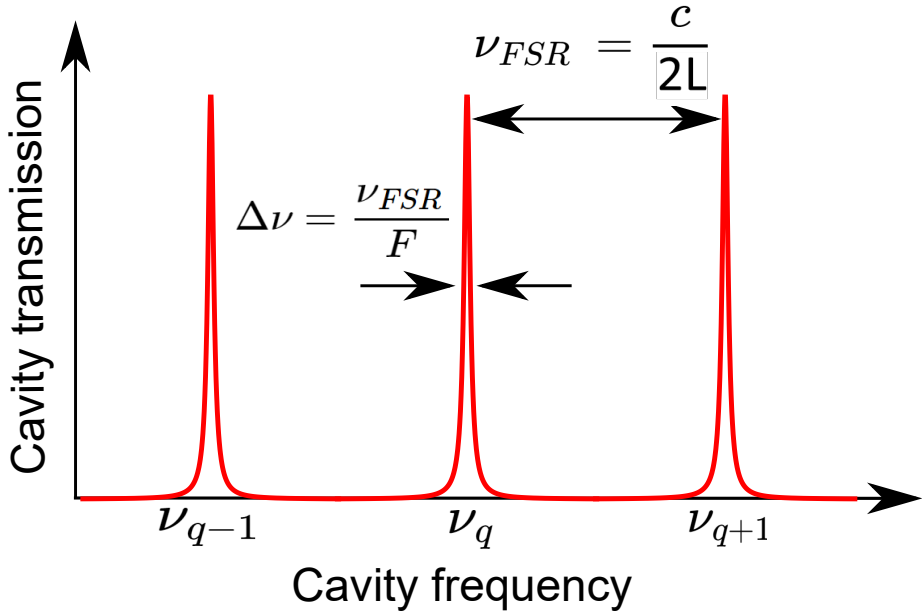


Figure 3.2: Transmission of a planar cavity of length L and Finesse F , with cavity resonances at frequencies $\nu_q = q \frac{c}{2L}$ separated by ν_{FSR} displaying a Lorentzian profile with linewidth $\Delta\nu$.

We notice that for large Finesse values, the intensity spectrum is sharply peaked around the cavity resonance frequencies ν_{q+N} for $N = 1, 2, \dots$ (Figure 3.2).

Viewing Finesse as a number of bounces the photon makes before leaking out of the cavity, the lifetime of a photon inside the cavity τ_{cav} is given by the relation:

$$\tau_{cav} = \frac{F L}{\pi c} = \frac{1}{2\pi\Delta\nu}, \quad (3.12)$$

and we define the cavity decay rate κ as:

$$\kappa = \frac{1}{\tau_{cav}} = 2\pi\Delta\nu, \quad (3.13)$$

establishing the relation between the resonant mode linewidth and the cavity loss rate.

We conclude the discussion on the cavity parameters by introducing the Quality Factor which is defined as:

$$Q = 2\pi \frac{\text{Stored energy}}{\text{Energy loss per cycle}}. \quad (3.14)$$

It relates the cavity linewidth to its frequency and represents the field storage time of

the resonator in units of the optical period $T = 1/\nu_0$:

$$Q = \frac{\nu_0}{\Delta\nu}. \quad (3.15)$$

3.2. GAUSSIAN BEAMS IN SPHERICAL-MIRROR RESONATORS

A 1D planar resonator is a special case of a more general type of 3D cavities in which one or both mirrors are spherical with radii of curvature R_1 and R_2 ($R_1 = R_2 = \infty$ in the planar mirror case). The advantage of this configuration is greater robustness to mirror misalignment which increases the capability of containing the field inside the cavity, translating to higher finesse values. In our experiments, we will utilize an asymmetric cavity which consists of one planar and one curved mirror with the radius of curvature R . The choice of an asymmetric cavity is made with respect to easier incorporation of the diamond sample into the cavity with one planar mirror, which will be discussed in the following chapter.

The stability condition for such a cavity is:

$$0 \leq \left(1 - \frac{L}{R}\right) \leq 1, \quad (3.16)$$

placing a requirement on the cavity length: $L \leq R$. For cavity lengths beyond this limit, the beam waist grows larger than the cavity mirror size, and the field is eventually lost. This will influence the fabrication process of the curved mirror, presented in the following chapters.

Solutions of the Helmholtz equation (Equation (3.1)) for the boundary conditions imposed by this mirror geometry are Gaussian beams shown in Figure 3.3:

$$U(\mathbf{r}) = A_0 \frac{W_0}{W(z)} \exp\left(-\frac{\rho^2}{W^2(z)}\right) \exp\left(-ikz - ik\frac{\rho^2}{2R(z)} + i\zeta(z)\right), \quad (3.17)$$

where we assume the beam is traveling along the z direction and $\rho = x^2 + y^2$. The parameter $\zeta(z)$ represents the phase retardation relative to a planar wave, the Gouy phase shift. $W(z)$ is the width of the Gaussian beam i.e. the distance from the beam axis where the intensity drops by a factor of $1/e^2$. Parameter z_0 called the Rayleigh range, indicates the position on the cavity axis where the radius of curvature of the Gaussian beam $R(z)$ is minimal and the distance over which the beam is approximately collimated ($W = \sqrt{2}W_0$ with W_0 being the minimum value of the beam width)[2]. The relations between these parameters are described by the following set of equations:

$$z_0 = \frac{\pi W_0^2}{\lambda}; \quad W(z) = W_0 \sqrt{1 + \left(\frac{z}{z_0}\right)^2}; \quad R(z) = z \left(1 + \left(\frac{z_0}{z}\right)^2\right). \quad (3.18)$$

We set the origin of the Gaussian wave ($z = 0$) at the location where it behaves like a planar wave ($R = \infty$) and notice that the beam at this position has minimal width. For an asymmetric cavity employing a planar mirror at $z = 0$ and a mirror with curvature R placed at $z = L$ we find:

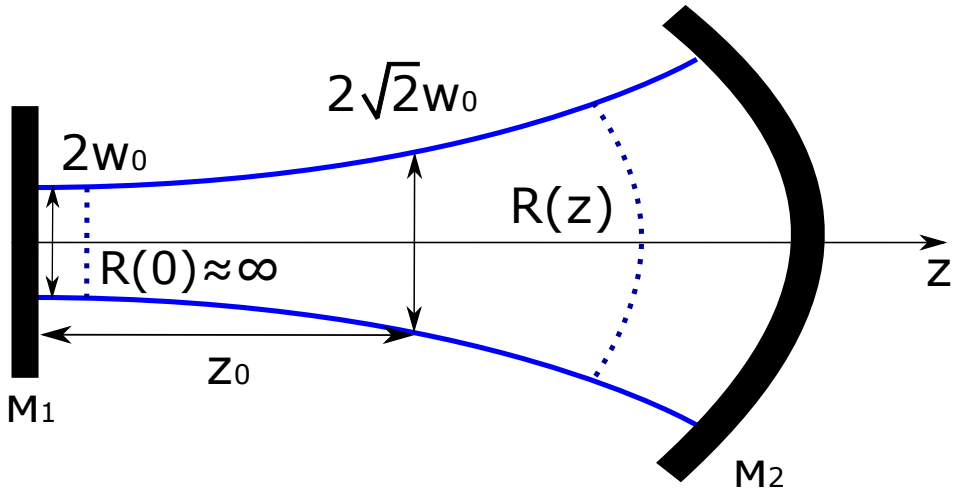


Figure 3.3: Gaussian beam in a cavity consisting of a planar mirror M_1 and curved mirror M_2 propagating along the z -axis. Smallest width of this Gaussian beam is W_0 , its Rayleigh range is z_0 and its radius of curvature is $R(z)$.

$$z_0 = \sqrt{L(R-L)}; \quad W_0^2 = \frac{\lambda}{\pi} \sqrt{L(R-L)}, \quad (3.19)$$

and calculate the cavity mode volume as[3]:

$$V_m = \left(\frac{W_0}{2}\right)^2 \pi L = \frac{\lambda}{4} \sqrt{L^3(R-L)}. \quad (3.20)$$

Mode volume along with the quality factor (Equation 3.15) will be the dominant parameter describing the nature of the emitter-cavity coupling, which we discuss in the following section.

3.3. EMITTERS IN CAVITIES

The goal of this section is to introduce the relevant parameters governing the interplay between a cavity and an emitter placed within its volume following the approach in Fox[4].

The character of a cavity-emitter interaction is defined by the three parameters: cavity decay rate - κ , emitter decay rate - γ and an emitter-cavity coupling rate - g_0 (Figure 3.4).

Cavity field decay rate κ has already been discussed in the section 3.1, Equation (3.13).

The emitter decay rate determines its Fourier-limited linewidth, in the absence of other broadening mechanisms:

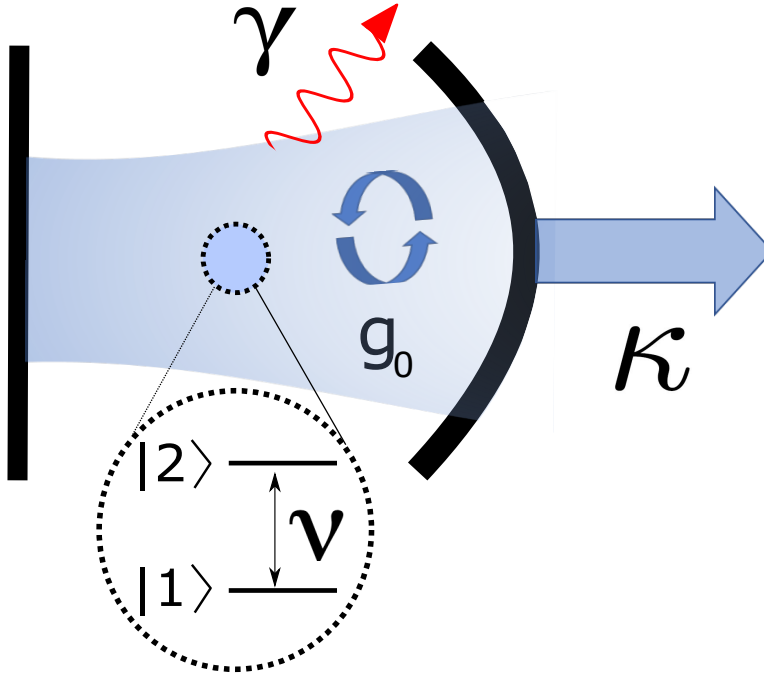


Figure 3.4: A two-level emitter with the transition frequency ν is coupled to an optical cavity at rate g_0 . This coherent process competes with the cavity decay rate κ and non-resonant emitter decay rate γ .

$$\gamma_{NV} = \frac{\mu_{NV}^2 \omega^3}{3\pi\epsilon_0 \hbar c^3}, \quad (3.21)$$

where μ_{NV} represents the total dipole moment of the NV center and ω is the transition frequency. The branching ratio or the Debye-Waller factor ζ is then given by:

$$\zeta = \frac{\gamma_{ZPL}}{\gamma_{NV}} = \frac{\mu_{ZPL}^2}{\mu_{NV}^2} \approx 3\% \quad (3.22)$$

where γ_{ZPL} and μ_{ZPL} are the decay rate and the dipole moment of the ZPL transition, respectively.

Lets consider the case of the NV center coupling to a cavity resonant with its ZPL transition. The NV-cavity coupling constant g_0 is determined by the ZPL transition dipole moment μ_{ZPL} interacting with the vacuum fluctuations of the electromagnetic field within the cavity volume V :

$$g_0 = \sqrt{\frac{\mu_{ZPL}^2 \omega}{2\hbar\epsilon_0 V}}. \quad (3.23)$$

The relation between these three parameters defines the regime of the cavity-emitter coupling. In the strong coupling regime $g_0 \gg (\kappa, \gamma)$ the exchange of the energy quanta

between the cavity and the emitter is faster than the photon loss meaning that the photon has a higher chance of being reabsorbed by the emitter in a coherent process instead of leaking out of the cavity. The weak coupling regime, the one relevant to this thesis, covers the non-coherent case: $g_0 \ll (\kappa, \gamma)$ where the photon emission is irreversible. However, in this regime, the existence of the cavity surrounding the emitter can still have a significant effect on the emission properties which we discuss in the following paragraph.

The transition rate of spontaneous emission is governed by the Fermi's Golden Rule:

$$W = \frac{2\pi}{\hbar^2} |M_{12}|^2 g(\omega), \quad (3.24)$$

where M_{12} is the matrix element of the transition and $g(\omega)$ photon density of states.

For determining the matrix element we use the electric dipole interaction:

$$M_{12} = \mu_{12} \epsilon_{vac} = \sqrt{\frac{\mu_{12}^2 \hbar \omega}{2\epsilon_0 V_0}}. \quad (3.25)$$

The photon density of states for the emitter in free space is given by:

$$g_f(\omega) = \frac{\omega^2}{\pi^2 c^3} V_0. \quad (3.26)$$

We calculate the transition rate for the free space emitter and multiply the result with factor $\frac{1}{3}$ which represents averaging over all possible dipole orientations:

$$W_{free} = \frac{\mu_{12}^2 \omega^3}{3\pi\epsilon_0 \hbar c^3}, \quad (3.27)$$

equivalent with Equation (3.21).

Now lets consider the effect of embedding the emitter in the optical cavity, such as the one described in Section 3.2. Using the form of its Lorentzian lineshape from Figure 3.2 (Equation (3.7)) the density of states function for the emitter in the cavity with linewidth $\Delta\omega$ and frequency ω_c is:

$$g_c(\omega) = \frac{2}{\pi} \frac{\Delta\omega_c}{4(\omega - \omega_c)^2 + \Delta\omega_c^2}, \quad (3.28)$$

The resonant condition between the atom and the cavity is satisfied for $\omega = \omega_c$ which leads to:

$$g_c(\omega) = \frac{2}{\pi\Delta\omega} = \frac{2Q}{\pi\omega}. \quad (3.29)$$

This represents the crucial difference in comparison to the emitter in free space (Equation (3.26)). Cavity modifies the photonic density of states thus having a significant effect on the transition probabilities in Fermi's golden rule (Equation (3.24)). Transition element M_{12} is an intrinsic property of the emitter and thus remains unchanged so the W_{cav} is:

$$W_{cav} = \frac{2Q\mu_{12}^2}{\hbar\epsilon_0 V_0} \xi^2, \quad (3.30)$$

where ξ is the normalized dipole orientation taking into account the spatial overlap between the emitter and the cavity field anti-node.

Comparing the transition rate between the emitter in the cavity and in free space, we define the Purcell factor F_P as:

$$F_P = \frac{W_{cav}}{W_{free}} = \frac{3Q\lambda^3}{4\pi^2 V_0}, \quad (3.31)$$

for the cavity on resonance and the emitter dipole located in the field maximum and oriented along the cavity field.

A Purcell factor larger than unity indicates enhancement of the emission rate due to the modified density of states of the emitter inside the cavity compared to the free-space case. We notice that it is governed by two parameters directly connected to the cavity properties; for maximum Purcell enhancement, we would require cavities with high quality factors and low mode volumes. The Purcell factor can also be expressed through the ratio between the coupling strength of the emitter to the cavity and their decay rates as defined above, also called the cooperativity:

$$C = \zeta F_P = \frac{4g_0^2}{\kappa\gamma_{NV}}. \quad (3.32)$$

One way to experimentally determine the Purcell factor is through the measurement of the emitter lifetime reduction. Compared to the lifetime of the NV center in freespace, $\frac{1}{\tau} = \frac{1}{\tau_{ZPL}} + \frac{1}{\tau_{PSB}}$, the lifetime of the excited state of an NV center coupled to the cavity decreases to $\frac{1}{\tau_{cav}} = \frac{1+F_P}{\tau_{ZPL}} + \frac{1}{\tau_{PSB}}$. From this point it is straightforward to calculate the Purcell factor as:

$$F_P = \frac{\tau/\tau_{cav} - 1}{\zeta}. \quad (3.33)$$

Finally, the ratio of the ZPL emission into the cavity mode compared to the total emission is given by:

$$\beta = \frac{F_P\gamma_{ZPL}}{F_P\gamma_{ZPL} + \gamma_{NV}}. \quad (3.34)$$

In the discussion so far, we have assumed that the emitter linewidth is much smaller than the cavity decay rate i.e. $\gamma \ll \kappa$, which is often the case for atomic transitions in cavity experiments using cold atoms or trapped ions. However, in case of the emitters embedded in the solid state matrix such as an NV center in diamond, broadening of the emitter linewidth, due to mechanisms such as coupling to phonons or spectral diffusion introduced in Chapter 2, can greatly reduce the Purcell factor. This can be described through an effective quality factor Q_{eff} given by following equation:

$$\frac{1}{Q_{eff}} = \frac{1}{Q_{cav}} + \frac{1}{Q_{emitter}} ; Q_{emitter} = \frac{\nu}{\gamma}, \quad (3.35)$$

illustrating that Q_{eff} can also be limited by the broad emitter linewidths. This highlights the importance of narrow NV center linewidths in our experiments, placing a strict requirement on the cavity and diamond sample design and the need for performing measurements in cryogenic conditions where the phononic contributions do not broaden the spectral line[5]. On the other hand, while low temperatures reduce the pure dephasing broadening mechanism of all NV spectral lines, they have no influence on the vibrational ground state relaxation rates of the PSB (on the order of ≈ 80 THz) indicating that, at low temperatures, the PSB rate of emission into the cavity remains unaltered[6] apart from the cavity feeding mechanism[7].

The following paragraph presents a short overview of experimentally designed cavities with embedded NV centers and discusses their performance.

3.4. AN OVERVIEW OF NITROGEN-VACANCY CENTERS IN CAVITIES SO FAR

In the previous section we introduced the theoretical principles governing the enhanced emission properties of an emitter coupled to the cavity. Here we present an overview of the experiments demonstrating coupling between NV centers and optical cavities with different cavity designs.

Three main design approaches have so far been established for demonstrating Purcell enhancement of the NV centers. An "integrated" design relies on fabricating a periodic series of holes etched into a single crystal diamond substrates creating regions with alternating refractive index, forming a photonic crystal cavity (PhC)[8–12]. These structures are either fabricated around already existing NV centers within the diamond substrate or the NV centers have been subsequently implanted into the optimal position with respect to the cavity field maximum. This design greatly benefits from strong field confinement with cavity mode volumes reaching $\approx (\frac{\lambda}{n})^3$. An example of 1D and 2D PhC is presented in Figure 3.5. Spectral cavity tuning is performed either reversibly by introducing gas (usually Xe) into the cavity changing its refractive index and red-shifting the wavelength of its modes or irreversibly by etching the cavity material.

However achieving precise emitter placement within the cavity center is extremely challenging which can be tackled by adopting a hybrid approach. This approach relies on fabricating similar structures out of non-diamond material (Gallium Phosphide for example) followed by positioning nanodiamonds containing NV centers into the cavity center to which they couple via an evanescent field[14–16]. Still, two main challenges to both approaches remain. First, the quality factor of these cavities is significantly reduced ($Q \approx 5000$) due to the imperfections of the etching process, creating a rough cavity side-walls and non-uniform hole structures. An even greater limitation of this architecture lies in the optical properties of the embedded NV centers. Shallow NV centers, as well as ones found in nanodiamonds, are positioned tens of nanometers away from the di-

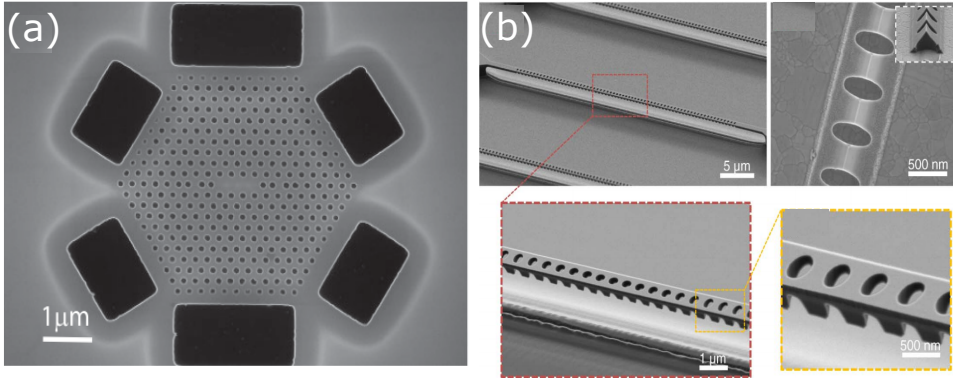


Figure 3.5: An integrated cavity design. (a) An SEM image of a 2D photonic crystal cavity created in diamond[8]. (b) An SEM of a 1D nanobeam photonic crystal cavity[13].

among surface and suffer from surface proximity effects which broaden their linewidth by several orders of magnitude compared to their bulk diamond counterpart.

An alternative approach is embedding NV centers in an open, tunable Fabry-Perot microcavity which enables *in-situ* spatial and spectral cavity tuning to the emitter. Compared to the PhC design, these cavities can possess significantly higher quality factors but also larger mode volumes. This tunable cavity design, where one mirror can be spatially moved, relaxes the constraint for perfect emitter placement in the heart of the cavity which opens up new possibilities in the diamond substrate selection. However, additional spatial degrees of freedom also correspond to vulnerability to mechanical vibrations, which will be further explored in Chapter 6.

So far, several experiments utilizing this configuration have been performed using nanodiamonds[6, 17–19] (Figure 3.6(a)) which suffer from spectral diffusion effects as discussed above. The main advantage of this design is fully utilized by inserting micrometers thin diamond slabs into the cavity architecture[20–22] in which emitters could retain their bulk-like properties, while enabling strong field confinement (Figure 3.6(b)).

Following chapter will describe the fabrication of the components and an assembly of an open Fabry-Perot microcavity with an integrated diamond membrane.

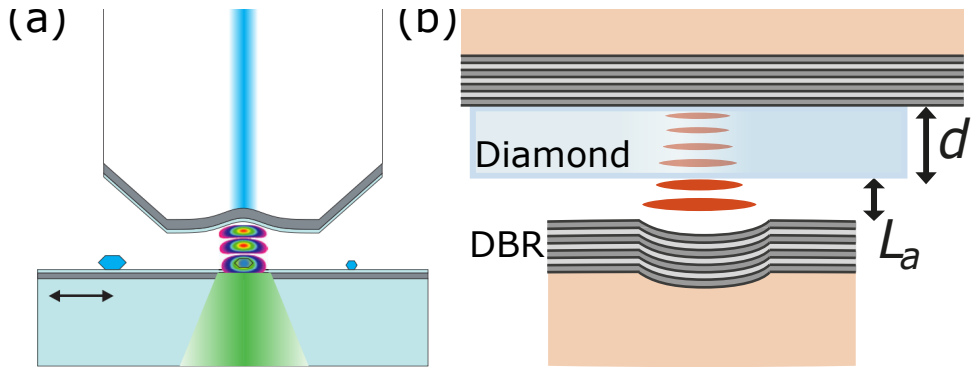


Figure 3.6: Fabry-Perot cavity design. (a) Sketch of the Fabry-Perot microcavity using nanodiamond containing NV centers[19]. (b) Sketch of the fiber-based Fabry-Perot microcavity containing a thin diamond membrane with thickness d and air length L_a [21].

REFERENCES

- [1] B. E. A. Saleh and M. C. Teich, *Fundamentals of Photonics*. New York: Wiley, 1991.
- [2] M. Ruf, "Fiber-based fabry-perot microcavities," 2016.
- [3] D. Hunger, T. Steinmetz, Y. Colombe, C. Deutsch, T. W. Hänsch, and J. Reichel, "A fiber fabry-perot cavity with high finesse," *New J. Phys.*, vol. 12, no. 6, p. 065038, 2010.
- [4] M. Fox, *Quantum Optics*. Oxford University Press., 2006.
- [5] K.-M. C. Fu, C. Santori, P. E. Barclay, L. J. Rogers, N. B. Manson, and R. G. Beausoleil, "Observation of the dynamic jahn-teller effect in the excited states of nitrogen-vacancy centers in diamond," *Phys. Rev. Lett.*, vol. 103, p. 256404, Dec 2009.
- [6] R. Albrecht, A. Bommer, C. Deutsch, J. Reichel, and C. Becher, "Coupling of a single nitrogen-vacancy center in diamond to a fiber-based microcavity," *Phys. Rev. Lett.*, vol. 110, p. 243602, Jun 2013.
- [7] A. Auffèves, D. Gerace, J.-M. Gérard, M. F. m. c. Santos, L. C. Andreani, and J.-P. Poizat, "Controlling the dynamics of a coupled atom-cavity system by pure dephasing," *Phys. Rev. B*, vol. 81, p. 245419, Jun 2010.
- [8] A. Faraon, C. Santori, Z. Huang, V. M. Acosta, and R. G. Beausoleil, "Coupling of nitrogen-vacancy centers to photonic crystal cavities in monocrystalline diamond," *Phys. Rev. Lett.*, vol. 109, p. 033604, Jul 2012.
- [9] B. J. M. Hausmann, B. J. Shields, Q. Quan, Y. Chu, N. P. de Leon, R. Evans, M. J. Burek, A. S. Zibrov, M. Markham, D. J. Twitchen, H. Park, M. D. Lukin, and M. Lončar, "Coupling of nv centers to photonic crystal nanobeams in diamond," *Nano Lett.*, vol. 13, no. 12, p. 5791, 2013.

- [10] J. C. Lee, D. O. Bracher, S. Cui, K. Ohno, C. A. McLellan, X. Zhang, P. Andrich, B. Alemán, K. J. Russell, A. P. Magyar, I. Aharonovich, A. Bleszynski Jayich, D. Awschalom, and E. L. Hu, “Deterministic coupling of delta-doped nitrogen vacancy centers to a nanobeam photonic crystal cavity,” *Appl. Phys. Lett.*, vol. 105, no. 26, p. 261101, 2014.
- [11] L. Li, T. Schröder, E. H. Chen, M. Walsh, I. Bayn, J. Goldstein, O. Gaathon, M. E. Trusheim, M. Lu, J. Mower, M. Cotlet, M. L. Markham, D. J. Twitchen, and D. Englund, “Coherent spin control of a nanocavity-enhanced qubit in diamond,” *Nat. Commun.*, vol. 6, p. 6173, Jan 2015.
- [12] J. Riedrich-Möller, S. Pezzagna, J. Meijer, C. Pauly, F. Mücklich, M. Markham, A. M. Edmonds, and C. Becher, “Nanoimplantation and purcell enhancement of single nitrogen-vacancy centers in photonic crystal cavities in diamond,” *Appl. Phys. Lett.*, vol. 106, no. 22, p. 221103, 2015.
- [13] M. J. Burek, J. D. Cohen, S. M. Meenehan, N. El-Sawah, C. Chia, T. Ruelle, S. Meesala, J. Rochman, H. A. Atikian, M. Markham, D. J. Twitchen, M. D. Lukin, O. Painter, and M. Lončar, “Diamond optomechanical crystals,” *Optica*, vol. 3, pp. 1404–1411, Dec 2016.
- [14] D. Englund, B. Shields, K. Rivoire, F. Hatami, J. Vučković, H. Park, and M. D. Lukin, “Deterministic coupling of a single nitrogen vacancy center to a photonic crystal cavity,” *Nano Lett.*, vol. 10, no. 10, p. 3922, 2010.
- [15] J. Wolters, A. W. Schell, G. Kewes, N. Nüsse, M. Schoengen, H. Döscher, T. Hannappel, B. Löchel, M. Barth, and O. Benson, “Enhancement of the zero phonon line emission from a single nitrogen vacancy center in a nanodiamond via coupling to a photonic crystal cavity,” *Applied Physics Letters*, vol. 97, no. 14, p. 141108, 2010.
- [16] T. van der Sar, J. Hagemeyer, W. Pfaff, E. C. Heeres, S. M. Thon, H. Kim, P. M. Petroff, T. H. Oosterkamp, D. Bouwmeester, and R. Hanson, “Deterministic nanoassembly of a coupled quantum emitter–photonic crystal cavity system,” *Appl. Phys. Lett.*, vol. 98, no. 19, p. 193103, 2011.
- [17] H. Kaupp, C. Deutsch, H.-C. Chang, J. Reichel, T. W. Hänsch, and D. Hunger, “Scaling laws of the cavity enhancement for nitrogen-vacancy centers in diamond,” *Phys. Rev. A*, vol. 88, p. 053812, Nov 2013.
- [18] S. Johnson, P. R. Dolan, T. Grange, A. A. P. Trichet, G. Hornecker, Y. C. Chen, L. Weng, G. M. Hughes, A. A. R. Watt, A. Auffèves, and J. M. Smith, “Tunable cavity coupling of the zero phonon line of a nitrogen-vacancy defect in diamond,” *New J. Phys.*, vol. 17, no. 12, p. 122003, 2015.
- [19] H. Kaupp, T. Hümmer, M. Mader, B. Schleder, J. Benedikter, P. Haeusser, H.-C. Chang, H. Fedder, T. W. Hänsch, and D. Hunger, “Purcell-enhanced single-photon emission from nitrogen-vacancy centers coupled to a tunable microcavity,” *Phys. Rev. Applied*, vol. 6, p. 054010, Nov 2016.

- [20] E. Janitz, M. Ruf, M. Dimock, A. Bourassa, J. Sankey, and L. Childress, “Fabry-perot microcavity for diamond-based photonics,” *Phys. Rev. A*, vol. 92, p. 043844, Oct 2015.
- [21] S. Bogdanović, S. B. van Dam, C. Bonato, L. C. Coenen, A. J. Zwerver, B. Hensen, M. S. Z. Liddy, T. Fink, A. Reiserer, M. Lončar, and R. Hanson, “Design and low-temperature characterization of a tunable microcavity for diamond-based quantum networks,” *Applied Physics Letters*, vol. 110, no. 17, p. 171103, 2017.
- [22] D. Riedel, I. Söllner, B. J. Shields, S. Starosielec, P. Appel, E. Neu, P. Maletinsky, and R. J. Warburton, “Deterministic enhancement of coherent photon generation from a nitrogen-vacancy center in ultrapure diamond,” 2017.

4

EXPERIMENTAL METHODS

S. Bogdanović

The goal of this chapter is to introduce the components which constitute a diamond-based Fabry-Perot microcavity and describe the experimental setup. We utilize a tunable cavity design where one cavity element is mounted onto a piezo positioner for combined lateral scanning of the diamond membrane and spectral cavity tuning.

The chapter begins by describing the preparation of the fiber interface onto which coatings for cavity mirrors are deposited. The properties of these coatings including residual transmission, loss and penetration depth are then discussed, followed by a description of the diamond sample fabrication method and subsequent incorporation into the cavity system. We finish the chapter with the description of the piezo positioner and the cryostation housing the cavity itself.

4.1. FIBER INTERFACE

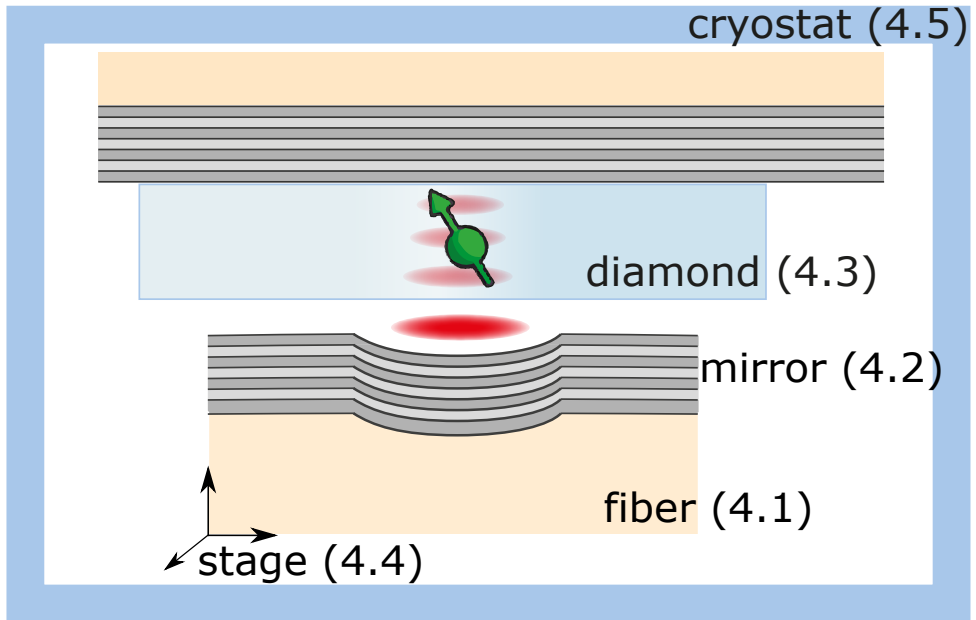


Figure 4.1: Schematic of the cavity consisting of a concave fiber tip and a plane mirror onto which a thin diamond membrane is bonded. The cavity is mounted onto a piezo stage and cooled down to cryogenic temperatures.

The high-finesse microcavity used in this thesis consists of a flat, low roughness, fused silica plates and curved fiber tips coated with high reflectivity mirrors (Figure 4.1). A dimple in the fiber tip is created using CO_2 laser ablation technique[1, 2]. Using a circularly polarized laser pulse focused onto the tip of the fiber, the fiber surface is melted creating a concave depression with the radius of curvature dependent on the power of the laser pulse. Due to the ablation nature of this process, produced depression exhibits a low surface roughness which is imperative for reducing scattering loss in the high finesse optical cavity. Created depressions have a radius of curvature between 10 - 25 μm and surface roughness of ≤ 0.2 nm RMS measured using atomic force microscope.

4.2. MIRROR PROPERTIES

In order to achieve high cavity finesse, optical coatings with low residual transmission are required. Using the Ion-Beam Sputtering (IBS) technique alternating layers of high and low refractive index are deposited onto the fused silica plates and curved fiber interfaces (Laseroptik) forming a Distributed Bragg Reflector (DBR) with each layer having a quarter wave optical thickness. These coatings are created at ultra-high vacuum condi-

tions forbidding the use of regular fibers due to outgassing issues. To prevent this, special fibers (Cu600 IVG) have been utilized whose copper coating serves as a protection against the outgassing in the mirror deposition chamber.

The stopband of the created DBR stack is centered around 637 nm (Figure 4.2), optimized for > 70% transmission at 532 nm.

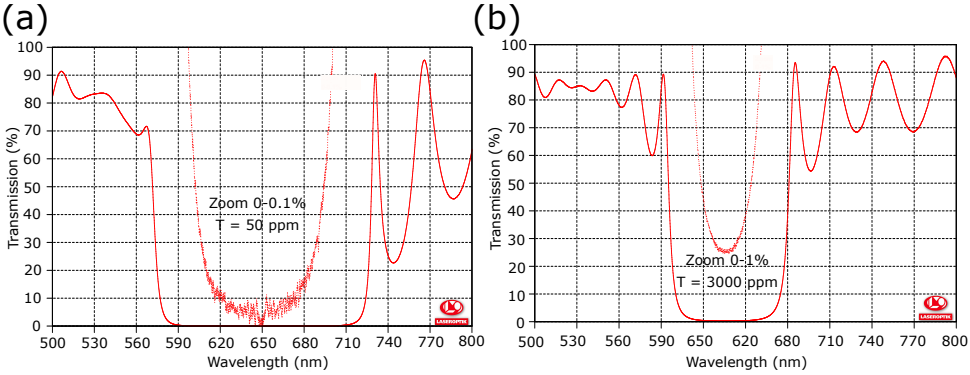


Figure 4.2: Measured stopband for the IBS coatings (Laseroptik) consisting of alternating layers of Ta_2O_5 (refractive index $n_H = 2.04$) and SiO_2 (refractive index $n_L = 1.45$) for (a) low transmission mirror and (b) high transmission mirror with narrow stopband.

Transmission of the DBR stack is dependent on the number of layers applied and is given by Equation (4.1)[3]:

$$T = 4n_0 \frac{n_L^{N-1}}{n_H^{N+1}}, \quad (4.1)$$

where n_0 is the refractive index of the silica substrate, $n_0 \approx 1.45$. Using Equation (4.1) we calculate the expected transmission of the low transmission DBR stack consisting of $N = 31$ layers to be $T \approx 50$ ppm (Figure 4.2(a)). An optional coating design aimed at efficient extraction of NV center PSB photons (up to 750 nm) through the mirror stack relies on creating a narrow stopband by changing the individual layer thickness (Figure 4.2(b)). This can enable locating the NV centers inside the diamond enclosed by these mirrors.

The field loss within the resonator can occur due to two effects: Scattering of the light into the other spatial modes and absorption of light within the resonator. Scattering loss is dependent on the surface roughness of the substrates and applied coatings and can be calculated from the following equation[4]:

$$S \approx \left(\frac{4\pi\sigma}{\lambda}\right)^2, \quad (4.2)$$

where σ is the roughness of the mirror surface. Using the measured surface roughness of the fiber and fused silica interface (≈ 0.3 nm RMS), we expect $S = 15$ ppm per mirror.

The absorption loss is inherent to the coating process itself and can be reduced to $A = 10$ ppm by annealing the mirrors for 5 hours at the temperature of 300° C.

The last effect we take into account is the increase of effective cavity length due to the finite field penetration within the mirror stack, the effective cavity length is modified by $L_{eff} = L_{cav} + 2L_{pen}$ with:

$$L_{pen} = \frac{\lambda}{4(n_H - n_L)}. \quad (4.3)$$

In our case $L_{pen} = 0.27 \mu\text{m}$ per mirror stack[3].

4.3. DIAMOND MEMBRANE

4

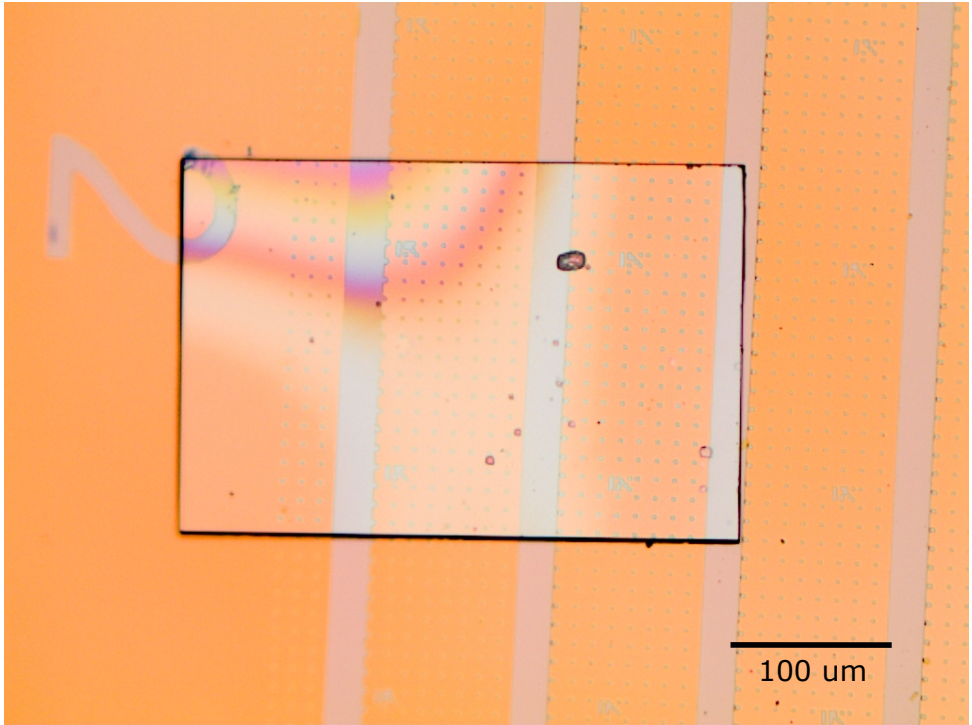


Figure 4.3: Optical microscope image of a $4 \mu\text{m}$ thin diamond membrane bonded to the patterned mirror surface containing microwave striplines and markers.

Choice of the diamond sample is restricted by the requirement of maintaining good optical properties of the emitters while maximizing the values of the Purcell factor. The former condition can be met by using the emitters located far away from the diamond surface embedded inside a diamond membrane where NV centers are expected to exhibit bulk-like properties. However large Purcell factors require small cavity mode volume, which would require thinning down the diamond membrane to only a few micrometers thickness. To create such membranes we start from commercially available 0.5 mm

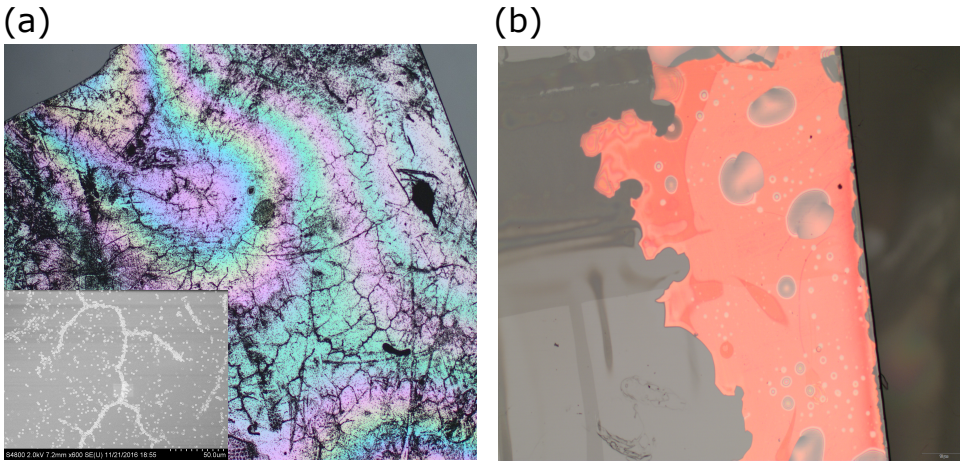


Figure 4.4: Damaged diamond membrane and coatings during the preparation process. (a) Optical microscope image of a damaged diamond surface after 20 minutes of O_2 plasma etching. The inset shows an SEM image of one of the damaged areas. (b) Mirror coatings deposited directly to the diamond membrane delaminated after 1 hour of $ArCl_2$ plasma etching.

thick diamond (Element Six) which is cleaved and polished to membranes of ≈ 30 micrometer thickness (Delaware Diamond Knives). The membranes are then cleaned for 1 hour in the triacid solution (1:1:1 of Perchloric : Sulphuric : 30% Nitric solution) followed by Aceton and IPA clean. The diamond membrane is then etched to the desired thickness of several micrometers using Inductive Coupled Plasma Reactive Ion Etching (ICP RIE) and bonded to the patterned mirror surface using Van der Waals forces (Figure 4.3). A step-by-step fabrication recipe and the procedure details are described in Chapter 5.

As a cautionary tale, two failed methods of diamond membrane preparation are described.

First, the use of oxygen as an etching gas in the ICP RIE process exacerbates surface damages created via diamond membrane polishing, resulting in the creation of pits in the diamond surface (Figure 4.4(a)). In order to bypass this, first few micrometers of diamond need to be removed using Argon-Chlorine recipe, in order to remove the layer damaged from polishing. This type of etch is more chemical which is favorable for diamond surface roughness[5, 6].

Second, an attempt was made to apply low transmission coatings directly on a thick, unetched diamond membrane which would reduce the difficulty in handling and bonding of the thin diamond. However etching the diamond from the uncoated side still caused a drastic coating delamination (Figure 4.4(b)) likely due to the mismatch of the coefficient of thermal expansion between the diamond and the coatings material.

4.4. PIEZO POSITIONER

In order to scan the sample for the emitters within the cavity architecture and tune the cavity on resonance with the emitter spectral line, we mount the fiber mirror onto a piezo positioner. Keeping the tunable cavity stable under cryogenic conditions requires special consideration in the choice of this element.

Low-temperature experiments are performed using a custom designed Cryo Positioning Stage High Resonance (CPSHR) manufactured by Janssen Precision Engineering (JPE) in which three separate linear actuators push the plate on which the fiber is mounted enabling coarse movement of this cavity element while keeping the planar mirror fixed. The advantage of this design lies in its high mechanical resonant frequency which improves the stability of the assembled cavity in the presence of low frequency vibrations of the cryostation floor. The first natural frequency of the unloaded stage is specified to be at 1.5 kHz with the coarse scanning range of 0.5 mm in all directions[7]. Three high resolution piezo elements beneath the fiber mounting plate provide the mechanism for fine cavity tuning with the sensitivity of 5 nm/V at 5 K and scanning range of 0.5 micrometers.

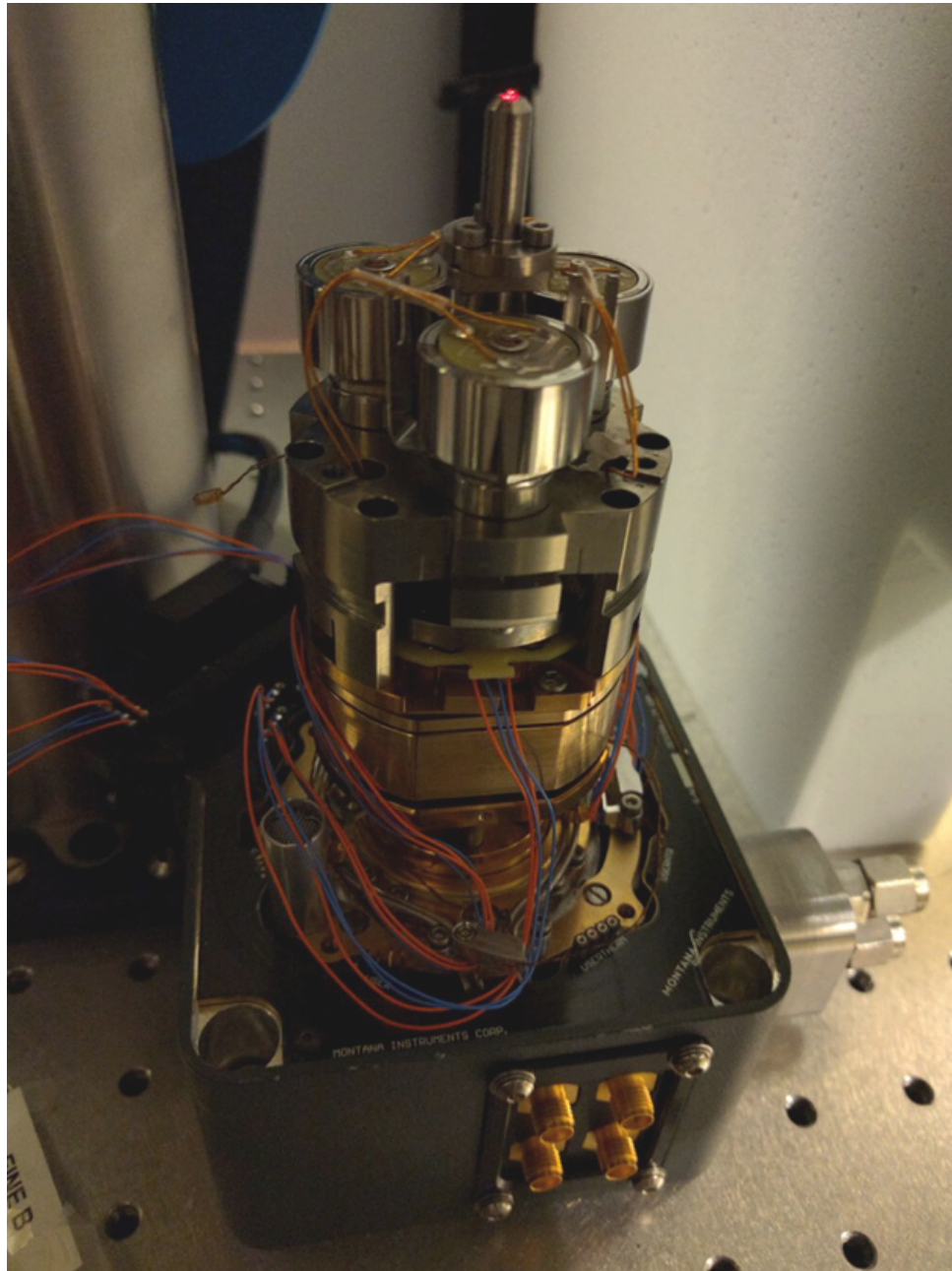
To further decouple the system from the mechanical vibrations of the cryostation base, the whole stage is suspended on a passive vibration isolation platform (CVIP1) with 40 Hz cut-off frequency, acting as a low-pass filter for the mechanical noise reaching the cavity. The whole construction is mounted on a Montana cryostation platform, shown in Figure 4.5.

4.5. CRYOSTATION

The described cavity with the piezo positioner stack is mounted inside a Montana Instruments closed-cycle cryostation. Utilizing an optical fiber as one of the cavity components provides a convenient way to deliver laser light inside the cavity. Fiber is introduced into the cryostat chamber using a Swagelok compression feedthroughs and spliced to another single mode fiber outside of the chamber. Reaching sufficiently low temperature at the diamond membrane location residing on the top of the piezo stage is possible by bypassing the stage using custom designed Montana thermal links. These links are designed to provide a very loose connection to the cryostation floor in order to prevent the propagation of the vibrations to the top of the cavity which would circumvent the vibration isolation elements.

Another strategy to further reduce the vibrations originating from the operation of the cryostation pulse tube is synchronizing our measurements acquisition to Hall probe sensor placed on the operating unit cold head. In Figure 4.6 we present the result of the vibration measurements of the cavity linewidth with respect to the cryostation sync signal. Every point represents the average of 30 linewidth measurements. The details of the linewidth measurements will be presented in Chapter 5. Using the results presented in Figure 4.6 we identify the measurement timings during which the mechanical noise is greatly reduced.

Having introduced the components constituting our cavity and the environment in



4

Figure 4.5: JPE Cryo Positioning Stage High Resonance with a passive vibration isolation add-on, mounted on a base platform of a Montana. Red laser excitation is visible at the tip of the fiber mounted on top of the stage.

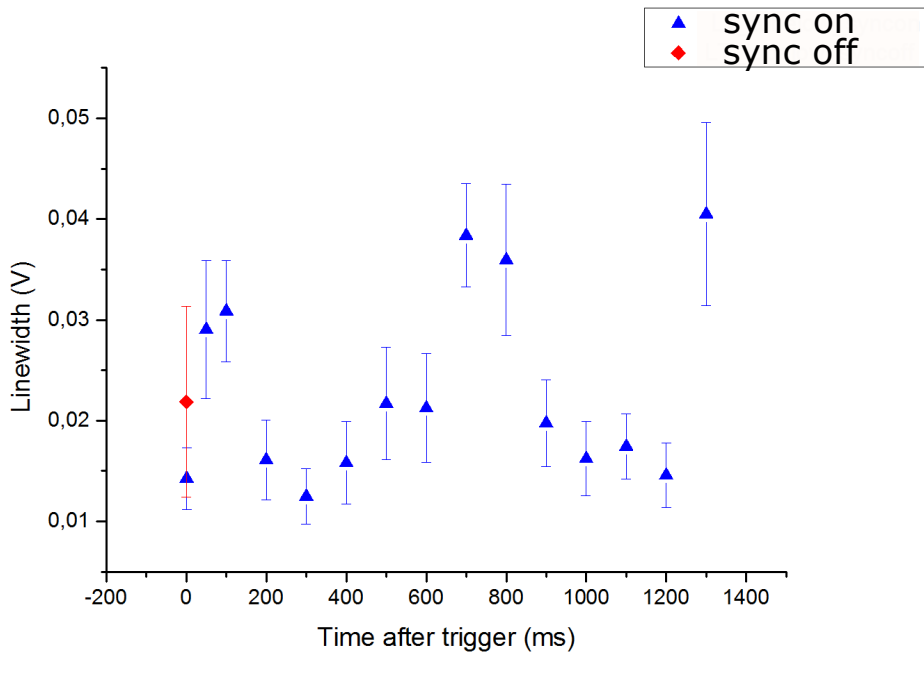


Figure 4.6: Linewidth dependence on measurement time with respect to the synchronization signal.

which the cavity is housed, we proceed with describing the detailed fabrication process of the cavity elements which will be the topic of the next chapter.

REFERENCES

- [1] D. Hunger, T. Steinmetz, Y. Colombe, C. Deutsch, T. W. Hänsch, and J. Reichel, "A fiber fabry-perot cavity with high finesse," *New J. Phys.*, vol. 12, no. 6, p. 065038, 2010.
- [2] D. Hunger, C. Deutsch, R. J. Barbour, R. J. Warburton, and J. Reichel, "Laser micro-fabrication of concave, low-roughness features in silica," *AIP Adv.*, vol. 2, no. 1, p. 012119, 2012.
- [3] C. J. Hood, H. J. Kimble, and J. Ye *Phys. Rev. A*, vol. 64, p. 033804, Aug 2001.
- [4] T. Klaassen, M. P. van Exter, and J. P. Woerdman, "Characterization of scattering in an optical fabry-perot resonator," *Appl. Opt.*, vol. 46, p. 5210, Aug 2007.
- [5] J. Enlund, J. Isberg, M. Karlsson, F. Nikolajeff, J. Olsson, and D. J. Twitchen, "Anisotropic dry etching of boron doped single crystal cvd diamond," *Carbon*, vol. 43, no. 9, p. 1839, 2005.
- [6] C. Lee, E. Gu, M. Dawson, I. Friel, and G. Scarsbrook, "Etching and micro-optics fabrication in diamond using chlorine-based inductively-coupled plasma," *Diamond Relat. Mater.*, vol. 17, no. 7–10, p. 1292, 2008.
- [7] <http://www.janssenprecisionengineering.com/page/cryo-positioning-stage-high-resonance/>.



5

ROBUST NANO-FABRICATION OF AN INTEGRATED PLATFORM FOR SPIN CONTROL IN A TUNABLE MICRO-CAVITY

S. Bogdanović*, M. S. Z. Liddy*, S. B. van Dam, L. C. Coenen, T. Fink,
M. Lončar and R. Hanson

Coupling nitrogen-vacancy centers in diamond to optical cavities is a promising way to enhance the efficiency of diamond based quantum networks. An essential aspect of the full toolbox required for the operation of these networks is the ability to achieve microwave control of the electron spin associated with this defect within the cavity framework. Here, we report on the fabrication of an integrated platform for microwave control of an NV center electron spin in an open, tunable Fabry-Pérot microcavity. A critical aspect of the measurements of the cavity's finesse reveals that the presented fabrication process does not compromise its optical properties. We provide a method to incorporate a thin diamond slab into the cavity architecture and demonstrate control of the NV center spin. These results show the promise of this design for future cavity-enhanced NV center spin-photon entanglement experiments.

This chapter has been accepted for publication in *APL Photonics*.

*These authors contributed equally to this study.

5.1. INTRODUCTION

Nitrogen-vacancy (NV) colour centers in diamond have emerged as attractive candidates for quantum photonic applications. Their electronic spin can be optically initialized, read out in a single shot[1], and coherently manipulated with the use of microwave signals[2]. This spin-photon interface provides a platform for distant entanglement generation [3], while additional coupling to nearby carbon-13 nuclear spins forms a multi-qubit quantum node[4–7]. These aspects make the NV center a good candidate for quantum network protocols[8–10]. The efficiency of entanglement generation between network nodes is currently limited by the NV center's low ($\approx 3\%$) emission rate of the resonant zero-phonon line (ZPL) photons. This problem can be addressed by coupling NV centers to optical microcavities[11–23], enhancing the ZPL emission rate and providing efficient photon extraction by means of the Purcell effect[24]. An appealing cavity design consists of an open, tunable Fabry-Pérot microcavity housing a large area diamond membrane[25–27] in which emitters retain their bulk-like properties[28]. The tunability of this design enables both spectral positioning of the cavity to be resonant with the emitter as well as selective lateral placement of the emitter within the center of the cavity mode. However, in order to use these emitters in quantum information protocols, microwave control must be integrated into the cavity architecture. Here, we present fabrication methods used to create a platform that integrates microwave control of an NV center spin within an optical cavity while maintaining the cavity's high finesse properties. While microwave addressing of a single NV center spin has already been realized in thin diamond slabs[29] and photonic crystal cavities[21], this is the first demonstration of NV center spin addressing within a framework tailored to the implementation of a tunable microcavity.

The cavity consists of a dimpled fiber tip and polished fused silica plate, both coated with a highly reflective dielectric mirror stack (Figure 5.1(A)). Microwave striplines and marker arrays are fabricated on the planar mirror surface in order to locate the NV centers and address their spin within the diamond slab bonded to the mirror.

5.2. FIBER DIMPLE

The curved fiber profile was fabricated using a CO₂ laser ablation technique[30, 31]: A single 1 ms long circularly polarized laser pulse is focused onto the cleaved fiber facet. As a result of thermal evaporation and subsequent melting, a concave depression with low surface roughness of $\sigma_{\text{rms}} \leq 0.20 \pm 0.02$ nm is created. The depth and diameter of this depression can be controlled by varying a combination of the pulse power, duration, and beam waist. Due to the small fiber core diameter, care must be taken to center the depression onto the cleaved facet to ensure a good coupling efficiency to the cavity mode. Following dimple creation, the surface geometry is measured, *in situ*, with an interferometer. Figure 5.1(B) shows an exemplary phase measurement and the corresponding reconstructed surface profile (Figure 5.1(C)). The shape of the depression closely resembles that of a two dimensional Gaussian. In its center, it can be approxi-

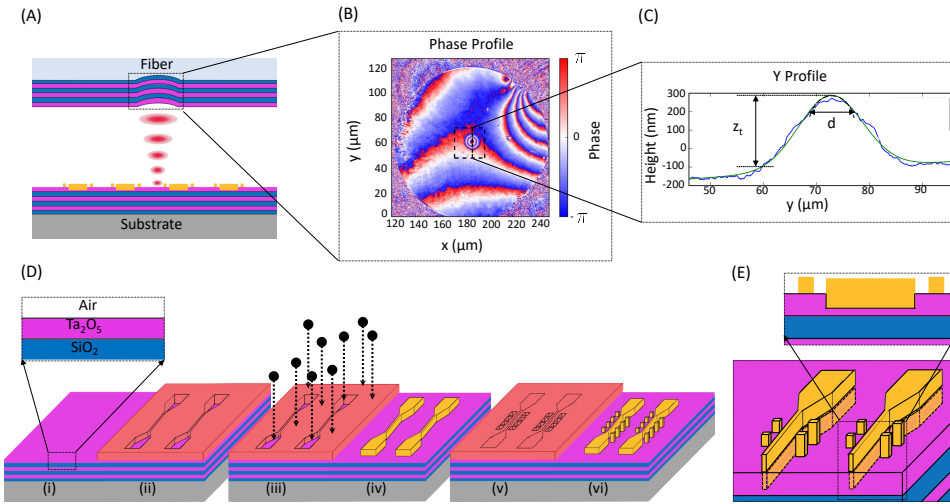


Figure 5.1: (Colour Online) Fabrication of the Fabry-Pérot cavity components. (A) The design of the Fabry-Pérot cavity, comprised of a processed planar mirror and laser ablated fiber interface. (B) Phase profile of the ablated fiber facet measured using an interferometer. (C) Reconstructed surface profile of the region denoted by the black rectangle in (B) (blue line) and fit with a Gaussian function (green line). The extracted parameters are $d = 8.3 \mu\text{m}$ and $z_t = 403 \text{ nm}$. The fiber radius of curvature R , is $22.4 \mu\text{m}$. (D) Planar mirror processing stages: (i) Mirror coatings consist of 31 layers of alternating high (Ta_2O_5 , 75 nm thickness) and low (SiO_2 , 100 nm thickness) refractive index materials deposited onto a low roughness fused silica plate and ablated fiber tip. (ii) Patterned and developed optical photoresist mask for the microwave striplines. (iii) Etching 65 nm of material into the mirror stack using an SF_6 and O_2 ICP RIE recipe followed by (iv) evaporation of 5 nm (65 nm) of titanium (gold) and an overnight liftoff. (v) Patterned and developed optical resist mask for marker array, aligned to the gold striplines. (vi) Evaporation of 5 nm (5 nm) titanium (gold) followed by one hour of liftoff. (E) Cross-section of the mirror post processing revealing the embedded microwave striplines and surface marker array.

mated by a hemisphere with radius of curvature, $R \approx d^2 / (8z_t)$, where d and z_t are the diameter and depth of the dimple, respectively[30]. Low-ellipticity profiles with comparable radii of curvature along the x - and y -direction are required in order to minimize polarization splitting of the cavity mode[32]. The extracted ellipticity of the fiber used in this experiment is 1.3 %.

5.3. MIRROR COATINGS

Following laser ablation of the fibers, a mirror stack forming a Distributed Bragg Reflector (DBR) is deposited onto both the fiber facets and polished fused silica plates (Laseroptik). The residual transmission of this stack is measured to be 50 ppm at 637 nm wavelength. The observed fiber and specified fused silica surface roughness (0.2 nm and 0.5 nm RMS, respectively) correspond to scattering losses of 25 and 100 ppm [33]. Following coating, the planar mirror is annealed in vacuum at 300°C for 5 hours, which reduces the absorption losses of the stack from ≈ 50 ppm to ≤ 10 ppm[34]. The total losses give an expected value of the cavity finesse of $F \approx 22\,000$.

5

5.4. STRIPLINES AND MARKER FIELD

In order to address the spin and index the location of the NV centers, parallel microwave striplines and a field of uniquely identifiable markers are fabricated on the planar mirror surface. For successful diamond bonding, the processed mirrors must possess a low profile for all patterned surface features. A two-step fabrication procedure was devised, which includes first patterning embedded microwave striplines into the planar mirror, followed by the deposition of a small marker array on the surface. The fabrication procedure is presented in Figure 5.1(D). To begin the processing, optical photoresist, AZ 3007, is deposited on the planar mirror at a thickness of 1 μm , followed by a soft bake at 90°C for 60 s. 4 mm long by 45 μm wide masks for the striplines are patterned with a laser writer (DMO Microwriter ML-2), and developed in MF-321 for 45 s (Figure 5.1(D,i-ii)). Using an SF_6 and O_2 based Inductively Coupled Plasma Reactive Ion Etch (ICP RIE) to remove 65 nm of material, the mask for the microwave striplines is transferred into the planar mirror (Figure 5.1(D,iii)) (Methods). After etching, a 5 nm layer of titanium is evaporated as an adhesion layer followed by 65 nm of gold (Temescal FC2000). The first stage of the fabrication is completed by removing all excess gold with an overnight liftoff in photoresist stripper (PRS) at 70°C, leading to the result shown in (Figure 5.1(D,iv)). The second stage of the fabrication procedure proceeds with the same photoresist deposition method, followed by patterning the marker array, aligned adjacent to the microwave striplines, and then developed (Figure 5.1(D,v)). 5 nm layers of Ti and Au are evaporated consecutively, followed by 1 hour of liftoff in PRS at 70°C to complete the fabrication (Figure 5.1(D,vi)).

Essential to the desired cavity architecture is the possibility to bond a several micrometer thin diamond membrane over the structures on the planar mirror. Irregular structures and frills on the edges of the fabricated striplines have been found to deter successful bonding. Furthermore, a microwave stripline that is fully recessed in the

etched trench acts as a capillary channel for water used during the bonding process, preventing a good diamond-mirror bond. A uniform raised profile of a feature above the mirror surface by no more than 20 nm was found to allow for successful bonding.ng.

5.5. CAVITY FINESSE

To verify that the presented fabrication procedure does not introduce additional losses to the planar mirror, the finesse of a cavity with a processed and unprocessed planar mirror is compared while keeping the fiber mirror unaltered. The finesse F is calculated from the cavity linewidth $\delta\nu$ and free spectral range (FSR) ν_{FSR} :

$$F = \frac{\nu_{FSR}}{\delta\nu} = \frac{c}{2 \cdot L_{cav} \cdot \delta\nu}, \quad (5.1)$$

where c is the speed of light and L_{cav} the cavity length.

The cavity linewidth is obtained by exciting the cavity with a 637 nm laser through the fiber port while modulating the planar mirror position with a 40 Hz sinusoidal signal scanning the cavity across the resonance. The measurement setup is presented in Figure 5.2(A). Before entering the cavity, the light passes through an electro-optic modulator (EOM) creating sidebands with a fixed frequency separation, used to convert the measured linewidth in length to frequency. The imperfect elliptical curvature in the fiber profile induces a polarization splitting of the cavity mode which is filtered using a polarizer in the detection path before the transmitted signal reaches the photodiode. An example of a measured linewidth for a cavity consisting of an unprocessed (processed) planar mirror is presented in Figure 5.2(B) (Figure 5.2(C)) for two different cavity lengths. The measured linewidth is an average over ten such single sweeps. It is to be noted that all cavity measurements were performed in the absence of a diamond slab, to compare only the processing effects on the mirror properties. For a study of the effects of a diamond slab incorporated into the cavity, see references [25,26].

The FSR is obtained by coupling a broadband supercontinuum laser into the cavity and measuring the transmitted signal on a spectrometer. Figure 5.2(D) (Figure 5.2(E)) shows the results of the FSR measurement for a cavity with an unprocessed (processed) planar mirror. Fundamental cavity modes can be seen as well as higher order modes at higher frequencies, which are confirmed by their shape in a camera image (not shown). Using the measured linewidth and FSR, the finesse value of the unprocessed mirror cavity is calculated (Equation (5.1)) to be $F = (23 \pm 3) \cdot 10^3$, while the finesse of the processed mirror is $F = (20 \pm 2) \cdot 10^3$. Measured finesse values are in good agreement with the finesse values calculated from the mirror transmission and losses. We conclude that our fabrication procedure preserves good optical properties of the mirrors.

5.6. DIAMOND MEMBRANE PREPARATION AND BONDING

For integration into the cavity system the large-area diamond membranes must be bonded to the processed planar mirrors. Diamond membranes are obtained by slicing and mechanically polishing 2 mm × 2 mm × 0.5 mm <100> bulk diamonds (Element Six), into 30

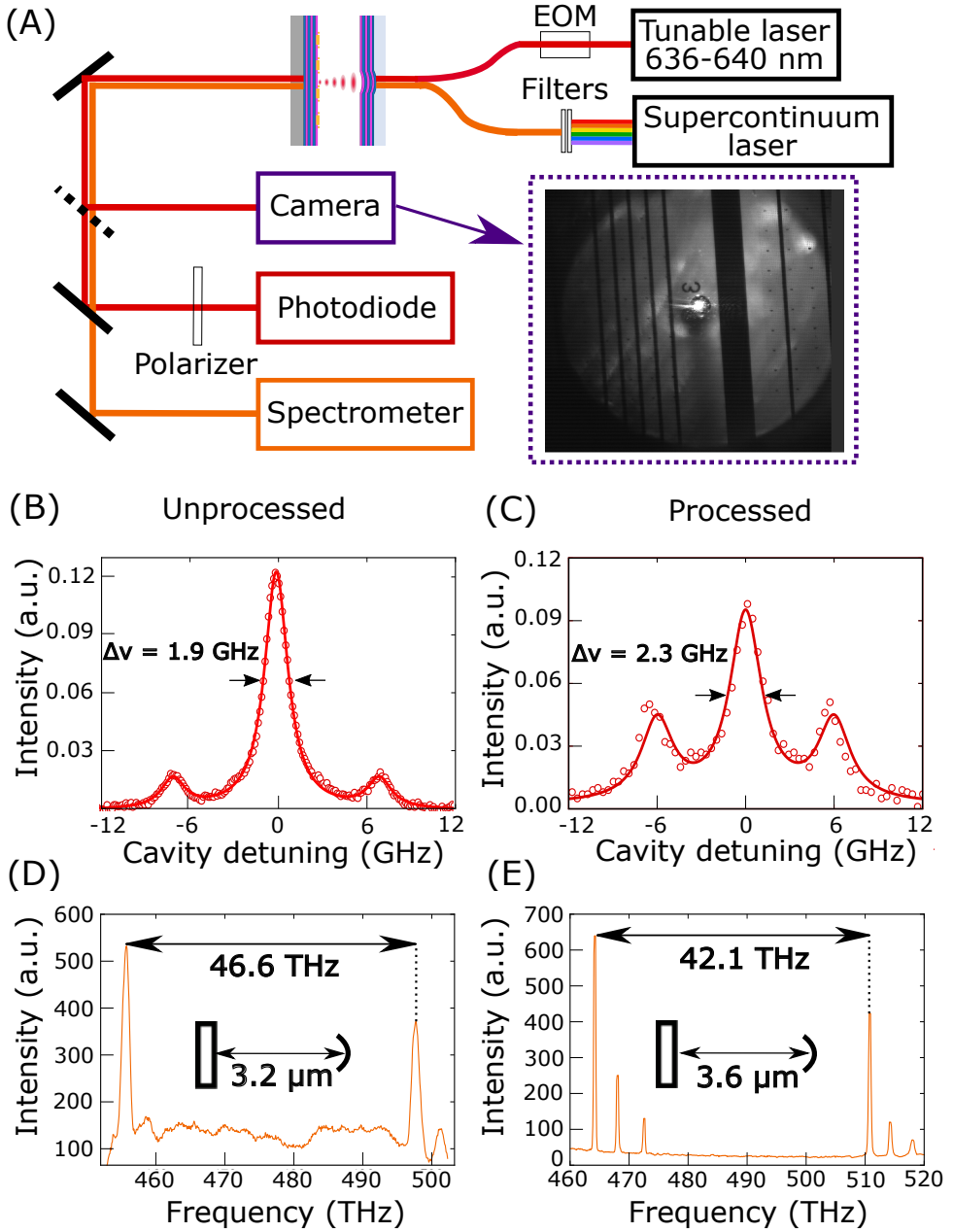


Figure 5.2: (Colour online) Measurement of the cavity finesse. (A) Schematic of the cavity finesse measurement setup. The cavity consists of the mirror coated ablated fiber tip glued to a custom designed fiber mount and screwed into a Newport (462-XYZ-M) stage for coarse positioning, and a planar mirror glued onto a piezo stage (PI E509.X1) for fine spectral cavity tuning. The inset shows a camera image of the patterned planar mirror and fiber microcavity on resonance. (B) Linewidth measurements of the unprocessed and (C) processed cavity are performed by exciting the cavity with a 637 nm laser (Newfocus TLB-6304) while modulating the cavity length. An EOM (Jenoptik) induces sidebands in the laser profile with 6 GHz separation that enable measuring the linewidth in frequency units. The transmitted light is collected on a photodiode (Thorlabs APD130A2) and read out on an oscilloscope. (D) Unprocessed and (E) processed cavity transmission spectra measured by coupling a supercontinuum broadband laser (Fianium SC400) into the cavity and measuring transmitted light on the spectrometer (Princeton Instruments Acton SP2500). The distance between the fundamental modes determines the cavity length (Equation (5.1)).

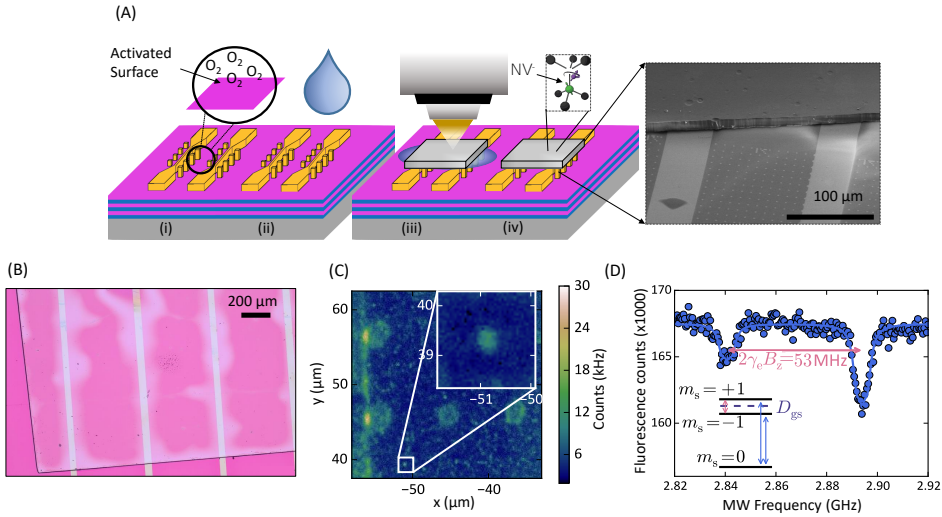


Figure 5.3: (Colour Online) Diamond membrane bonding and NV center spin control. (A) Diamond bonding to the patterned mirror: (i) Surface activation of the processed mirror chip with an oxygen plasma at low vacuum. (ii) Water is pipetted onto the activated surface. (iii) The diamond membrane is placed onto the patterned surface followed by drying of the water using the light from the microscope objective. (iv) The diamond membrane containing NV centers is bonded to the mirror. Inset: A scanning electron microscope (SEM) image of a bonded diamond membrane atop a patterned planar mirror. (B) Optical image of an etched $2\text{ mm} \times 2\text{ mm} \times 8\text{ }\mu\text{m}$ diamond, bonded to the processed planar mirror with microwave striplines and marker array. (C) Scanning optical confocal image showing a single NV center (inset). The scans were performed at the depth of $\approx 1.5\text{ }\mu\text{m}$ below the surface of the diamond membrane. The $2\text{ }\mu\text{m} \times 2\text{ }\mu\text{m}$ spots correspond to the photoluminescence from the square gold markers. Part of the microwave stripline is visible on the left. (D) Optically detected electron spin resonance spectrum demonstrating NV spin addressing with the embedded microwave striplines. The spectrum exhibits two resonances associated with the $m_s = 0 \rightarrow m_s = \pm 1$ spin transitions (inset), centered at the zero field splitting $D_{gs} = 2.87\text{ GHz}$. Two resonances are separated by the Zeeman splitting $2\gamma_e B_z$ where γ_e is the NV electron spin gyromagnetic ratio and B_z is the static external magnetic field. Individual electron spin resonance dips are fitted using three Lorentzian profiles with a splitting of 2.16 MHz to account for the hyperfine splitting from the NV interaction with its host ^{14}N nuclear spin ($I_N = 1$) [35].

μm thick slabs (Delaware Diamond Knives). Leftover residue and surface damage from the mechanical polishing is removed by submerging the diamond in a boiling mixture of 1:1:1 (Perchloric : Nitric : Sulfuric) acid for 1 hour, followed by the removal of several μm on the top side of the polished diamond membrane using an Ar/Cl₂ based ICP RIE (Methods). Chlorine based etching produces smooth diamond surfaces which are required to minimize scattering loss at the diamond interface within the cavity[36, 37]. The final diamond roughness, measured with Atomic Force Microscopy, was found to be 0.2 nm RMS. However, prolonged exposure to chlorine etch gas has been linked to degrading optical properties of the NV centers. Introducing an O₂ based plasma etching step has been found to resolve the surface chlorine contamination[27, 28].

In order to preserve optical properties of the cavity, the diamond must be fixed to the mirror without adhesives, constraining the type of bonding techniques permitted. First attempts to etch the diamond slab with the bottom surface coated with the dielectric mirror stack resulted in coating delamination, likely due to the difference in thermal expansion coefficients of the materials. Successful bonding of the diamond membrane to a processed planar mirror with an activated hydrophilic surface has been achieved via Van der Waals forces. Addition of a water droplet between the two interfaces promotes bonding via strong interfacial forces creating good optical contact between the diamond and the mirror, removing the need for adhesives.[38, 39].

To prepare the processed mirror for bonding, it is placed in an Oxygen plasma environment at 0.4 mbar for 45 s with 100 W, altering the hydrophobicity of the surface (Figure 5.3(A,i)). Water is pipetted onto the surface of the mirror (Figure 5.3(A,ii)) followed by placing the diamond membrane on top of a patterned region. Using the light from an optical microscope objective, the water is evaporated while the bonding process is monitored simultaneously (Figure 5.3(A,iii)). The quality of the bond can be evaluated with visual cues as well as with a profile measurement. Figure 5.3(A,iv) and Figure 5.3(B) show SEM and optical images respectively of the bonded diamond. A poor bond can be identified by the appearance of Newton rings, indicative of an uneven surface and the existence of an air gap between the mirror and diamond. In the optical image, a well bonded diamond is indicated by a uniform colouration. The "milky" colouration seen near the striplines highlights the slightly elevated areas. Profilometer measurements revealed an overall height variation of 100 nm over the diamond surface bonded on top of the patterned area.

5.7. CONCLUSION

In conclusion, we have presented the fabrication of an integrated platform for microwave control in an open, high finesse Fabry-Pérot microcavity enclosing a thin diamond membrane. Finesse measurements of the processed mirrors confirm that the fabrication procedure does not compromise their optical properties. We present a diamond bonding method that allows placing large area diamond membranes onto the cavity mirror while simultaneously enabling the microwave control of the NV center spin. The presented cavity architecture is well suited for enabling enhancement of the NV centers resonant emission along with the control of their spins.

5.8. METHODS

Markers and stripline etching procedure: The planar mirrors are etched with an SF₆ and O₂ based ICP RIE technique in an (Oxford Instruments PlasmaLab 100) etcher with the following parameters: SF₆(Ar) gas flow - 50(10) sccm, ICP (RF) Power - 700(150) W, Base Pressure - 0.026 mBar, Temperature - 50°C, Time - 26 s followed by O₂ gas flow - 50 sccm, ICP(RF) Power - 750(20) W, Base Pressure - 0.030 mBar, Temperature - 50°C, Time - 8 s at a combined rate of 1.9 nm/s, removing 65 nm of mirror material.

The diamond etch parameters are: Ar(Cl₂) gas flow-10(20) sccm, ICP (RF) Power - 500(200) W, Base Pressure - 0.01 mBar, Temperature - 30°C with a resulting etch rate of 2.5 μm/hr.

REFERENCES

- [1] L. Robledo, L. Childress, H. Bernien, B. Hensen, P. F. A. Alkemade, and R. Hanson, “High-fidelity projective read-out of a solid-state spin quantum register,” *Nature*, vol. 477, pp. 574–578, Sep 2011.
- [2] F. Jelezko, T. Gaebel, I. Popa, A. Gruber, and J. Wrachtrup, “Observation of coherent oscillations in a single electron spin,” *Phys. Rev. Lett.*, vol. 92, p. 076401, Feb 2004.
- [3] H. Bernien, B. Hensen, W. Pfaff, G. Koolstra, M. S. Blok, L. Robledo, T. H. Taminiau, M. Markham, D. J. Twitchen, L. Childress, and R. Hanson, “Heralded entanglement between solid-state qubits separated by three metres,” vol. 497, pp. 86–90, May 2013.
- [4] M. V. G. Dutt, L. Childress, L. Jiang, E. Togan, J. Maze, F. Jelezko, A. S. Zibrov, P. R. Hemmer, and M. D. Lukin, “Quantum register based on individual electronic and nuclear spin qubits in diamond,” *Science*, vol. 316, no. 5829, pp. 1312–1316, 2007.
- [5] P. Neumann, J. Beck, M. Steiner, F. Rempp, H. Fedder, P. R. Hemmer, J. Wrachtrup, and F. Jelezko, “Single-shot readout of a single nuclear spin,” *Science*, vol. 329, no. 5991, pp. 542–544, 2010.
- [6] T. H. Taminiau, J. J. T. Wagenaar, T. van der Sar, F. Jelezko, V. V. Dobrovitski, and R. Hanson, “Detection and control of individual nuclear spins using a weakly coupled electron spin,” *Phys. Rev. Lett.*, vol. 109, p. 137602, Sep 2012.
- [7] A. Reiserer, N. Kalb, M. S. Blok, K. J. M. van Bemmelen, T. H. Taminiau, R. Hanson, D. J. Twitchen, and M. Markham, “Robust quantum-network memory using decoherence-protected subspaces of nuclear spins,” *Phys. Rev. X*, vol. 6, p. 021040, Jun 2016.
- [8] H. J. Kimble, “The quantum internet,” *Nature*, vol. 453, pp. 1023–1030, Jun 2008.
- [9] N. Kalb, A. A. Reiserer, P. C. Humphreys, J. J. W. Bakermans, S. J. Kamerling, N. H. Nickerson, S. C. Benjamin, D. J. Twitchen, M. Markham, and R. Hanson, “Entanglement distillation between solid-state quantum network nodes,” *Science*, vol. 356, no. 6341, pp. 928–932, 2017.
- [10] S. B. van Dam, P. C. Humphreys, F. Rozpedek, S. Wehner, and R. Hanson, “Multiplexed entanglement generation over quantum networks using multi-qubit nodes,” *Quantum Science and Technology*, vol. 2, no. 3, p. 034002, 2017.
- [11] J. Wolters, A. W. Schell, G. Kewes, N. Nüsse, M. Schoengen, H. Döscher, T. Hannappel, B. Löchel, M. Barth, and O. Benson, “Enhancement of the zero phonon line emission from a single nitrogen vacancy center in a nanodiamond via coupling to a photonic crystal cavity,” *Applied Physics Letters*, vol. 97, no. 14, p. 141108, 2010.
- [12] P. E. Barclay, K. M. C. Fu, C. Santori, A. Faraon, and R. G. Beausoleil, “Hybrid nanocavity resonant enhancement of color center emission in diamond,” *Phys. Rev. X*, vol. 1, no. 1, p. 011007, 2011.

- [13] T. van der Sar, J. Hagemeyer, W. Pfaff, E. C. Heeres, S. M. Thon, H. Kim, P. M. Petroff, T. H. Oosterkamp, D. Bouwmeester, and R. Hanson, "Deterministic nanoassembly of a coupled quantum emitter–photonic crystal cavity system," *Appl. Phys. Lett.*, vol. 98, no. 19, p. 193103, 2011.
- [14] A. Faraon, C. Santori, Z. Huang, V. M. Acosta, and R. G. Beausoleil, "Coupling of nitrogen-vacancy centers to photonic crystal cavities in monocrystalline diamond," *Phys. Rev. Lett.*, vol. 109, p. 033604, Jul 2012.
- [15] H. Kaupp, C. Deutsch, H.-C. Chang, J. Reichel, T. W. Hänsch, and D. Hunger, "Scaling laws of the cavity enhancement for nitrogen-vacancy centers in diamond," *Phys. Rev. A*, vol. 88, p. 053812, Nov 2013.
- [16] R. Albrecht, A. Bommer, C. Deutsch, J. Reichel, and C. Becher, "Coupling of a single nitrogen-vacancy center in diamond to a fiber-based microcavity," *Phys. Rev. Lett.*, vol. 110, p. 243602, Jun 2013.
- [17] B. J. M. Hausmann, B. J. Shields, Q. Quan, Y. Chu, N. P. de Leon, R. Evans, M. J. Burek, A. S. Zibrov, M. Markham, D. J. Twitchen, H. Park, M. D. Lukin, and M. Lončar, "Coupling of nv centers to photonic crystal nanobeams in diamond," *Nano Lett.*, vol. 13, no. 12, p. 5791, 2013.
- [18] J. C. Lee, D. O. Bracher, S. Cui, K. Ohno, C. A. McLellan, X. Zhang, P. Andrich, B. Alemán, K. J. Russell, A. P. Magyar, I. Aharonovich, A. Bleszynski Jayich, D. Awschalom, and E. L. Hu, "Deterministic coupling of delta-doped nitrogen vacancy centers to a nanobeam photonic crystal cavity," *Appl. Phys. Lett.*, vol. 105, no. 26, p. 261101, 2014.
- [19] J. Riedrich-Möller, S. Pezzagna, J. Meijer, C. Pauly, F. Mücklich, M. Markham, A. M. Edmonds, and C. Becher, "Nanoimplantation and purcell enhancement of single nitrogen-vacancy centers in photonic crystal cavities in diamond," *Appl. Phys. Lett.*, vol. 106, no. 22, p. 221103, 2015.
- [20] D. Englund, B. Shields, K. Rivoire, F. Hatami, J. Vučković, H. Park, and M. D. Lukin, "Deterministic coupling of a single nitrogen vacancy center to a photonic crystal cavity," *Nano Lett.*, vol. 10, no. 10, p. 3922, 2010.
- [21] L. Li, T. Schröder, E. H. Chen, M. Walsh, I. Bayn, J. Goldstein, O. Gaathon, M. E. Trusheim, M. Lu, J. Mower, M. Cotlet, M. L. Markham, D. J. Twitchen, and D. Englund, "Coherent spin control of a nanocavity-enhanced qubit in diamond," *Nat. Commun.*, vol. 6, p. 6173, Jan 2015.
- [22] S. Johnson, P. R. Dolan, T. Grange, A. A. P. Trichet, G. Hornecker, Y. C. Chen, L. Weng, G. M. Hughes, A. A. R. Watt, A. Auffèves, and J. M. Smith, "Tunable cavity coupling of the zero phonon line of a nitrogen-vacancy defect in diamond," *New J. Phys.*, vol. 17, no. 12, p. 122003, 2015.
- [23] H. Kaupp, T. Hümmer, M. Mader, B. Schleder, J. Benedikter, P. Haeusser, H.-C. Chang, H. Fedder, T. W. Hänsch, and D. Hunger, "Purcell-enhanced single-photon

- emission from nitrogen-vacancy centers coupled to a tunable microcavity,” *Phys. Rev. Applied*, vol. 6, p. 054010, Nov 2016.
- [24] E. M. Purcell, H. C. Torrey, and R. V. Pound, “Resonance absorption by nuclear magnetic moments in a solid,” *Phys. Rev.*, vol. 69, p. 37, Jan 1946.
- [25] E. Janitz, M. Ruf, M. Dimock, A. Bourassa, J. Sankey, and L. Childress, “Fabry-perot microcavity for diamond-based photonics,” *Phys. Rev. A*, vol. 92, p. 043844, Oct 2015.
- [26] S. Bogdanović, S. B. van Dam, C. Bonato, L. C. Coenen, A. J. Zwerver, B. Hensen, M. S. Z. Liddy, T. Fink, A. Reiserer, M. Lončar, and R. Hanson, “Design and low-temperature characterization of a tunable microcavity for diamond-based quantum networks,” *Applied Physics Letters*, vol. 110, no. 17, p. 171103, 2017.
- [27] D. Riedel, I. Söllner, B. J. Shields, S. Starosielec, P. Appel, E. Neu, P. Maletinsky, and R. J. Warburton, “Deterministic enhancement of coherent photon generation from a nitrogen-vacancy center in ultrapure diamond,” 2017.
- [28] Y. Chu, N. de Leon, B. Shields, B. Hausmann, R. Evans, E. Togan, M. J. Burek, M. Markham, A. Stacey, A. Zibrov, A. Yacoby, D. Twitchen, M. Loncar, H. Park, P. Maletinsky, and M. Lukin, “Coherent optical transitions in implanted nitrogen vacancy centers,” *Nano Lett.*, vol. 14, no. 4, p. 1982, 2014.
- [29] J. S. Hodges, L. Li, M. Lu, E. H. Chen, M. E. Trusheim, S. Allegri, X. Yao, O. Gaathon, H. Bakhru, and D. Englund, “Long-lived nv spin coherence in high-purity diamond membranes,” *New Journal of Physics*, vol. 14, no. 9, p. 093004, 2012.
- [30] D. Hunger, T. Steinmetz, Y. Colombe, C. Deutsch, T. W. Hänsch, and J. Reichel, “A fiber fabry–perot cavity with high finesse,” *New J. Phys.*, vol. 12, no. 6, p. 065038, 2010.
- [31] D. Hunger, C. Deutsch, R. J. Barbour, R. J. Warburton, and J. Reichel, “Laser micro-fabrication of concave, low-roughness features in silica,” *AIP Adv.*, vol. 2, no. 1, p. 012119, 2012.
- [32] M. Uphoff, M. Brekenfeld, G. Rempe, and S. Ritter *New J. Phys.*, vol. 17, no. 1, p. 13053, 2014.
- [33] T. Klaassen, M. P. van Exter, and J. P. Woerdman, “Characterization of scattering in an optical fabry–perot resonator,” *Appl. Opt.*, vol. 46, p. 5210, Aug 2007.
- [34] “Laseroptik, internal communication..”
- [35] P. Neumann, R. Kolesov, V. Jacques, J. Beck, J. Tisler, A. Batalov, L. Rogers, N. B. Manson, G. Balasubramanian, F. Jelezko, and J. Wrachtrup, “Excited-state spectroscopy of single nv defects in diamond using optically detected magnetic resonance,” *New Journal of Physics*, vol. 11, no. 1, p. 013017, 2009.

- [36] J. Enlund, J. Isberg, M. Karlsson, F. Nikolajeff, J. Olsson, and D. J. Twitchen, "Anisotropic dry etching of boron doped single crystal cvd diamond," *Carbon*, vol. 43, no. 9, p. 1839, 2005.
- [37] C. Lee, E. Gu, M. Dawson, I. Friel, and G. Scarsbrook, "Etching and micro-optics fabrication in diamond using chlorine-based inductively-coupled plasma," *Diamond Relat. Mater.*, vol. 17, no. 7–10, p. 1292, 2008.
- [38] E. Yablonovitch, D. M. Hwang, T. J. Gmitter, L. T. Florez, and J. P. Harbison, "Van der waals bonding of gaas epitaxial liftoff films onto arbitrary substrates," *Applied Physics Letters*, vol. 56, no. 24, pp. 2419–2421, 1990.
- [39] P. Latawiec, V. Venkataraman, M. J. Burek, B. J. M. Hausmann, I. Bulu, and M. Lončar, "On-chip diamond raman laser," *Optica*, vol. 2, p. 924, Nov 2015.



6

DESIGN AND LOW-TEMPERATURE CHARACTERIZATION OF A TUNABLE MICROCAVITY FOR DIAMOND-BASED QUANTUM NETWORKS

S. Bogdanović, S. B. van Dam, C. Bonato, L. C. Coenen, A. J. Zwerver,
B. Hensen, M. S. Z. Liddy, T. Fink, A. Reiserer, M. Lončar and R.
Hanson

We report on the fabrication and characterization of a Fabry-Perot microcavity enclosing a thin diamond membrane at cryogenic temperatures. The cavity is designed to enhance resonant emission of single nitrogen-vacancy centers by allowing spectral and spatial tuning while preserving the optical properties observed in bulk diamond. We demonstrate cavity finesse at cryogenic temperatures within the range of $F = 4,000 - 12,000$ and find a sub-nanometer cavity stability. Modeling shows that coupling nitrogen-vacancy centers to these cavities could lead to an increase of remote entanglement success rates by three orders of magnitude.

This chapter has been published in *Appl. Phys. Lett.* **110**, 171103 (2017).

6.1. INTRODUCTION

Nitrogen-vacancy (NV) centers in diamond are promising building blocks for realizing quantum networks for computation, simulation and communication. The NV center electron spin and nearby nuclear spins form a robust multi-qubit quantum network node that is fully controlled by microwave and optical pulses[1, 2]. Separate network nodes can be entangled through spin-photon entanglement and subsequent two-photon interference and detection [3–5]. The success rate of such entangling protocols is limited by the low probability (few percent) of the NV center emitting into the resonant zero phonon line (ZPL). Coupling of an NV center to an optical cavity can greatly increase the rate of generation and collection of ZPL photons through Purcell enhancement[6]. Purcell enhancement of the ZPL has been demonstrated in several cavity architectures such as diamond photonic crystal cavities[7–11], microring resonators[12] and hybrid structures with evanescently coupled nanodiamonds[13–16]. In recent years the open Fabry-Perot microcavity [17] has emerged as a promising platform for diamond emitters[18–22]. Such a microcavity provides *in-situ* spatial and spectral tunability, while reaching strong field confinement due to its small mode volume V and high quality factor Q . Moreover, this architecture allows for the use of diamond slabs[23] in which the NV center can be relatively far removed from surfaces and thus exhibit bulk-like optical properties, as required for quantum network applications.

6

6.2. CAVITY DESIGN

Here we report on the realization of a high-finesse tunable microcavity enclosing a diamond membrane and its characterization under cryogenic conditions as relevant for quantum network applications. Our cavity employs a concave fiber tip fabricated using a CO₂ laser ablation technique[24] coated with a dielectric mirror stack, and a high reflectivity plane mirror onto which a thin diamond membrane is bonded (see Figure 6.1(a)). This cavity configuration is mounted inside a closed-cycle cryostation (Montana Instruments). To minimize scattering loss as required for a high finesse optical cavity, low surface roughness at the mirror-diamond and diamond-air interfaces is essential. We fabricate the diamond membrane (Figure 6.1(b)) by etching a polished 30 μm thick diamond sheet (ElementSix) down to $\approx 4 \mu\text{m}$ using Ar/Cl₂ inductively coupled plasma reactive ion etching. This etching process is known to preserve the surface smoothness of the diamond[25, 26]. Using AFM, we measure a final diamond roughness value of 0.35 nm RMS. Finally the membrane is bonded to the plane mirror by Van der Waals forces[27].

6.3. CAVITY MODE STUDY

We first study the cavity modes by recording transmission spectra as a function of cavity length using broadband excitation from a supercontinuum laser (see Figure 6.1(c)). From these spectra we extract the frequency of the fundamental modes of the cavity.

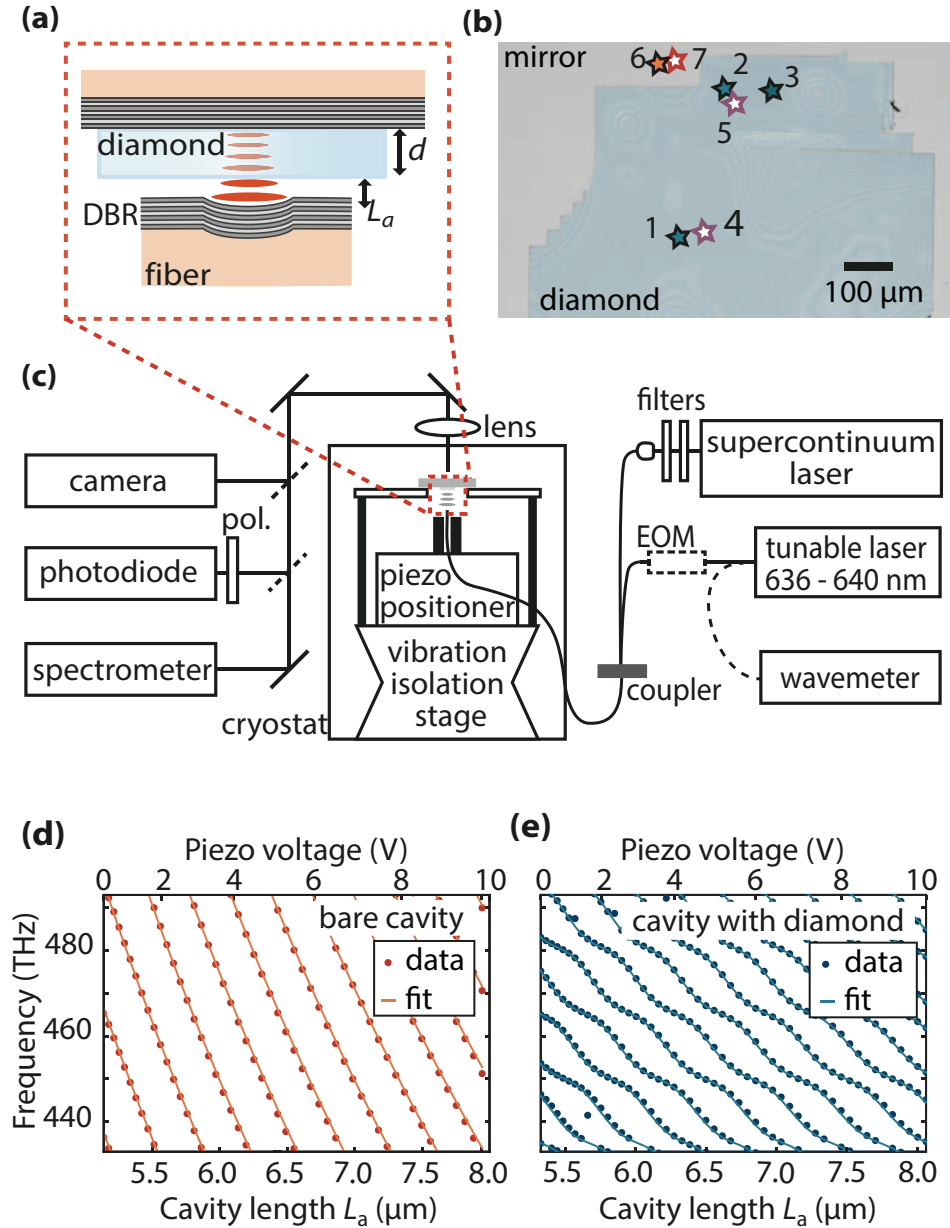


Figure 6.1: (Color Online) Design of the setup and the cavity transmission spectra. (a) Schematic of the cavity showing the concave fiber-tip and the plane mirror onto which a diamond membrane is bonded. The fiber-tip concavity (radius of curvature of $18.4 \mu\text{m}$) is fabricated by CO_2 laser ablation and coated with a dielectric mirror (LASEROPTIK). The residual transmission of the fiber mirror is 50 ppm and losses are ≈ 70 ppm. The reflectivity of the plane mirror is $\approx 99.99\%$. From this follows an expected finesse of $F \approx 29,000$. (b) Microscope image of the $4 \mu\text{m}$ thick bonded diamond membrane. Positions at which cavity properties are measured at 300 K (11 K) are marked with filled (open) markers. (c) Overview of the experimental setup. Effects of mechanical noise sources such as the cryostat pulse tube operation are mitigated with a high-frequency resonance cryo-positioning stage and a low-frequency resonance passive vibration isolation stage (Janssen Precision Engineering CPSHR1-s and CVIP1). See Supplementary Material for low temperature mechanical noise spectrum. (d),(e) The cavity fundamental modes dependency on the cavity length, for a bare cavity (position 6 in (b)) and a cavity containing diamond (position 1 in (b)). Higher order modes are removed to show only the fundamental mode which we fit with the resonant frequencies given by $\nu = cm/2L_a$ for (d) and by Eq. 1 for (e).

The fiber mirror can be moved laterally to obtain an empty cavity (spectrum in Figure 6.1(d)), or a cavity including a diamond membrane (Figure 1(e)). The notably different length dependency for the two cases is a direct consequence of the presence of the high refractive index ($n_d = 2.417$) diamond membrane within the optical cavity. The partially reflecting interface between diamond and air creates a configuration in which the cavity field can be localized in air-like modes, with a length dependency similar to Figure 1(d), and in diamond-like modes, that are largely insensitive to changes in the cavity length. Due to the coupling between these modes, the behaviour of the fundamental modes in Figure 6.1(e) displays avoided crossings. The resulting resonant cavity frequencies ν are determined from a one-dimensional lossless cavity model[21, 28]:

$$\nu \approx \frac{c}{2\pi(L_a + n_d d)} \left\{ \pi m - (-1)^m \times \arcsin \left(\frac{n_d - 1}{n_d + 1} \sin \left(\frac{m\pi(L_a - n_d d)}{L_a + n_d d} \right) \right) \right\}, \quad (6.1)$$

and fit to the measured resonant frequencies to extract the diamond thickness d and the length of the air layer in the cavity L_a with an accuracy up to $\lambda/2$.

6.4. FINESSE MEASUREMENT

6

The intrinsic cavity properties are described by the finesse that we calculate using the cavity length (as determined by the transmission spectra) and the cavity linewidth in frequency. To measure the latter we couple light with a frequency of 471.3 THz from a narrow-linewidth (< 1 MHz) diode laser into the cavity and detect the transmitted signal using a photodiode as we scan the cavity length across the resonance. Phase-modulation was used to create laser sidebands at a fixed 6 GHz separation to directly determine the cavity linewidth in frequency (Figure 6.2(a,b)). We obtain the finesse of the cavity for different cavity lengths. These measurements are repeated at different positions on the diamond membrane and at different temperatures (300 K and 11 K). The results are summarized in Figure 6.2(c). For intermediate cavity lengths, high finesse values of approximately 10,000 are supported by our cavity architecture. For cavity lengths larger than $55 \times \frac{\lambda}{2}$, we observe a distinct drop in finesse which we attribute to clipping losses[17]. At short cavity lengths ($< 45 \times \frac{\lambda}{2}$, $L_{air} \approx 4 \mu\text{m}$) the finesse values show significant fluctuations. We note that similar scatter of finesse values at short microcavity lengths has been previously observed[17, 21]; potential causes are cavity misalignment and contact between the fiber and the plane mirror.

We further investigate the variation of the average finesse as a function of the character (air-like versus diamond-like) of the cavity mode. Cavities formed at the steepest part of a mode (Figure 6.1(e)) are assigned an ‘air-like character’ of 1, whereas the cavities at the flat part have air-like character of 0. Intermediate values are obtained from a linear interpolation by frequency. The bare cavity, that we approximate to have an air-like character of 1, has a finesse of $F \approx 28,000$ (Figure 6.2(d)), which is in agreement with the value expected from the mirrors’ parameters. Inserting the diamond membrane into the cavity reduces the finesse. We attribute this reduction to several effects. First, adding a

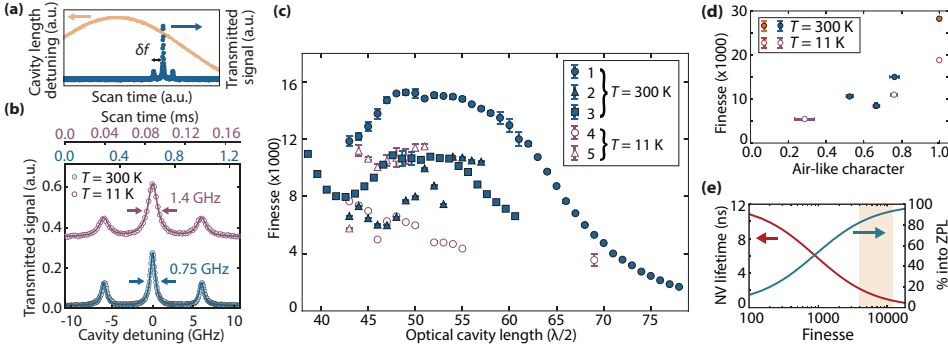


Figure 6.2: (Color online) Measurements of intrinsic cavity properties. (a) Cavity linewidth measurements are performed by scanning the cavity length (orange) around the laser resonance and measuring the signal on the photodiode (blue). The laser frequency is modulated at $\delta f = 6$ GHz. (b) Two representative linewidth scans measured at $T = 300$ K and $T = 11$ K. A single polarization eigenmode is selected using a polarizer in the detection path. At cryogenic temperatures some scans show a deformation as a result of the system vibrations. To represent the intrinsic (vibration-independent) linewidth, we use only scans to which three Lorentzians could be reliably fitted. (c) Finesse dependence on cavity length measured at five different positions on the diamond membrane at $T = 300$ K (closed markers) and $T = 11$ K (open markers). Per cavity length 40-100 scans as in (b) are averaged to obtain the linewidth in frequency. (d) Finesse dependence on the air-like character of the cavity mode, averaged over $L = 47 \times \frac{\lambda}{2}$ to $L = 55 \times \frac{\lambda}{2}$. The data points with an air-like character of 1 represent measurements of the bare cavity finesse. (e) Simulations of the excited state lifetime and emission probability into the cavity mode via the ZPL for an NV center embedded in this optical cavity with $L = 45 \times \frac{\lambda}{2}$. The shaded region shows the finesse range 4,000 – 15,000 measured for cavities containing diamond.

diamond interface into the optical cavity introduces an additional loss mechanism due to scattering from the diamond surface. Given the measured surface roughness of the diamond membrane we expect a reduction in finesse due to scattering to $F \approx 21,000$ [29]. Second, the refractive index of the plane mirror coating is optimized for bare cavity applications. Inserting a diamond membrane (which has a higher refractive index than air) will lower its effective reflectivity, reducing the finesse threefold[21]. The influence of these mechanisms is strongly dependent on the character of the mode in the cavity. The modes with a diamond-like character have an antinode at the air-diamond interface, and therefore are most susceptible to scattering at the diamond surface. The trend in the data in Figure 6.2(d) is consistent with the above consideration, where modes with a more air-like character show a higher finesse.

We estimate the effect that the cavities realized here would have on an embedded NV center's excited state lifetime as well as the probability that emission occurs via the ZPL into the cavity mode (Figure 6.2(e)). We use the Purcell factor F for an ideally placed and oriented NV:

$$F = \frac{3}{4\pi^2} \left(\frac{c}{n_d v} \right)^3 \frac{Q}{V}, \quad (6.2)$$

and use bulk-like free-space values for the branching ratio into the ZPL (3%) and excited state lifetime (12 ns)[12]. A more complex model that explicitly takes dephasing, phonon side-band emission and other cavity modes into account [19, 30] yields quantitatively similar results (not shown). We find that the emission properties of the NV center

would be greatly improved, with a probability of emission into the cavity mode via the ZPL above 80% for the current finesse values, compared to the $\approx 3\%$ probability into all modes for the uncoupled case. Thus, both the relative contribution of ZPL photons to the emission as well as the collection efficiency may be significantly enhanced using these cavities.

6.5. CAVITY STABILITY MEASUREMENT

The linewidth measurements in Figure 6.2 probe the intrinsic cavity properties at time scales comparable to the scan time (0.1 ms at $T = 11$ K). Cooling the system to cryogenic temperatures introduces significant low-frequency (up to about 10 kHz) mechanical noise from the cryostation pulse tube, which results in cavity linewidth broadening when averaging over time scales longer than $(10 \text{ kHz})^{-1}$. We probe the effect of the low-frequency noise on the system by measuring the cavity transmission signal as a function of the laser frequency at a fixed cavity length ($50 \times \frac{\lambda}{2}$). The laser frequency is swept slowly compared to the pulse tube cycle time, ensuring that the full effect of pulse-tube-induced vibrations is visible in the data. The resulting signal is shown in the orange curve in Figure 6.3(b). The broadened cavity linewidth is fitted with a Gaussian function, for which a full width half maximum (FWHM) of 22.2 ± 0.7 GHz is found. This value is a direct measure of the cavity displacement from its resonance position of 0.80 ± 0.03 nm.

Synchronization of our measurement to the 1-Hz cycle of the cryostation pulse tube gives further insight into the effect of the mechanical noise. In Figure 6.3(c) we present the dependence of the effective cavity linewidth on the measurement delay with respect to the cryostation sync signal (Figure 6.3(a)). We find that the vibrations of the system are strongly dependent on the timing within the cryostation cycle, with the cavity linewidth broadening varying from 14 GHz to 50 GHz. The open red datapoints in Figure 6.3(b) show the photodiode signal for the lowest vibration time-bin, 250-300 ms after the sync signal, for which the Gaussian fit gives a cavity length displacement of 0.48 ± 0.03 nm. Cavity displacement can be further reduced by employing active cavity stabilization methods such as the Pound-Drever-Hall technique [31].

Figure 6.3(d) shows the effect of the low-frequency vibrations on the expected fraction of the NV center's emission into the ZPL as calculated in Figure 6.2(d). We use a Gaussian distribution of the displacements as found in the vibration-sensitive measurement of Figure 6.3(b) and a target cavity finesse of 5,000. For the measured vibration levels, we expect the resulting emission via the ZPL into the cavity mode to be 33% which still greatly surpasses the native NV center's emission. In the analysis, we assume the case of an ideally placed emitter within the cavity field (Figure 6.3(d) (solid line)). We additionally explore the effect of a non-ideal dipole orientation and emitter location, resulting in an emission probability of 26% (Figure 6.3(d) (dashed line)). In practice, close-to-ideal conditions could be achieved by utilizing a $\langle 111 \rangle$ -oriented diamond crystal and achieving a high NV-center concentration through nitrogen implantation [32] or nitrogen delta-doping growth [33]. Stable implanted NV centers with the desired linewidths have already been reported [32].

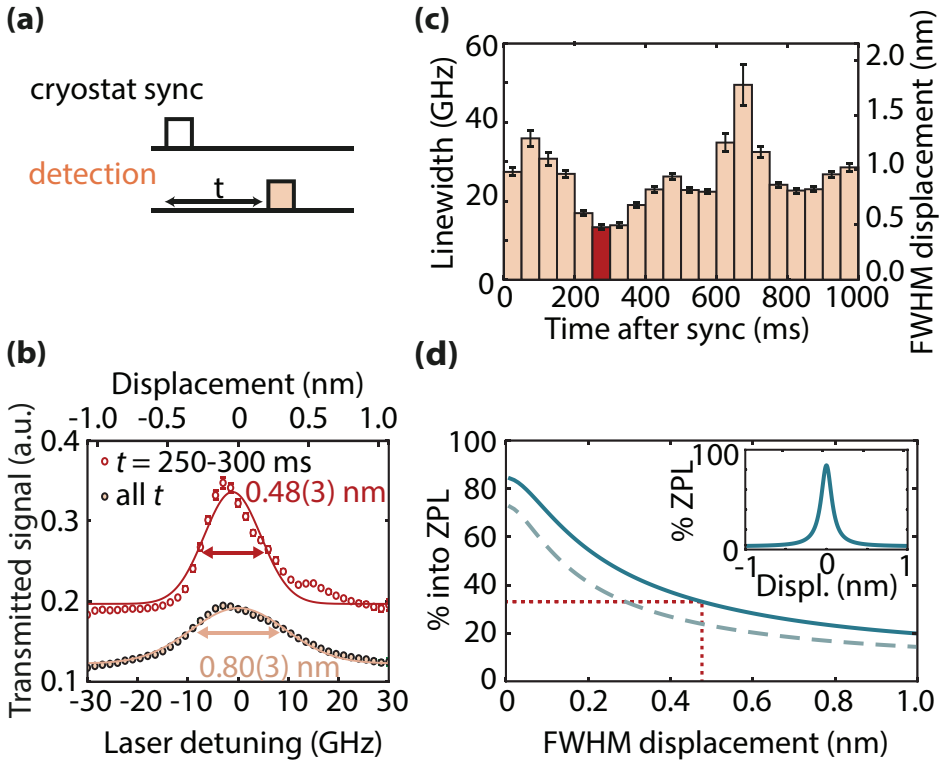


Figure 6.3: (Color online) Vibration-sensitive measurements of the cavity linewidth. (a) Timing of the cavity linewidth detection with respect to the cryostation synchronization signal. (b) Measurement of the cavity transmitted signal, performed by sweeping the laser frequency over the cavity resonance during 41 cycles of the cryostat pulse tube. The center of 50 sweeps is overlapped and averaged, and fitted with a Gaussian curve, for data collected throughout the cryostation tube cycle (orange curve), and for data collected in the time bin 250-300 ms after the sync signal (red curve). (c) Cavity linewidth dependency on the measurement time with respect to the sync signal. (d) Simulation of the NV center emission via the ZPL for a cavity with length $45 \times \frac{\lambda}{2}$ subject to vibrations. The results include a perfectly oriented emitter in the cavity anti-node (solid line) and for an emitter with 30° dipole mismatch and $\frac{\lambda}{10}$ deviation of the emitter position from the cavity anti-node (dashed line). The inset shows the dependency of the NV center's emission into the ZPL on the cavity displacement from its resonance position.

6.6. CONCLUSION

In conclusion, our tunable, high-finesse Fabry-Perot microcavity with an embedded diamond membrane reaches high finesse values of $F \approx 12,000$ at cryogenic temperatures. The demonstrated 0.48 nm length stability under these conditions would enable an approximately 13 times increase in the NV ZPL photon emission. Additionally, these resonant photons are all fed into the well-defined spatial cavity mode that is well suited for collection, leading to an estimated 3 times enhanced collection efficiency. For demonstrated NV center remote entangling schemes that rely on two-photon interference^[3, 5] the resulting boost in the generation and collection of resonant photons in the presented architecture would thus offer an $(3 \times 13)^2 \approx 10^3$ increase in success probability.

6.7. SUPPLEMENTARY MATERIAL

In order to determine the frequency spectrum of the mechanical noise of our cavity system operating at low temperature, we analyze the cavity transmission signal measured on the photodiode. By tuning the cavity on the fringe of a resonance and disconnecting the electronic elements of the piezo circuit, we are able to isolate and measure only the mechanical noise contribution. Using the Welch method¹ to analyze 100 ms long traces of the photodiode signal with 0.8 μs resolution, we obtain the noise power spectral density (Figure 6.4(a)) as well as cumulative noise power (Figure 6.4(b)). We attribute the frequency component at 1.2 kHz to the first natural resonant frequency of the cryo positioning stage².

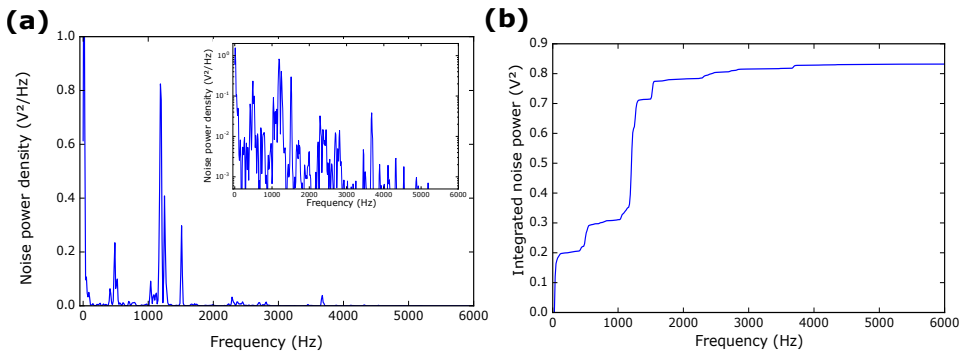


Figure 6.4: (Color Online) Measurement of the cavity mechanical noise spectral properties. (a) Noise power spectral density. The inset shows the plot on a logarithmic scale. (b) Cumulative noise power contribution.

¹Welch, P. D. (1967), IEEE Transactions on Audio and Electroacoustics, AU-15 (2), 70–73

²<http://www.janssenprecisionengineering.com/page/cryo-positioning-stage-high-resonance/>

REFERENCES

- [1] M. V. G. Dutt, L. Childress, L. Jiang, E. Togan, J. Maze, F. Jelezko, A. S. Zibrov, P. R. Hemmer, and M. D. Lukin, "Quantum register based on individual electronic and nuclear spin qubits in diamond," *Science*, vol. 316, no. 5829, p. 1312, 2007.
- [2] T. H. Taminiau, J. Cramer, T. van der Sar, V. V. Dobrovitski, and R. Hanson, "Universal control and error correction in multi-qubit spin registers in diamond," *Nat. Nanotech.*, vol. 9, p. 171, Mar 2014.
- [3] S. D. Barrett and P. Kok, "Efficient high-fidelity quantum computation using matter qubits and linear optics," *Phys. Rev. A*, vol. 71, p. 060310, Jun 2005.
- [4] W. B. Gao, A. Imamoglu, H. Bernien, and R. Hanson, "Coherent manipulation, measurement and entanglement of individual solid-state spins using optical fields," *Nat. Photon.*, vol. 9, p. 363, Jun 2015.
- [5] B. Hensen, H. Bernien, A. E. Dreau, A. Reiserer, N. Kalb, M. S. Blok, J. Ruitenbergh, R. F. L. Vermeulen, R. N. Schouten, C. Abellan, W. Amaya, V. Pruneri, M. W. Mitchell, M. Markham, D. J. Twitchen, D. Elkouss, S. Wehner, T. H. Taminiau, and R. Hanson, "Loophole-free bell inequality violation using electron spins separated by 1.3 kilometres," *Nature*, vol. 526, p. 682, Oct 2015.
- [6] E. M. Purcell, H. C. Torrey, and R. V. Pound, "Resonance absorption by nuclear magnetic moments in a solid," *Phys. Rev.*, vol. 69, p. 37, Jan 1946.
- [7] A. Faraon, C. Santori, Z. Huang, V. M. Acosta, and R. G. Beausoleil, "Coupling of nitrogen-vacancy centers to photonic crystal cavities in monocrystalline diamond," *Phys. Rev. Lett.*, vol. 109, p. 033604, Jul 2012.
- [8] B. J. M. Hausmann, B. J. Shields, Q. Quan, Y. Chu, N. P. de Leon, R. Evans, M. J. Burek, A. S. Zibrov, M. Markham, D. J. Twitchen, H. Park, M. D. Lukin, and M. Lončar, "Coupling of nv centers to photonic crystal nanobeams in diamond," *Nano Lett.*, vol. 13, no. 12, p. 5791, 2013.
- [9] J. C. Lee, D. O. Bracher, S. Cui, K. Ohno, C. A. McLellan, X. Zhang, P. Andrich, B. Alemán, K. J. Russell, A. P. Magyar, I. Aharonovich, A. Bleszynski Jayich, D. Awschalom, and E. L. Hu, "Deterministic coupling of delta-doped nitrogen vacancy centers to a nanobeam photonic crystal cavity," *Appl. Phys. Lett.*, vol. 105, no. 26, p. 261101, 2014.
- [10] L. Li, T. Schröder, E. H. Chen, M. Walsh, I. Bayn, J. Goldstein, O. Gaathon, M. E. Trusheim, M. Lu, J. Mower, M. Cotlet, M. L. Markham, D. J. Twitchen, and D. Englund, "Coherent spin control of a nanocavity-enhanced qubit in diamond," *Nat. Commun.*, vol. 6, p. 6173, Jan 2015.
- [11] J. Riedrich-Möller, S. Pezzagna, J. Meijer, C. Pauly, F. Mücklich, M. Markham, A. M. Edmonds, and C. Becher, "Nanoimplantation and purcell enhancement of single nitrogen-vacancy centers in photonic crystal cavities in diamond," *Appl. Phys. Lett.*, vol. 106, no. 22, p. 221103, 2015.

- [12] A. Faraon, P. E. Barclay, C. Santori, K.-M. C. Fu, and R. G. Beausoleil, “Resonant enhancement of the zero-phonon emission from a colour centre in a diamond cavity,” *Nat. Photon.*, vol. 5, p. 301, May 2011.
- [13] D. Englund, B. Shields, K. Rivoire, F. Hatami, J. Vučković, H. Park, and M. D. Lukin, “Deterministic coupling of a single nitrogen vacancy center to a photonic crystal cavity,” *Nano Lett.*, vol. 10, no. 10, p. 3922, 2010.
- [14] J. Wolters, A. W. Schell, G. Kewes, N. Nüsse, M. Schoengen, H. Döscher, T. Hannappel, B. Löchel, M. Barth, and O. Benson, “Enhancement of the zero phonon line emission from a single nitrogen vacancy center in a nanodiamond via coupling to a photonic crystal cavity,” *Applied Physics Letters*, vol. 97, no. 14, p. 141108, 2010.
- [15] P. E. Barclay, K. M. C. Fu, C. Santori, A. Faraon, and R. G. Beausoleil, “Hybrid nanocavity resonant enhancement of color center emission in diamond,” *Phys. Rev. X*, vol. 1, no. 1, p. 011007, 2011.
- [16] T. van der Sar, J. Hagemeyer, W. Pfaff, E. C. Heeres, S. M. Thon, H. Kim, P. M. Petroff, T. H. Oosterkamp, D. Bouwmeester, and R. Hanson, “Deterministic nanoassembly of a coupled quantum emitter–photonic crystal cavity system,” *Appl. Phys. Lett.*, vol. 98, no. 19, p. 193103, 2011.
- [17] D. Hunger, T. Steinmetz, Y. Colombe, C. Deutsch, T. W. Hänsch, and J. Reichel, “A fiber fabry–perot cavity with high finesse,” *New J. Phys.*, vol. 12, no. 6, p. 065038, 2010.
- [18] H. Kaupp, C. Deutsch, H.-C. Chang, J. Reichel, T. W. Hänsch, and D. Hunger, “Scaling laws of the cavity enhancement for nitrogen-vacancy centers in diamond,” *Phys. Rev. A*, vol. 88, p. 053812, Nov 2013.
- [19] R. Albrecht, A. Bommer, C. Deutsch, J. Reichel, and C. Becher, “Coupling of a single nitrogen-vacancy center in diamond to a fiber-based microcavity,” *Phys. Rev. Lett.*, vol. 110, p. 243602, Jun 2013.
- [20] S. Johnson, P. R. Dolan, T. Grange, A. A. P. Trichet, G. Hornecker, Y. C. Chen, L. Weng, G. M. Hughes, A. A. R. Watt, A. Auffèves, and J. M. Smith, “Tunable cavity coupling of the zero phonon line of a nitrogen-vacancy defect in diamond,” *New J. Phys.*, vol. 17, no. 12, p. 122003, 2015.
- [21] E. Janitz, M. Ruf, M. Dimock, A. Bourassa, J. Sankey, and L. Childress, “Fabry-perot microcavity for diamond-based photonics,” *Phys. Rev. A*, vol. 92, p. 043844, Oct 2015.
- [22] H. Kaupp, T. Hümmer, M. Mader, B. Schleder, J. Benedikter, P. Haeusser, H.-C. Chang, H. Fedder, T. W. Hänsch, and D. Hunger, “Purcell-enhanced single-photon emission from nitrogen-vacancy centers coupled to a tunable microcavity,” *Phys. Rev. Applied*, vol. 6, p. 054010, Nov 2016.

- [23] A. P. Magyar, J. C. Lee, A. M. Limarga, I. Aharonovich, F. Rol, D. R. Clarke, M. Huang, and E. L. Hu, "Fabrication of thin, luminescent, single-crystal diamond membranes," *Appl. Phys. Lett.*, vol. 99, no. 8, p. 081913, 2011.
- [24] D. Hunger, C. Deutsch, R. J. Barbour, R. J. Warburton, and J. Reichel, "Laser micro-fabrication of concave, low-roughness features in silica," *AIP Adv.*, vol. 2, no. 1, p. 012119, 2012.
- [25] J. Enlund, J. Isberg, M. Karlsson, F. Nikolajeff, J. Olsson, and D. J. Twitchen, "Anisotropic dry etching of boron doped single crystal cvd diamond," *Carbon*, vol. 43, no. 9, p. 1839, 2005.
- [26] C. Lee, E. Gu, M. Dawson, I. Friel, and G. Scarsbrook, "Etching and micro-optics fabrication in diamond using chlorine-based inductively-coupled plasma," *Diamond Relat. Mater.*, vol. 17, no. 7–10, p. 1292, 2008.
- [27] P. Latawiec, V. Venkataraman, M. J. Burek, B. J. M. Hausmann, I. Bulu, and M. Lončar, "On-chip diamond raman laser," *Optica*, vol. 2, p. 924, Nov 2015.
- [28] A. M. Jayich, J. C. Sankey, B. M. Zwickl, C. Yang, J. D. Thompson, S. M. Girvin, A. A. Clerk, F. Marquardt, and J. G. E. Harris, "Dispersive optomechanics: a membrane inside a cavity," *New J. Phys.*, vol. 10, p. 095008, 2008.
- [29] T. Klaassen, M. P. van Exter, and J. P. Woerdman, "Characterization of scattering in an optical fabry-perot resonator," *Appl. Opt.*, vol. 46, p. 5210, Aug 2007.
- [30] A. Auffèves, D. Gerace, J.-M. Gérard, M. F. m. c. Santos, L. C. Andreani, and J.-P. Poizat, "Controlling the dynamics of a coupled atom-cavity system by pure dephasing," *Phys. Rev. B*, vol. 81, p. 245419, Jun 2010.
- [31] E. D. Black, "An introduction to pound-drever-hall laser frequency stabilization," *Am. J. Phys.*, vol. 69, no. 1, p. 79, 2001.
- [32] Y. Chu, N. de Leon, B. Shields, B. Hausmann, R. Evans, E. Togan, M. J. Burek, M. Markham, A. Stacey, A. Zibrov, A. Yacoby, D. Twitchen, M. Loncar, H. Park, P. Maletinsky, and M. Lukin, "Coherent optical transitions in implanted nitrogen vacancy centers," *Nano Lett.*, vol. 14, no. 4, p. 1982, 2014.
- [33] K. Ohno, F. Joseph Heremans, C. F. de las Casas, B. A. Myers, B. J. Alemán, A. C. Bleszynski Jayich, and D. D. Awschalom, "Three-dimensional localization of spins in diamond using 12c implantation," *Appl. Phys. Lett.*, vol. 105, no. 5, 2014.



7

OUTLOOK

S. Bogdanović

The work presented in this thesis describes a promising approach in establishing an efficient spin-photon interface by embedding an NV center in a tunable Fabry-Perot microcavity. In this chapter, we will review the current status of the experiment (Section 7.1) and outline the following steps necessary to achieve Purcell enhancement of the NV center (Section 7.2). Following this, we will suggest possible improvements to several aspects of the ongoing experimental effort (Section 7.3) and provide an overview of the future research directions (Section 7.4).

7.1. SUMMARY

The main goal of this thesis is to present the fabrication, characterization and an NV center spin addressing within a fiber-based, tunable Fabry-Perot microcavity enclosing a thin diamond membrane. The main points of this work can be summarized in the following manner:

- A fiber-based, tunable, Fabry-Perot microcavity was designed and constructed. The cavity was placed within a closed-cycle Montana cryostation with custom made cooling and passive stabilization elements.
- An array of markers and microwave delivery stripline were incorporated into the high reflectivity planar mirror forming the cavity without degrading its optical properties.
- A several micrometer thin diamond slab was fabricated and bonded to this mirror using Van der Waals forces.
- Microwave addressing of the NV center spin within this diamond was demonstrated.
- The mechanism of the cavity finesse reduction was investigated, probing its dependence on temperature, cavity length and presence of the diamond membrane. Special attention was given to the cavity stability issues.
- Cavity performance was estimated with respect to the expected improvement of the long distance entanglement protocols.

These results indicate that the coupling NV centers to these cavities represents a promising approach to increasing the emission of their resonant photons and correspondingly the success rate of the remote entanglement protocols. We will discuss the first steps required for demonstrating Purcell enhancement in the next section.

7.2. TOWARDS PURCELL ENHANCEMENT OF THE NV CENTER EMISSION

The first proof of the Purcell enhancement of the NV center coupled to the cavity can be provided by measuring the NV center lifetime reduction of the excited state compared to the uncoupled case using a pulsed green laser excitation (Equation (3.33)). This effect can be additionally confirmed by measuring the difference in the NV center saturation counts for the cavity on and off resonance. As the last step, the autocorrelation function measured in the Hanbury-Brown-Twiss experiment can reveal a modified emission profile of the NV center. Fulfilling these three checkpoints will unequivocally prove the Purcell enhancement of the NV center ZPL transition. Lifetime reduction of an NV center coupled to a tunable Fabry-Perot cavity has already been demonstrated[7], however

efficient photon extraction and improved collection efficiency are yet to be achieved.

The following step is probing the effect this cavity has on the NV properties necessary for quantum network operation. Spin addressing in these structures has been demonstrated in Chapter 5 although the NV center spin coherence times have not been investigated. Coherence times of up to a hundred microseconds have been reported in thin diamond membranes[9] and several hundreds of microseconds in shallow NV centers[10–12] indicating that spin properties can be preserved in these diamonds.

Increasing the branching ratio of the NV center ZPL would mean lower emission into the PSB that does not couple to the cavity. This would reduce the fidelity of the single shot readout (SSRO) protocol[3] which currently relies only on the PSB photon detection. This could be circumvented by including the ZPL photons to the SSRO scheme however strict care needs to be taken in filtering the resonant laser excitation photons from the ones emitted by the NV center. Some of the existing strategies that rely on time and polarization filtering will need to be adapted to the case of the emission in the cavity by, for example, using shorter excitation pulses with stricter time filtering. Alternatively, as a more advanced filtering strategy, the NV center excitation could be performed through a fabricated diamond waveguide, perpendicular to the cavity spatial mode.

The Purcell enhanced NV center emission will also have an increased probability of the direct decay into the ground state, bypassing the metastable spin singlet state. This could have an effect on the electron spin reset time, which would modify the nuclear spin dephasing during the successive remote entanglement attempts[15].

After describing the first experiments in the direction of the NV center Purcell enhancement of the NV center, in the following section we outline the possible improvements to the current experimental effort.

7.3. POSSIBLE EXPERIMENTAL ADVANCEMENT

Enhancing current experimental capabilities can be achieved by improving the cavity itself as well as the emitter properties within these cavities.

In Chapter 6, the emphasis is placed on the cavity stability and the linewidth broadening mechanism due to vibrations. Currently, cavity vibrations are reduced by employing a passive vibration isolation stage (Chapter 4). The cavity stability can be further improved by implementing an active cavity stabilization, using well established techniques such as Pound-Drever-Hall (PDH)[1]. However, the wavelength for obtaining the error signal cannot overlap with the NV center operation wavelength due to its interference with NV center resonant excitation. This would in practice mean stabilizing the cavity using wavelengths close to the edge of the mirror coating stopband or adapting the mirror coatings for two distinct stopbands, one resonant with the NV center transition and one for the PDH stabilization.

Another way of boosting the Purcell factor can be realized by reducing the cavity mode volume. By employing advanced fiber ablation techniques removing the redundant fiber material, even closer fiber approach to the planar mirror is possible[2]. Reducing the cavity mode volume can also be achieved by investigating the minimal diamond thickness that can still shield the NV centers from spectral diffusion effects described in Chapter 2.

It has already been stated throughout this thesis that broad emitter linewidths can have a detrimental effect on the long distance entanglement rates through two mechanisms. Equation (3.35) shows that the limitation to the Purcell factor can come from the increase of the emitter linewidth reducing the effective quality factor. Second, inhomogeneous spectral broadening will render the NV emitted photons distinguishable and will therefore reduce the fidelity of any heralded entangled state. Resonance checks can be employed to tackle this issue, starting the entanglement sequence only when two emitters are on resonance with each other[3] however, this will as a consequence induce a significant drop in the duty cycle of the experiment reducing the entanglement rates. Furthermore, this strategy is only effective in case of a slow changing NV center environment in which the spectral line is stable for several milliseconds after passing the check, corresponding to several hundred or thousands of entangling attempts.

From the above-mentioned arguments, it is clear that the investigation of the dynamics and the timescale of the NV center spectral jumps is of great importance. Comparison of the NV center linewidth we observed in the etched and unetched membranes shows a varying degree of linewidth broadening post-etching (up to several tens of GHz), consistent with other reports[4]. This effect is present even in the NV centers residing several micrometers deep within the diamond membrane, casting uncertainty on the mechanism of this broadening. It is suspected that prolonged chlorine etch in general has a detrimental effect on the NV center optical stability inducing, for example, emitter blinking. It has been shown that this can be mitigated by using more elaborate etching recipes with subsequent annealing steps[5] however additional confirmation is required.

The reduction of the NV center lifetime through Purcell effect can provide another mechanism in combating the issues of spectral diffusion mentioned above. Namely, this reduction would signify an increase in the lifetime limited ZPL linewidth. In the regime where this linewidth becomes larger than the spectral diffusion broadening, the fast decay into the cavity mode will make the energy uncertainty from the spectral jumps negligible[8].

As the last point, NV centers in the bonded diamond membranes experience a greater range of possible strain values, reaching hundreds of GHz. The fine structure of the NV center excited state at such high strain remains largely unexplored and the cyclicity of the optical transitions in this regime will need to be investigated[6].

7.4. FUTURE EXPERIMENTS

The crucial contribution of the Purcell effect will be through speedup of the long distance entanglement protocols which we discuss in the following paragraphs. The current collection efficiency of the ZPL photons using a 0.95 NA objective is 20%. With only 3% emission of the ZPL photons and the photon loss from additional optics elements in our setup, the probability to detect a ZPL photon is $\approx 10^{-3}$. Furthermore, using the long distance entanglement schemes which rely on the Barrett-Kok protocol[13, 14] the total success probability has to be squared reducing the entanglement success probability to 1 event in approximately million attempts, neglecting the fiber loss. This is incompatible with any quantum information protocol requiring information storage on longer lived nuclear spin states which are robust only for several thousands of entangling attempts[15].

Purcell enhanced NV center emission can address this bottleneck in several ways. First, the cavity will change the branching ratio and increase the ZPL photon emission rate compared to the total NV center emission. The cavities presented in this work will be able to increase the photon emission into the ZPL to 33% (Chapter 6), an order of magnitude increase compared to the uncoupled case. Moreover, these photons will be emitted into the cavity mode (Equation (3.34)) boosting their collection efficiency by approximately another factor of 4.

These gains would enable a speedup of our current entangling schemes roughly by a factor of $10^2 * 4^2 = 1600$ which would enable successful entanglement event in several hundred attempts. This would allow entering the regime where we can successfully store and preserve the quantum information on the nuclear spin until the success of the long distance entanglement protocol and finally teleport the information to the next network node.

Additionally, entangling schemes that provide a linear or near-linear scaling of entangling rates with loss (compared to the quadratic one in Barrett-Kok protocol), such as the extreme photon loss protocol[16, 17] and single photon heralded entanglement[18], can also be utilized at the expense of reduced fidelity.

Finally, an experiment complementary to the NV center Purcell enhancement would tackle the issue of NV center resonant emission wavelength which lies in the visible part of the spectrum at 637 nm and is incompatible with long distance transmission through optical fibers due to their internal losses of 8 dB/km. Converting the resonant emission from visible to a telecom band, where losses are drastically reduced, will enable longer photon propagation however at the expense of reducing the total photon number due to the low efficiency of this process.

We finish this section with the suggestions of the possible experiments outside of the scope of the Purcell-enhanced NV center emission. Having a cavity system mounted within a Montana cryostation allows exploring the NV - cavity coupling mechanism at

different temperature regimes. The proposed experiment would include temperature tuning of the emitter linewidth and probe the switch to the phonon-assisted cavity coupling as proposed by Auffeves et al[19, 20].

In Chapter 3, we introduced the regime of the coherent exchange of the excitation between the emitter and the cavity, i.e. strong coupling regime. Here we compare the parameters of the cavity presented in this thesis for fulfilling the strong coupling condition and discuss the necessary improvements in order to demonstrate it. We calculate the emitter-cavity coupling rate from Equation (3.23) taking mode volume from Equation (3.20) with cavity parameters described in Chapter 4 calculated to be $V_{mod} \approx 16 \mu m^3$. This would correspond to $g_0 \approx 600$ MHz which has to be compared to the emitter linewidth (Equation (3.21)) and the cavity decay rate (Equation (3.13)). For the cavities presented in this thesis (Chapter 6) the linewidth of several GHz is identified as the most dominant loss channel.

Minimizing the diamond thickness to few hundreds of nanometers and taking into account the depth of the fabricated fiber dimple and the mirror penetration depth, the effective cavity length could be reduced to $\approx 2 \mu m$ increasing the g_0 by a factor of 3. Employing better optical coatings and implementing already discussed advanced cavity stabilization techniques could enable cavity linewidth reduction which would fulfill the strong coupling condition. The effects of the reversible exchange of the excitation between the atom and the cavity field can be utilized in the experiments of the non-destructive photon readout[21], heralded state transfer in an absorption based regime[22] along with demonstrating atom-photon quantum gates[23] which are a key ingredient in many quantum information experiments[24].

7.5. CONCLUSION

This chapter has outlined the possible advancement of the existing experimental setup and highlighted the NV center optical properties in diamond membranes as the necessary point of improvement. We presented next steps for the demonstration of Purcell enhancement along with an analysis of the potential speedup of the current long distance entanglement protocols. Coupling NV centers to tunable Fabry-Perot cavities described in this thesis could open an exciting possibility of realizing a long standing goal of quantum networks, enabling secure quantum communication on a global scale.

REFERENCES

- [1] E. D. Black, “An introduction to pound–drever–hall laser frequency stabilization,” *Am. J. Phys.*, vol. 69, no. 1, p. 79, 2001.
- [2] H. Kaupp, T. Hümmer, M. Mader, B. Schleder, J. Benedikter, P. Haeusser, H.-C. Chang, H. Fedder, T. W. Hänsch, and D. Hunger, “Purcell-enhanced single-photon emission from nitrogen-vacancy centers coupled to a tunable microcavity,” *Phys. Rev. Applied*, vol. 6, p. 054010, Nov 2016.
- [3] L. Robledo, L. Childress, H. Bernien, B. Hensen, P. F. A. Alkemade, and R. Hanson, “High-fidelity projective read-out of a solid-state spin quantum register,” *Nature*, vol. 477, pp. 574–578, Sep 2011.
- [4] D. Riedel, I. Söllner, B. J. Shields, S. Starosielec, P. Appel, E. Neu, P. Maletinsky, and R. J. Warburton, “Deterministic enhancement of coherent photon generation from a nitrogen-vacancy center in ultrapure diamond,” 2017.
- [5] Y. Chu, N. de Leon, B. Shields, B. Hausmann, R. Evans, E. Togan, M. J. Burek, M. Markham, A. Stacey, A. Zibrov, A. Yacoby, D. Twitchen, M. Loncar, H. Park, P. Maletinsky, and M. Lukin, “Coherent optical transitions in implanted nitrogen vacancy centers,” *Nano Lett.*, vol. 14, no. 4, p. 1982, 2014.
- [6] B. Hensen, *Measurement-based Quantum Computation with the Nitrogen-Vacancy center in Diamond*. Delft, University of Technology: Master Thesis, 2011.
- [7] D. Riedel, I. Sollner, B. J. Shields, S. Starosielec, P. Appel, E. Neu, P. Maletinsky, and R. J. Warburton, “Deterministic enhancement of coherent photon generation from a nitrogen-vacancy center in ultrapure diamond,” *Phys. Rev. X*, vol. 7, p. 031040, Sep 2017.
- [8] Y. Chu and M. D. Lukin, “Quantum optics with nitrogen-vacancy centers in diamond,” 2015.
- [9] J. S. Hodges, L. Li, M. Lu, E. H. Chen, M. E. Trusheim, S. Allegri, X. Yao, O. Gaathon, H. Bakhr, and D. Englund, “Long-lived nv spin coherence in high-purity diamond membranes,” *New Journal of Physics*, vol. 14, no. 9, p. 093004, 2012.
- [10] K. Ohno, F. J. Heremans, L. C. Bassett, B. A. Myers, D. M. Toyli, A. C. B. Jayich, C. J. Palmstrøm, and D. D. Awschalom, “Engineering shallow spins in diamond with nitrogen delta-doping,” *Applied Physics Letters*, vol. 101, no. 8, p. 082413, 2012.
- [11] T. Ishikawa, K.-M. C. Fu, C. Santori, V. M. Acosta, R. G. Beausoleil, H. Watanabe, S. Shikata, and K. M. Itoh, “Optical and spin coherence properties of nitrogen-vacancy centers placed in a 100 nm thick isotopically purified diamond layer,” *Nano Letters*, vol. 12, no. 4, pp. 2083–2087, 2012. PMID: 22404419.
- [12] L. Li, T. Schröder, E. H. Chen, M. Walsh, I. Bayn, J. Goldstein, O. Gaathon, M. E. Trusheim, M. Lu, J. Mower, M. Cotlet, M. L. Markham, D. J. Twitchen, and D. Englund, “Coherent spin control of a nanocavity-enhanced qubit in diamond,” *Nat. Commun.*, vol. 6, p. 6173, Jan 2015.

- [13] H. Bernien, B. Hensen, W. Pfaff, G. Koolstra, M. S. Blok, L. Robledo, T. H. Taminiau, M. Markham, D. J. Twitchen, L. Childress, and R. Hanson, “Heralded entanglement between solid-state qubits separated by three metres,” *Nature*, vol. 497, pp. 86–90, May 2013. Letter.
- [14] B. Hensen, H. Bernien, A. E. Dreau, A. Reiserer, N. Kalb, M. S. Blok, J. Ruitenbergh, R. F. L. Vermeulen, R. N. Schouten, C. Abellan, W. Amaya, V. Pruneri, M. W. Mitchell, M. Markham, D. J. Twitchen, D. Elkouss, S. Wehner, T. H. Taminiau, and R. Hanson, “Loophole-free bell inequality violation using electron spins separated by 1.3 kilometres,” *Nature*, vol. 526, p. 682, Oct 2015.
- [15] A. Reiserer, N. Kalb, M. S. Blok, K. J. M. van Bemmelen, T. H. Taminiau, R. Hanson, D. J. Twitchen, and M. Markham, “Robust quantum-network memory using decoherence-protected subspaces of nuclear spins,” *Phys. Rev. X*, vol. 6, p. 021040, Jun 2016.
- [16] N. H. Nickerson, Y. Li, and S. C. Benjamin, “Topological quantum computing with a very noisy network and local error rates approaching one percent,” vol. 4, pp. 1756 EP –, Apr 2013. Article.
- [17] S. B. van Dam, P. C. Humphreys, F. Rozpedek, S. Wehner, and R. Hanson, “Multiplexed entanglement generation over quantum networks using multi-qubit nodes,” *Quantum Science and Technology*, vol. 2, no. 3, p. 034002, 2017.
- [18] N. Kalb, A. A. Reiserer, P. C. Humphreys, J. J. W. Bakermans, S. J. Kamerling, N. H. Nickerson, S. C. Benjamin, D. J. Twitchen, M. Markham, and R. Hanson, “Entanglement distillation between solid-state quantum network nodes,” *Science*, vol. 356, no. 6341, pp. 928–932, 2017.
- [19] A. Auffèves, J.-M. Gérard, and J.-P. Poizat, “Pure emitter dephasing: A resource for advanced solid-state single-photon sources,” *Phys. Rev. A*, vol. 79, p. 053838, May 2009.
- [20] A. Auffèves, D. Gerace, J.-M. Gérard, M. F. m. c. Santos, L. C. Andreani, and J.-P. Poizat, “Controlling the dynamics of a coupled atom-cavity system by pure dephasing,” *Phys. Rev. B*, vol. 81, p. 245419, Jun 2010.
- [21] A. Reiserer, S. Ritter, and G. Rempe, “Nondestructive detection of an optical photon,” *Science*, vol. 342, no. 6164, pp. 1349–1351, 2013.
- [22] N. Kalb, A. Reiserer, S. Ritter, and G. Rempe, “Heralded storage of a photonic quantum bit in a single atom,” *Phys. Rev. Lett.*, vol. 114, p. 220501, Jun 2015.
- [23] A. Reiserer, N. Kalb, G. Rempe, and S. Ritter, “A quantum gate between a flying optical photon and a single trapped atom,” *Nature*, vol. 508, pp. 237–240, Apr 2014. Letter.
- [24] L.-M. Duan and H. J. Kimble, “Scalable photonic quantum computation through cavity-assisted interactions,” *Phys. Rev. Lett.*, vol. 92, p. 127902, Mar 2004.

SUMMARY

A quantum network would allow the distribution of a quantum state over many spatially separated quantum nodes which individually possess the ability to generate, process and store quantum information. Connecting these nodes through quantum communication channels would enable sending quantum information over arbitrarily long distances, secret key distribution with guaranteed secure communication and distributed quantum computing. An appealing platform for implementation of quantum networks is the nitrogen-vacancy (NV) center in diamond.

An NV center is an optically active defect in diamond created by the substitution of two adjacent carbon atoms in the diamond crystal matrix by a nitrogen atom and a neighboring vacancy. The NV center fits remarkably well in the described quantum network framework. Its electronic spin can be optically initialized, read out in a single shot, coherently manipulated and coupled to the nearby carbon-13 nuclear spins. These properties represent necessary ingredients of a multi-qubit quantum node. The possibility of the entanglement between the state of the NV center spin and a photon establishes a photonic quantum link which can enable the entanglement of the quantum nodes, forming a quantum network.

First building blocks of the proposed quantum networks based on NV centers were demonstrated by performing entanglement between two distant NV centers separated by more than a kilometer. However, the current success rate of the entangling protocols is greatly reduced due to the low emission probability of the NV center photons into the resonant zero phonon line (ZPL) and the inefficient photon extraction from the diamond. This is the central problem which prevents promoting our experiments beyond proof-of-principle demonstration towards practical implementation of the proposed quantum networks.

The goal of this thesis is tackling these issues by coupling NV centers to optical cavities which would greatly increase the rate of generation and collection of the ZPL photons through the mechanism of Purcell enhancement.

The design and the fabrication of the components constituting a diamond-based Fabry-Perot microcavity, as used in this thesis, are described in Chapter 4. For large enhancement of the NV center resonant emission, a low cavity mode volume is necessary. This is achieved by inserting a micrometers thin diamond slab into the cavity architecture; we present the fabrication details of such samples.

Chapter 5 describes the fabrication of an integrated platform for microwave signal delivery to the NV centers within a diamond membrane in the cavity architecture. Microwave striplines and arrays of unique markers are embedded in the mirror onto which the diamond is bonded. We investigate the mirror optical properties post fabrication and find that the fabrication method preserves the mirror optical performance. We describe the diamond bonding method and demonstrate addressing of the NV center spin.

In Chapter 6 we probe the properties of the cavity with the embedded diamond membrane through measurements of the cavity finesse. We investigate the cavity finesse dependence on length, mode structure and temperature. We further explore the operation at cryogenic temperatures by probing the effect of cryostation vibration on the cavity linewidth.

Finally, in Chapter 7 we discuss ways of improving the existing experimental capabilities, outline the first steps for demonstrating enhancement of the NV center resonant emission and suggest future experiments that can be performed with this system. We conclude that coupling of the NV centers to the cavities developed in this research could lead to an increase of remote entanglement success rates by more than three orders of magnitude.

SAMENVATTING

Een kwantum network zou het mogelijk maken om een kwantummechanische toestand te verdelen over een groot aantal ruimtelijk gescheiden kwantum knooppunten, die elk kwantum informatie kunnen genereren, verwerken en opslaan. Het verbinden van deze knooppunten door middel van kwantum communicatie kanalen maakt het mogelijk om kwantum informatie over arbitrair lange afstanden te verzenden, gegarandeerd veilig te communiceren door middel van “secret key distribution” en gedistribueerd kwantum rekenen. Een aantrekkelijk platform voor de implementatie van een kwantum network is het stikstof-gate roosterdefect (NV centrum) in diamant.

Een NV centrum is een optisch actief roosterdefect in diamant, dat wordt gevormd door de substitutie van twee aangrenzende koolstofatomen in het kristalrooster van de diamant door een stikstofaatom en een gat. Het NV centrum past opmerkelijk goed in het beschreven raamwerk voor een kwantum network. Zijn elektronspin kan optisch worden geïnitieerd, in een keer uitgelezen, coherent gemanipuleerd en gekoppeld aan naburige koolstof-13 kernspins. Deze eigenschappen vertegenwoordigen noodzakelijke ingrediënten voor een multi-qubit kwantum knooppunt. De mogelijkheid om de toestand van de NV center elektronspin te verstrengelen met de toestand van foton brengt een fotonische kwantum verbinding tot stand, waardoor kwantum knooppunten met elkaar kunnen worden verstrengeld, met als gevolg een kwantum network.

First building blocks of the proposed quantum networks based on NV centers were demonstrated by performing entanglement between two distant NV centers separated by more than a kilometer. However, the current success rate of the entangling protocols is greatly reduced due to the low emission probability of the NV center photons into the resonant zero phonon line (ZPL) and the inefficient photon extraction from the diamond. This is the central problem which prevents promoting our experiments beyond proof-of-principle demonstration towards practical implementation of the proposed quantum networks.

De eerste bouwstenen van het voorgestelde kwantum network gebaseerd op NV centra zijn gedemonstreerd door twee NV centra op een afstand van meer dan een kilometer met elkaar te verstrengelen. Echter, de huidige slagingskansen van verstrengeling protocollen wordt sterk gereduceerd door de kleine emissiekansen van fotonen in de fononen-transitie (zero phonon line, ZPL), en de inefficiënte uitkoppeling van fotonen uit de diamant. Dit is een het belangrijkste probleem, dat een praktische implementatie van het voorgestelde kwantum network die verder gaat dan een proof-of-principle demonstratie in de weg staat.

Het doel van dit proefschrift is om deze beperkingen aan te pakken door de NV centra

te koppelen aan optische trilholtes, waarbij de emissie van ZPL-fotonen en de uitkoppelfefficiëntie van ZPL-fotonen worden verhoogd door zogenoemde Purcell versterking.

Hoofdstuk 4 beschrijft het ontwerp en de fabricage van de componenten van de in dit proefschrift gebruikte Fabry-Perot trilholte. Voor een grote versterking van de ZPL emissie van een NV centrum is een kleine trilholte noodzakelijk. Dit wordt bereikt door een micrometer dun diamant plaatje in de trilholte te plaatsen; we presenteren de details van de fabricage van dergelijke samples.

Hoofdstuk 5 beschrijft de fabricage van een platform voor microgolfaflivering bij de NV-centra in een diamant membraan geïntegreerd in de trilholte. Microgolf transmissielijnen en rijen van unieke markers worden ingebed in de spiegel waarop de diamant wordt gebonden. We onderzoeken de optische eigenschappen van de spiegels en ontdekken dat deze niet worden aangetast door deze fabricage methode. We beschrijven de methode om de diamant op de spiegel te binden en we laten zien dat we de spin van het NV centrum in de diamant kunnen aansturen.

In hoofdstuk 6 bepalen we de eigenschappen van de trilholte met het ingesloten diamantmembraan door metingen van de finesse van de trilholte. We onderzoeken de lengte-, de mode-structuur- en de temperatuurafhankelijkheid van de finesse. We verkennen de werking bij cryogene temperaturen verder door het effect van cryostaattrillingen op de optische lijnbreedte van de trilholte te bepalen.

Tenslotte bespreken we in hoofdstuk 7 manieren om de bestaande experimentele opstelling te verbeteren en schetsen we potentiële toekomstige experimenten die kunnen worden uitgevoerd met dit systeem. We tonen aan dat verstrengeling van NV centra op grote afstanden met meer dan drie ordergroottes zou kunnen worden versneld door gebruik te maken van de trilholte die is ontwikkeld in dit onderzoek.

ACKNOWLEDGEMENTS

I'd like to start with a simple truth. Coming to QT to do a PhD was the best one of all decision I have ever made. Through ups and downs, from times of loneliness and insecurity to times of happiness and self-confidence and back, this fact has persisted. The most significant reason for this is the love, friendship and support of the amazing people I have encountered throughout this adventure and their influence on my life. These pages are dedicated to you and I sincerely hope that you know that my gratitude to you goes far beyond the few sentences written in this section.

I start the Acknowledgment with the person most responsible for this path. **Ronald**, you gave me the opportunity to work in this amazing team. Without you, these pages wouldnt have been written and this experience wouldnt have existed. Next to you I learned how to anticipate and tackle the problems early on, how to organize and lead the project, be efficient and proactive. All of these are traits that you excel at. I am grateful to you for everything that I've learned and I will carry with me to my next step, for the independence I have developed and for the scientist I have become. Beyond that, the harmony and the fantastic atmosphere in the group come from your hiring priorities and I feel this is the biggest reason for Team Diamond being such a friendly and successful place.

Starting the cavity project could not have been possible without you, **Cristian**. Your experience and help were invaluable in setting a path which my PhD will take. I hope Edinburgh is great to you and I wish you success at your future research. **Anne-Marije**, you joined next and together, we explored many pathways of this newborn project. While some of them turned to be blind alleys, I still feel like we both learned and grew together during this time. It makes me happy and proud that you continued on your PhD path after this challenge and I have no doubts that you will do great! **Andreas**, while you never officially joined the cavity team, your experience and advice surely left a significant mark on it. Thank you for your help and good luck with your Munich endeavor!

Suzanne, you joined the project at the end of my third year and it is no coincidence that this was the start of the happiest and most productive time of my PhD. Your presence marked the end of my lonely years and I couldn't have asked for a better and more compatible partner than you! Your analytical mind, your attention to details and your patience contributed to the project beyond measure but your influence on my PhD goes well beyond that. Be it measurements we did together, endless discussion of theoretical concepts or your support in writing this thesis, working with you always left me with so much enthusiasm and hope concerning the task at hand. Thank you!

Madeline, my cleanroom comrade in arms. Working with you turns a usually harsh and arduous work like cleanroom or paper writing into a fun and easy experience! We made a great team and I am so grateful for your help and your support during your time in Delft. The communication we still have, long after your departure from Delft, shows

me that this friendship will last and I will be happy to meet you soon, on the other side of the ocean!

Marko, from day one I was amazed by your endless supply of optimism, your positivity in face of difficult problems and your helpful and open approach. The influence you had on me and my attitude towards science was as important as was your practical help on the project, which was incredible! Your mindset and presence continue to inspire me and I am very happy for the opportunity to continue working together with you in the future!

Martin, your skill with optics are only matched by your upbeat attitude and your desire to discuss science. It was great having you in the cavity project, I have learned so much from you. **Max**, we didnt overlap much, but our short work together and our discussions left me with no doubts that you will do excellent! Thank you for your help with this thesis! **Wouter**, thank you for your contribution to the cavity project and your help with this thesis! I wish you good luck at your next position. **Oleksiy**, **Lisanne** and **Sophie**, while I have not supervised you directly, your contribution to the project was very valuable and you have my gratitude. **Airat**, welcome to the cavity team, I wish you a successful master project!

I had a fantastic fortune to work in the diamond team which introduced me to many talented and enthusiastic people! **Hannes** you were patient enough to train me in ways of optics and your openness and advice shaped me into a better scientist. Discussing physics with you was and still is so inspiring and every project you touch turns into an incredible success. I have no doubts that will continue to be the case in the future. **Wolfgang**, thank you for the room and for the great atmosphere you created during your time in the diamond team. Welcome back to Delft and hope to have a beer or two with you soon! **Tim**, your advice and feedback helped me on so many occasions through my times (years) of uncertainty and being lost. I didnt see you and **Clara** as much as I would have liked to, but you are amazing people and I always loved the time we spent together. Good luck to you and little Samuel and I truly hope to see you more before I leave. **Machiel**, my cleanroom mentor, wherever I end up there will always be a couch for you to crash on! **Bas**, you had a short role in the cavity project but it was a highly appreciated one. Good luck to you and your family in the lands down under! **Julia**, we started our PhD at the similar time and grew up together on this journey. While our PhD paths couldnt have been more different, the amount of support and motivation we could give to each other was something shared. It is fantastic to see you carving up your own, unique path in the world of science which is just one more proof of how creative and talented you are. **Norbert**, besides being one of the most talented scientists I've ever met, you are a great coworker, officemate, and a beer buddy. I am especially grateful to you for your help with the thesis, but even beyond that, your chill vibe and your helpful attitude is something that made my time in the diamond team so much better. **Mohamed**, I only got to know you better during our conference in Switzerland, but what I got to know is a very warm, considerate and supportive person. It is a pity that I will leave without hanging out with you more and I wish you all the best. May our paths cross again! **Maarten**, our time in cleanroom was short and fun. I think you picked a great project to work on and I wish you lots of success in the future. **Conor**, welcome to the team!

Besides diamond team, there are many more people I want to acknowledge, without their help my project and my PhD wouldn't have happened. **Raymond, Raymond** and **Marijn**, your patience for my silly and mundane electronic puzzles was boundless! To you, I owe much of the progress of the project but also of my knowledge as well! **Bram, Mark, Jelle, Remco, Olaf, Nico, Jason** and **Siebe**, to you I owe help in countless technical lab related issues. Thank you for keeping the labs running so well! My early cleanroom days would have been a nightmare without the help of its great staff, especially **Marco, Charles** and **Ewan**. Each of you in your own department had so much patience with me and offered a helping hand that made many challenging cleanroom problems so much easier. And **Marja, Yuki** and **Chantal**, it is thanks to you that things are running so smoothly and organized. I feel that QT and now QuTech takes pride in its efficiency and you are at the heart of it!

In my youth, I have lived in a several different countries without having to leave my hometown. Things transformed around me and took different names but friendships remained. So did the friendships I have made in Netherlands, be it in the Kavli, Casimir, Quantum Transport, QC Lab or QuTech. **Ale**, you are the creative genius in cleanroom and outside of it. You had patience to help me countless times with many cleanroom problems especially in my early days everything looked new and scary. **Chris**, conversations with you always leave me with a smile on my face. Lets make that Serbian music night happen in the following days! **Iman**, even a few casual hallway and cleanroom conversations were enough for us to click and form a friendship. Your help for my most recent interview proved so valuable in getting the position and for this I am very grateful to you! **Julien** and **Franciska** your incredible hospitality during our visit only reflects what an amazing people you are. I wish you many more adventures and Im sure we will see each other again! **Klaus**, you will always be an honorary housemate of Kloksteeg! I am sure we will play more board games in the future, maybe with the younger generation as well!

James, you are my paranymp, a true friend and a towel. I dont know if I've ever met a person with so many overlapping tastes, opinions and interests which is both remarkable and scary. We've spent together so many glorious moments in the previous years that forged our friendship, going through each of them would require a separate chapter. I hope there are many more to come and I will make an effort for this to happen. **Alex**, truly my brother from another Slavic matushka, it is always a delight chatting with you. I wish you a "red belly" and hope that our paths cross time and time again. **Michiel**, be it pub-quizzing, beer-drinking, Scotland-hiking or filling out government forms, the conversations we have and your subtle sense of humor (of at least 25 mTrevors) always brings out the best of it. Im especially grateful to you for all your recent help and I will show up at your door one of these days with a more concrete token of gratitude. **Jakob**, we shared many moments together, went on trips, concerts and parties. Your calming presence and your views on life make you a fantastic person to be around to. Keep dancing and see you at another adventure! **Kun** you were the perfect officemate and a great friend. I hope things are great in Japan and that I will be able to see you again! **Vincent** your presence and your friendship made my days in Delft so much better (and crazier!). You and **Marieke** are warm and wonderful people and any community will be so lucky

to have you. **Diana**, ever since our first conversation at our first party when I didnt even know you, I knew we will have a blast. I'm not sure even Munich is large enough for the energy of you and **Markus** and I wish you all the best in finding that out!

It was an incredible stroke of luck that many of my friends from Serbia ended up in the Netherlands where we can pick up and strengthen our bonds. If among these people are two of your best high school friends, there is no other way to call it than miracle.

Nemanja, you know me all too well. In times of trouble, I would turn to you with my emotional tirades and your sober advice would cut right through them, straight to the heart of the problem. This is what friends are for and I am so grateful to have you as one. You offered your support so many times and helped me develop as a scientist and as a person on this path. You yourself are at the crossroads at the time of writing these lines and I have no doubt you will make the right choice. I will be there to help in any way I can. **Zorane**, kume, our friendship is so old it reached the age of legal drinking! From late night sharing of our teenage dilemmas at the end of my alley in Čačak to our 'wiser' years this friendship persisted, we learned and supported each other and our bond only got stronger. Being part of your life and a friend to your family fills me with pride and joy.

Saša, the flame you carry inside you is enough to keep warm anyone lucky enough to be near you, let alone be considered your friend. I have relied on your moral compass for direction ever since I've known you and it steered my path while growing up besides you. You carry a lot of credit for the person that I am today and I'm sure I will continue to change for the better next to you. You wouldnt allow it otherwise! **Vlado**, I know the call of an adventure and our friendship will not let the ocean divide us. I can see you waiting at my door on the day I move in, with a pack of beer and a great story. I am actually counting on it! **Vidak**, there is a reason for the 'Vidak rule'. Your outgoing and chill presence kept me from becoming boring and dull and I owe the best times I had in Netherlands to you. I hope its not too much to ask of you to keep doing it! I'm sure we will find a way to stay close to each other in the future. **Miloše**, we started out as high school acquaintances traveling together to America, then we shared an occasional drink in Belgrade but only through our proximity in Netherlands did I get to chance to discover the emotional sevdah soul lying beneath your calm exterior. It brings me happiness that this soul became my friend and will remain to be no matter where we might end up.

I can easily say, without being overly dramatic that coming to live in Kloksteeg 23c changed my life. Its not a sentiment, its a matter of fact, especially if I compare my life before and after the move. People you spend your days with are like your second family and this section is dedicated to you. **Daniel**, I remember the day you and Onder invited me to live with you. You are the heart of every party and your hunger for exploration and new experiences expanded my views of life as well. I am sure that you and **Sara** are having an amazing adventure in Australia and I hope it is everything you have wished for and more. **Peter**, our friendship started way before you moved in. You were an ally in the lab and a great support through peaks of my 'imposter syndrome'. Even the writing of this thesis would have been so much tougher without your generous help. This thesis kept me away from hanging out with you more and being a better buddy and I'm sure we will pick it up now that it is done. I am looking forward to it!

Nodar, bromigo, I have lived with many people throughout my life but I haven't had a better housemate than you. As a credit to your character, at times you were a better host to my guests than even I was. You are a perfect partner for anything from watching stupid shows to talking about deep philosophical stuff, you simply cover the whole range. Keep evolving and growing, your vector is fantastic and your final form will be glorious to behold! My hope is that I will be there to witness it. I will miss you greatly but hopefully not for long!

Önder, your impact on my life and in such a short period of time, cannot be described by words but I will try. Your friendship brought me peace of mind because I knew I could trust you to correct me if I stumble on the wrong path. You taught me how to accept and not be harsh on myself, which is something I desperately needed, but to remain always critical and never take things for granted. You changed my opinions and views of life more than any other person I have ever met and made me realize I have so much to learn, especially from you. But above all, having you as my best friend made me a better person because I had to live up to the standards of being yours. Having you and **Tanja** in my life makes me not worry about the future, because I know I am in good hands. And now, we have converged again! See you soon my friend!

The final written lines of this thesis go to the ones closest to me. My **family** who laid the foundations of who I am and then had faith in me to choose the right path and help and advise but never interfere. Every success I have ever achieved has you in it, and so does this one. Coming back to you always filled me with your love and support which I needed to carry on. Yes, this means to you too, **Damjane**. :)

Anais, having someone like you with me gives me hope that I did something good in life. You brought more happiness into my life than I ever thought is possible. We had so many wonderful adventures and there are many more to come, and knowing that I will share them with you fills my heart with excitement and joy. Although we are far away, my every future step will be made to bring me closer to you and your shine that I cannot do without.



LIST OF PUBLICATIONS

3. **S. Bogdanović***, M. S. Z. Liddy*, S. B. van Dam, L. C. Coenen, T. Fink, M. Lončar and R. Hanson *Robust nano-fabrication of an integrated platform for spin control in a tunable micro-cavity*, accepted for publication in APL Photonics.
2. **S. Bogdanović**, S. B. van Dam, C. Bonato, L. C. Coenen, A. J. Zwerver, B. Hensen, M. S. Z. Liddy, T. Fink, A. Reiserer, M. Lončar and R. Hanson *Design and low-temperature characterization of a tunable microcavity for diamond-based quantum networks*, Applied Physics Letters **110**, 171103 (2017).
1. Z. V. Popović, N. Lazarević, **S. Bogdanović**, M. M. Radonjić, D. Tanasković, R. Hu, H. Lei, Č. Petrović, *Signatures of the spin-phonon coupling in $Fe_{1+y}Te_{1-x}Se_x$ alloys*, Solid State Communications **193**, 51-55 (2014).



CURRICULUM VITAE

Stefan Bogdanović

- December, 1985 Born in Čačak, Serbia.
- 2000 – 2004 Secondary Education:
Gymnasium, Čačak, Serbia.
- 2004 – 2012 B. Sc and M.Sc. Physics, Faculty of Physics, Belgrade.
Advisor: Prof. Dr. Zoran V. Popović, Center for Solid State
Physics
'Raman Spectroscopy of iron-based superconductors'.
- 1/2012 – 11/2012 Research assistant, Institute of Physics, Belgrade.
Center for Solid State Physics
- 2012 – 2017 PhD researcher, Delft University of Technology
Advisor: Prof. dr. ir. R. Hanson, QuTech
*'Diamond-based Fabry-Perot microcavities for quantum net-
works'.*

